THERMALLY RADIATIVE AND MAGNETOHYDRODYNAMIC FLOW OF HYBRID NANOFLUID IN THE PRESENCE OF JOULE HEATING

By

SAIRA KHAN

DEPARTMENT OF MATHEMATICS

NATIONAL UNIVERSITY OF MODERN LANGUAGES

ISLAMABAD

June, 2025

Thermally Radiative and Magnetohydrodynamic Flow of Hybrid Nanofluid in the presence of Joule Heating

By

SAIRA KHAN

Supervised By

DR. ANUM NASEEM

MS Mathematics, National University of Modern Languages, Islamabad, 2025

A THESIS SUBMITTED IN PARTIAL FULFILMENT OF

THE REQUIREMENTS FOR THE DEGREE OF

MASTER OF SCIENCE

In **Mathematics**

To

DEPARTMENT OF MATHEMATICS

FACULTY OF ENGINEERING & COMPUTING

NATIONAL UNIVERSITY OF MODERN LANGUAGES ISLAMABAD

NATIONAL UNIUVERSITY OF MODERN LANGUAGES FACULTY OF ENGINEERIING & COMPUTER SCIENCE

THESIS AND DEFENSE APPROVAL FORM

The undersigned certify that they have read the following thesis, examined the defense, are satisfied with overall exam performance, and recommend the thesis to the Faculty of Engineering and Computing for acceptance.

Thesis Title: Thermally Radiative and Magnetohydrodynamic Flow of Hybrid Nanofluid in the presence of Joule Heating

Submitted By: Saira Khan **Registration #:** 75 MS/Math/S23

Master of Science in Mathematics (MS Math)
Title of the Degree

Mathematics
Name of Discipline

Dr. Anum Naseem
Name of Research Supervisor

____
Signature of Research Supervisor

Dr. Sadia Riaz
Name of HOD (Math)

____
Signature of HOD (Math)

Dr. Noman Malik
Name of Dean (FEC)

____
Signature of Dean (FEC)

June 30th, 2025

AUTHOR'S DECLARATION

I Saira Khan

Daughter of Abdul Majeed

Registration # 75 MS/Math/S23

Discipline Mathematics

Candidate of **Master of Science in Mathematics (MS Math)** at the National University of Modern Languages do hereby declare that the thesis **Thermally Radiative and Magnetohydrodynamic Flow of Hybrid Nanofluid in the presence of Joule Heating** submitted by me in partial fulfillment of MS Mathematics degree, is my original work, and has not been submitted or published earlier. I also solemnly declare that it shall not, in future, be submitted by me for obtaining any other degree from this or any other university or institution. I also understand that if evidence of plagiarism is found in my thesis/dissertation at any stage, even after the award of a degree, the work may be cancelled and the degree revoked.

____
Signature of Candidate

Saira Khan
Name of Candidate

30th June, 2025
Date

ABSTRACT

Title: Thermally Radiative and Magnetohydrodynamic Flow of Hybrid Nanofluid in the presence of Joule Heating

Hybrid nanofluids are an advanced group of nanofluids which offer extremely efficient heat transfer and fluid flow properties when two distinct nanoparticles are blended with a basefluid. Consequently, they prove to be of great significance when the industrial, technological and engineering sectors are concerned. These fluids are playing a role in revolutionizing industries by offering superior heat transfer and energy efficiency. Their potential applications continue to expand, making them a critical innovation in thermal management, and energy systems. This analysis focuses on the examination of the Darcy Forchheimer flow of three unique fluids, two nanofluids ($ZnO/Kerosene\ oil$) and ($Al_2O_3/Kerosne\ oil$) and their resulting hybrid nanofluid ($Zno - Al_2O_3/Kerosene\ oil$). The fluids are flowing over a shrinking sheet placed in a porous medium. The effects of magnetohydrodynamics, thermal radiation, combined with Joule heating are also of importance in this study. The flow model, based on the partial differential equations, is reduced into a system of ordinary differential equations by employing sufficient similarity transformations. This model is further solved using the bvp4c tool in MATLAB software, which provides the numerical results along with graphical outcomes. Influence of various notable parameters on the velocity and temperature distribution have been investigated. It has been observed that the temperature profile increases for higher values of Eckert number, magnetic parameter, radiation parameter and Biot number respectively. The velocity profile declines when the porosity parameter, Forchheimer number, inclination angle and the nanoparticles concentration is enhanced. The critical parameters of Skin friction coefficient and Nusselt number have also been interpreted for different involved factors. The skin fraction coefficient amplifies for the velocity ratio parameter, magnetic and porosity parameter. On the other hand, Nusselt number reduces for the Eckert number, magnetic parameter as well as the radiation parameter.

TABLE OF CONTENTS

LIST OF TABLES

LIST OF FIGURES

LIST OF ABBREVIATIONS

Al_2O_3	Aluminium Oxide
ZnO	Zinc Oxide
MATLAB	Matrix Laboratory
Bvp4c	Boundary Value Problem for 4^{th} Order Collocation
PDEs	Partial Differential Equations
ODEs	Ordinary Differential Equations
MHD	Magnetohydrodynamic
C_f	Skin Friction
Nu	Nusselt Number

LIST OF SYMBOLS

x, y	Cartesian coordinates
u, v	Components of velocity
s_1	First nanoparticle
s_2	Second nanoparticle
ϕ_1	Volumetric Concentration of the first nanoparticle
ϕ_2	Volumetric Concentration of the second nanoparticle
$(C_p)_f$	Specific heat of base fluid
k_f	Thermal conductivity of base fluid
σ_f	Electrical conductivity of base fluid
ρ_f	Density of base fluid
μ_f	Dynamic viscosity of base fluid
$(\rho C_p)_f$	Heat capacity of base fluid
$(C_p)_{nf}$	Specific heat of nanofluid
k_{nf}	Thermal conductivity of nanofluid
σ_{nf}	Electrical conductivity of nanofluid
ρ_{nf}	Density of nanofluid
μ_{nf}	Dynamic viscosity of nanofluid
$(\rho C_p)_{nf}$	Heat capacity of nanofluid
$(C_p)_{hnf}$	Specific heat of hybrid nanofluid
k_{hnf}	Thermal conductivity of hybrid nanofluid
σ_{hnf}	Electrical conductivity of hybrid nanofluid
ρ_{hnf}	Density of hybrid nanofluid
μ_{hnf}	Dynamic viscosity of hybrid nanofluid
$(\rho C_p)_{hnf}$	Heat capacity of hybrid nanofluid
α	Angle of inclination
υ	Kinematic viscosity
q_r	Radiative heat flux

θ	Dimensionless temperature
T_f	Temperature of the wall
T_∞	Ambient temperature of the hybrid nanofluid
M	Magnetic field parameter
R	Radiation parameter
Pr	Prandtl number
Ec	Eckert number
Bi	Biot number
$\mathcal{F}$	Non-uniform inertia coefficient
Fr	Forchheimer number
ω_o	Porosity parameter
K_o^*	Porosity permeability
λ_1	Velocity ratio parameter
Re_x	Reynold's number

ACKNOWLEDGMENT

In the name of Allah, the Most Gracious, the Most Merciful. All praise is due to Allah, the Lord of the worlds, whose infinite blessings and guidance have illuminated my path throughout this academic journey. I am eternally grateful to Him for His countless blessings.

I would like to express my deepest and most heartfelt thanks to my beloved parents, whose endless sacrifices and encouragement have been my guiding light. Their unwavering faith in me and their constant prayers have been the foundation of my strength and success. I am truly blessed to have them in my life, and I am forever indebted and deeply thankful for their unwavering support, which has shaped me into the person I am today.

My sincere appreciation goes to my supervisor, Dr. Anum Naseem, whose thoughtful insights, expert guidance and inspiring mentorship have been crucial to this work.

May Allah (SWT) reward and bless all those who have contributed to my journey, and may He grant us success in this life and the Hereafter.

DEDICATION

This thesis work is a token of gratitude to my mother and father, whose immeasurable sacrifices and unwavering faith in my abilities have encouraged me to pursue my dreams and never give up.

Chapter 1

Introduction

1.1 Hybrid Nanofluids

Nanofluid is a form of a fluid emerging from the suspension of nanoparticles, having a typical diameter ranging from 1 to 100 nm, in a basefluid, such as water, oil-based fluids, ethylene glycol etc. When two distinct kinds of nanometer-sized particles are submerged in a unique base fluid, the resulting combination is generally referred to as a hybrid nanofluid. Researchers and scientists have discovered new and advanced methods to refine the thermo-physical as well as heat transfer characteristics of a fluid under consideration and creation of a hybrid nanofluid is one such crucial technique. By incorporating two nanoparticles with a basefluid, the resultant fluid not only enhances the rates of heat transfer, but also demonstrates boosted thermal conductivity, thermal consistency, augmented stability and overall heat transfer enhancement in contrast to other standard and conventional fluids. In other words, hybrid nanofluids were established to tackle the drawbacks and limitations of typical fluids and even mono nanofluids. This concept was initially described by Turcu *et al.* [1], elaborating their superior properties of transfer of heat, efficiency, cost-effectivity and thermal conduction. Hence hybrid nanofluids have a vast variety of applications and are utilized in industrial machinery, as coolants in machines and automobiles, biomedicine, solar thermal systems, aerospace, electronics etc. Mahmoud [3] considered a micropolar, hydromagnetic fluid on a stretching surface and studied how magnetic field, thermal radiation and heat conduction affected the fluid. Nadeem *et al.* [4] analyzed the stagnation point, time independent flow of a non-Newtonian, viscoelastic nanofluid past a stretching surface while accounting for thermal diffusion and Brownian motion. The process of homotopy analysis was employed to solve the problem. Abolbashari *et al.* [5] conducted an investigation on the nanoparticles (Al_2O_3, Cu, TiO_2, CuO) with H_2O and evaluated the entropy of a time dependent MHD fluid flow due to a porous, stretching surface by the procedure of homotopy analysis. The nanoparticles of copper (Cu) and titanium dioxide (TiO_2) along with the H_2O base fluid was taken up by Ghadikolaei *et al.* [6] to check the impact of magnetohydrodynamics on the stagnation point flow of fluid across a stretching surface. The RKF-45 technique was utilized for the attainment of numerical solutions. Jamaludin *et al.* [7] investigated the stagnation point flow of hybrid nanofluid ($Cu\text{-}Al_2O_3/H_2O$) along a stretching/shrinking permeable surface under the influence of heat generation/absorption, mixed convection and MHD. The mathematical equations were further simplified using the bvp4c module of MATLAB and a duality in the solutions was observed.

1.2 Magnetohydrodynamics

One of the major disciplines of mathematical physics, magnetohydrodynamics or MHD explores the motion, features and behavior of fluids subject to magnetism. The fluids under consideration are conductive fluids such as metallic liquids, plasma, and seawater. Alfven [2] was the one of the earliest scientists to introduce the concept of MHD. This field basically implies that current can be generated in an electroconductive fluid via magnetic forces which in turn gives rise to electric charges in the fluid and ultimately causes the magnetic field to vary. Some fundamental applications of magnetohydrodynamics include MHD power generators, atomic power stations, braking systems of automobiles, casting of metallic liquids and emission of solar plasma. Aly *et al.* [8] dealt with the implications of magnetohydrodynamics on the hybrid nanofluid comprising of Cu and Al_2O_3 mixed in pure H_2O. The heat transfer and fluid flow was studied near the stagnation point while the flow was induced due to a stretchable/shrinkable sheet under the effect of partial slip. The results revealed that the hybrid nanofluid works more effectively than a nanofluid. The work of Khan *et al.* [9] consisted of a hybrid ($Cu - Al_2O_3/Blood$) nanofluid over a continuous stretchable/shrinkable surface with magnetohydrodynamics, heat absorption, heat generation, slip conditions. The strategy of homotopy analysis was applied to garner analytical results. Yashkun *et al.* [10], considering the contribution of magnetohydrodynamics, studied the flow of a hybrid nanofluid (Cu-Al_2O_3/H_2O) past a stretching/shrinking sheet. The flow was also affected by the component of thermal radiation and suction. Further mathematical working was done using MATLAB, more specifically, bvp4c. It was found that the nanofluid was less competent than the hybrid nanofluid when it came to the transfer of heat. Kumbhakar and Nandi [11] worked on how the variables of viscous dissipation, convective boundary condition, nonlinear thermal radiation, Joule heating, heat source/heat sink affected the behavior of a magnetized, time-dependent hybrid nanofluid with constant density. It was also investigated that how the flow behaved in accordance with chemical reactions and velocity slip. The RKF-45 scheme was adopted for quantitative and graphical solutions. Noor *et al.* [12] examined the Jeffery hybrid nanofluid comprising of $Cu - Al_2O_3/C_6H_9NaO_7$ in the context of transfer of mass and heat and the magnetohydrodynamics flow of the fluid with the additional factors of chemical reaction, heat generation and absorption in a compressing channel was examined. Nadeem *et al.* [13] explored the magnetohydrodynamic, tangential and time dependent flow of a fuzzy hybrid nanofluid ($Cu - Al_2O_3/C_2H_6O_2$) while accounting for nonlinear thermal radiation, convective boundary conditions, boundary slip and Ohmic heating, in the presence of an exponentially expanding sheet. Further, the solutions were provided by the bvp4c technique in the MATLAB software. The results indicated that the efficiency of heat transfer was boosted with a rise in the volumetric fraction of nanoparticle and thermal radiation. Mumtaz *et al.* [14] worked on the two-dimensional flow of a magnetohydrodynamic flow of a ternary hybrid nanofluid ($Al_2O_3 - TiO_2 - Cu/H_2O$) and analyzed the effects of Brownian motion on the flow. The factors of mixed convection, chemical reaction was also part of the investigation. The ODEs were consequently solved by the MATLAB's efficient tool, bvp4c. The outcomes clarified that the velocity profile is optimized by the elevation in the parameter of curvature while rise in the magnetic parameter decreases it. Yahaya *et al.* [15] looked into the fluid properties of a hybrid nanofluid when the magnetic forces were taken into account and the fluid was in motion along a shrinking surface. The components of viscous dissipation and convective BCs were also a part of the study. Lisha *et al.* [16] studied the hydromagnetic three-dimensional flow of a Casson hybrid nanofluid ($MWCNT - SWCNT/H_2O$) onto an inclined, stretching surface with permeability, heat source/sink, homogeneous reaction, thermal radiation, and angle of inclination. Taking the basefluid to be water, the nanoparticles of single-walled and multi-walled carbon nanotubes were used in addition to certain shape factors. Kumar *et al.* [17] focused on the factors of magnetohydrodynamics, slip condition, and thermal radiation and their effect on the water, single-walled and multi-walled carbon nanotubes and aluminium oxide-based hybrid nanofluid. Hussain *et al.* [18] considered the hybrid nanofluid ($Ag - Cu - GO/C_{12}H_{26}C_{15}H_{32}$) and analyzed the implications of convective boundary conditions, activation energy and thermal diffusion on the magnetohydrodynamic flow across a stretching surface. Brownian motion and chemical reaction effects were also taken into account. The process of HAM was employed to obtain the mathematical and graphical results. Rehman *et al.* [19] dealt with the unsteady, Casson, hydromagnetic flow of hybrid nanofluid through a stretching sheet, while being influenced by magnetohydrodynamics and viscous dissipation. The graphical results were then compiled using the HAM scheme. Khan *et al.* [20] addressed the ($Fe_3O_4 - Al_2O_3/H_2O$) hybrid nanofluid onto a material with pores consisting of a stretchable surface within and its time-independent, boundary layer, incompressible and MHD flow is affected by thermal radiation, heat generation/absorption and slip conditions. The attained ODEs are then simplified by using the MAPLE software via the RK technique of solution.

1.3 Thermal Radiation

When heat energy is transmitted from a high temperature zone to a region of less temperature by means of waves, more specifically electromagnetic waves, the consequent phenomenon is classified as thermal radiation. This type of radiation is the only heat conduction mechanism that can traverse through air or even potentially through vacuum, without the requirement of propagative media. The movement of the sub-atomic particles (protons and electrons) of a material is the major cause of propagation of this radiative energy. The fundamental notion of thermal radiation is incorporated in a variety of technological equipment that are operated every day. One of the oldest instances is the heat of the sun. Apart from such a basic application, this form of energy transfer is employed in thermal imaging, indoor thermal devices such as gas and water heaters, luminescent light bulbs, firefighting resources, solar-powered stations, industrial and engineering practices etc. Hamad *et al.* [21] assessed the magnetohydrodynamics flow of a fluid through a flat, porous plate under the effect of thermal radiation and the convective boundary conditions. The Fehlberg scheme in Maple tool was considered for numerical computation. Lin *et al.* [22] studied the thermocapillary convection flow of a shear-thinning, non-Newtonian nanofluid consisting of nanoparticles of copper and the oxides of copper, titanium and aluminium with $(C_8H_{15}NaO_8 - H_2O)$ as base fluid, forming the nanofluid as $(Cu - CuO - TiO_2 - Al_2O_3/C_8H_{15}NaO_8 - H_2O)$. The flow is affected by thermal radiation, and the numerical calculations were demonstrated by the process of shooting. Taking thermal radiation as the driving force, Imtiaz *et al.* [23] examined the flow of an electromagnetic nanofluid over an exponentially stretching surface with Brownian motion and thermal diffusion. Ramesh *et al.* [24] illustrated the three-dimensional flow of the Maxwell fluid passing through a porous, dual-directional stretchable surface being directly influenced by thermal radiation. Usman *et al.* [25] employed the procedure of least squares to examine the unsteady, 3-D $(Al_2O_3 - Cu/H_2O)$ based hybrid nanofluid flow with nonlinear thermal radiation and magnetohydrodynamics. The findings of Yusuf *et al.* [26] explored the solution via shooting process when the nanoparticles of TiO_2 and Cu were immersed in H_2O and moved across a stretching surface with porosity while being under the impact of thermal radiation. The three dimensional and Darcy Forchheimer fluid flow with slip was considered to comprehend the entropy generation for conventional and hybrid nanofluids. Masood and Farooq [27] investigated the $(Ag - GO/H_2O)$ based hydromagnetic hybrid nanofluid flow over a stretching surface with an inclined magnetic field and thermal radiation. The method of homotopy was considered for dealing with the equations. The study of Ali *et al.* [28] aimed to deal with heat transfer of magnetohydrodynamic hybrid nanofluid $(Fe_2O_3 - CuO/H_2O)$ flowing over a stretching cylinder while accounting for the effect of thermal radiation. The predictor-corrector technique of Adams-Bashforth generated mathematical and graphical findings. Neethu *et al.* [29] took an exponentially stretching surface for the thermally radiative and MHD hybrid nanofluid flow while the combination of titanium dioxide, silver and H_2O constitute the hybrid nanofluid. Arshad *et al.* [30] analyzed the hybrid nanofluid $(TiO_2 - Al_2O_3/H_2O)$ with thermal radiation affecting the 3-D flow. The incompressible, time-independent, magnetized fluid was also bound by mixed convection and thermophoresis. Oke *et al.* [31] made use of the method of finite difference to numerically solve the model of nanofluid based on nanoparticles of copper, water and aluminium oxide nanoparticles flowing across a spinning plate, in the presence of thermal radiation, Coriolis force and inclined magnetohydrodynamics. Arshad *et al.* [32] addressed the model of rotating conventional as well as hybrid nanofluids and examined how thermal radiation worked for the flow. This MHD, 3-D flow of the fluid, subjected to an angled magnetic force and chemical reactions were also observed. The investigation of Nagaraja *et al.* [33] had the primary purpose of dealing with the ternary hybrid $(TiO_2 - Al_2O_3 - Ag/H_2O)$ nanofluid, possessing both the opposed and aided flow with the consideration of thermal radiation, chemical reaction. Ibrahim *et al.* [34] worked on a model based on water as the host fluid while the nanoparticles of the compound aluminium oxide and the element copper created the hybrid nanofluid flowing along a curved stretching/shrinking sheet under the effects of thermal radiation, suction/injection and mixed convection. Bvp4c provided numerical computations while several parameters and their implications were under consideration. Arshad *et al.* [35] compared the mixed convection flow of three nanofluids, comprising of pure water with alumina, pure water with aluminum oxide and copper, and pure water with titanium dioxide, which is a tri-hybrid nanofluid and accessed the unified implications of thermal diffusion and Dufour effects on the fluid problem with the presence of thermal radiation and chemical reactions.

Hashim *et al.* [36] encountered the problem of a time-dependent, two-dimensional nanofluid flow which is a combination of alumina and water with copper nanomaterials. The problem is investigated in the presence of thermal radiation with fluid flowing on a surface being stretched/shrunk. Varatharaj *et al.* [37] determined how the fluid responded when Ohmic heating, viscous dissipation and majorly thermal radiation affect the flow. The intricate combination of ($CuO - CH_3OH - GO$) gave rise to the Casson, hydromagnetic fluid upon which the slip boundary condition was also applied. The Keller-box algorithm gave information about the numerous components of the model. The objective of the examination of Rahman *et al.* [38] was to model a Darcy Forchheimer flow of a Maxwell hybrid nanofluid ($Cu - TiO_2/H_2O$) across a porous stretching surface, while considering the effects of thermal radiation, heat source/sink. Madhu *et al.* [39] dealt with the flow of hybrid nanofluid ($Fe_2O_4 - MnZnFe_2O_4/H_2O$) over a stretching cylinder under the effect of thermal radiation and activation energy. Waseem *et al.* [40] studied the entropy generation for a fluid comprising of $Cu - TiO_2$ nanoparticles and the fluid flow over a dual-directional sheet with the effects of Ohmic heat, magnetohydrodynamics and thermal radiation being factors of scrutinization. The model is further simplified by the optimal homotopy asymptotic method in the software of Mathematica. Dealing with the Cattaneo-Christov model of heat flux, Farooq *et al.* [41] combined multi-walled carbon nanotubes with copper and single-walled carbon nanotubes with silver and then mixed them both with $NaC_6H_7O_6$ to study the transfer of heat with thermal radiation for the fluids ($Cu - MWCNT/\ NaC_6H_7O_6$) and ($Ag - SWCNT/\ NaC_6H_7O_6$).

1.4 Stagnation Point

In the discipline of fluid mechanics, a stagnation point signifies the location where the fluid flow comes to a stop momentarily, making the fluid velocity to be zero at that point. Located at an object's surface where the fluid movement halts, stagnation points generally split the flow into two streams on the two sides of the object. This type of flow is of profound appeal to the researchers and scientists worldwide, concerning mainly the industries of aerospace and engineering. In the construction of rockets, ships and aircrafts, stagnation point plays a key role in assessing the distribution of pressure and heat. Examining the mechanism of boundary layer, heat protectants for vehicles and spacecrafts, hydrodynamics and meteorological processes etc. are some of the prominent implementations of stagnation point. In accordance with the work of Nazar *et al.* [42], a time-independent, micropolar flow of a fluid having constant density was studied over a stretchable sheet adjacent to the stagnation point. The mathematical and graphical evidence was obtained via the Keller-box approach. Abbas *et al.* [43] dealt with a time-independent Maxwell fluid and explored the effects of mixed convection on the 2D flow near the point of stagnation along a vertically stretching/shrinking surface. Noor *et al.* [44] studied the influence of mixed convection on a micropolar nanofluid flowing over a stretching surface near the stagnation point. The numerical algorithm of Fehlberg was employed to deal with the ODEs system. It was observed that the fluid flow was greatly influenced by the velocity slip condition. Rostami *et al.* [45] considered a hybrid nanofluid ($Al_2O_3 - SiO_2/H_2O$) to examine the mixed convection phenomenon on a hydromagnetic, time-independent flow across a porous plate adjacent to the stagnation point. The numerical solution of the system of transformed ODEs from the PDEs was obtained by utilizing the MATLAB tool, specifically its program, bvp4c. Jamaludin *et al.* [46] studied the flow due to mixed convection within close range of the stagnation point. The study took into account the (Al_2O_3/H_2O), (TiO_2/H_2O) and (Cu/H_2O) nanofluids and analyzed the impact of heat generation/absorption and thermal radiation on the fluid. The consequences of suction were also explored through a vertical surface. The converted ODEs were then dealt with by the MATLAB's tool known as bvp4c and a numerical solution was generated. The impact of various parameters on the flow was assessed and the results were elaborated graphically. Zainal *et al.* [47] considered the numerical study of stagnation point, mixed convective, time-dependent hydromagnetic flow of a copper along with aluminium oxide water-based hybrid nanofluid flowing over a porous sheet. The fluid problem was solved by means of the bvp4c tool of the popular MATLAB application. Waqas *et al.* [48] inspected the magnetohydromagnetic hybrid nanofluid based on magnetite and cupric oxide nanoparticles with water as the basefluid ($CuO - Fe_3O_4/H_2O$) when the factors of thermal radiation and viscous dissipation were involved. MATLAB software generated the graphical and mathematical solutions of the model of the fluid near a stagnation point. Shatnawi *et al.* [49] delved into the unsteady flow of Casson hybrid nanofluid ($MWCNT - SWCNT/H_2O$) by considering multi and single-walled nanotubes of carbon with H_2O and the fluid flows over a Riga surface near a stagnation point while Lorentz forces, thermal radiation and viscous dissipation were under study. The physical factors integrated on the velocity and fluid's temperature were tabulated and exhibited graphically. Kayalvizhi and Kumar [50] studied the entropy generation in a copper-water-aluminium oxide-based hybrid nanofluid stagnation point flow. The model took the parameters of radiation, melting heat transfer and viscous dissipation into account for the investigation. Mahmood and Khan [51] characterized the nanoparticles of alumina, titanium dioxide and cupric oxide to form a ternary hybrid nanofluid ($CuO - TiO_{2-}Al_2O_3/polymer$) which was reliant on mass suction in addition to heat generation. The Runge-Kutta scheme of order 4 was applied and Mathematica was utilized to get a comparative evaluation. Lone *et al.* [52] deployed the scheme of bvp4c to numerically analyze the radiative fluid flow of an unsteady nanofluid composed of ($CuO - TiO_2/engine\ oil$) and the flow was studied near the stagnation region of a surface. The mixed convection and convective conditions were also considered for the flow. Zainal *et al.* [53] investigated the Arrhenius energy model for the laminar hybrid nanofluid flowing via a stretchable/shrinkable sheet in the vicinity of the stagnation point. The nanoscale copper particles, aluminum oxide partciles and pure water were incorporated. Zainal *et al.* [54] examined the 3-D flow of a hydromagnetic hybrid nanofluid at the boundary layer adjacent to the stagnation point. Using the aluminium alloy 7072 and aluminium alloy 7075 with water, Alharbi *et al.* [55] scrutinized the implications of thermal radiation and stagnation point flow of the hybrid nanofluid around a spinning orbital sphere. The acquired differential equations are solved parametrically. Karthik and Kumar [56] dispersed dust particles in the fluid comprised of an alloy of titanium along with $Ag, H_2O, C_2H_6O_2$, giving rise to ($Alloy\ of\ titanium - Ag/H_2O - C_2H_6O_2$). Solar radiation was factored in for this flow near to the stagnation point. Fadhel *et al.* [57] employed a stretchable/shrinkable surface to computationally evaluate the stagnation point flow of Casson fluid, making a blend of nanosized particles of copper, nanoparticles of alumina as well as sodium alginate basefluid. The numerical outputs were interpreted by the bvp4c framework, which ultimately revealed a dual nature of the achieved solution. Mahmood *et al.* [58] studied the influence of thermal radiation on the stagnation point flow of hybrid nanofluid, by suspending nanoscale particles of copper as well as those of alumina in water, across a vertical porous sheet while also including mixed convection and magnetohydrodynamic. The findings illustrated how different parameters impacted the motion of the fluid and heat transfer attributes. Ouyang *et al.* [59] determined the fluid flow of time-dependent nanofluid, hybrid nanofluid and tri-hybrid nanofluid flowing over a shrinking sheet in a permeable medium near a stagnation point with heat absorption and generation. Singla *et al.* [60] investigated stagnation point fluid flow of the copper-alumina nanoparticles immersed in water and the flow was subjected to mixed convection and slip velocity condition.

1.5 Joule Heating

When a solid or a liquid (conductor) possessing resistance allows electric current to flow through it, the electrical energy is transformed into heat and the entire framework is described as Joule heating. Since this heating is a direct consequence of resistance, it is also referred to as resistive heating. The free movement of electrons is hindered as the current traverses through an electric conductor. This resistance then turns the current's energy into thermal energy. This essential principle has countless uses in our day-to-day activities, including heaters, toasters, geysers, ovens, stoves operating via electricity, heat sensor gadgets, fuse panels, circuit wirings, metals melding and fusion, medical equipment of heat therapy etc. Nawaz *et al.* [61] gained an insight into how the Genetic Algorithm works for the Newtonian and non-Newtonian fluid flow when the fluid is under the impact of Joule heating. The stagnation point flow over the stretching sheet was observed numerically by the Downhill simplex (Nelder-Mead) method while the OHAM scheme generated analytical computations. Hayat *et al.* [62] submerged copper in pure H_2O and examined the flow over a stretching surface with porosity and Joule heating. The fluid has constant density and depiction of numerous variables on the profiles of temperature and velocity were obtained. Kamran *et al.* [63] studied the mechanism of Casson nanofluid while being subject to magnetism and condition of slip. The surface of flow was being stretched while Joule heating was also affected strongly on the flow. The algorithm of Keller-box was adopted to access the conduct of multiple factors. Ghadikolaei *et al.* [64] examined the performance of a non-Newtonian hydromagnetic, micropolar fluid of constant density as it flows past a stretching plate while being simultaneously altered by nonlinear thermal radiation and Joule heating. Aziz *et al.* [65] considered a nanofluid ($Cu - C_2H_6O_2$) and a hybrid nanofluid ($Cu - Fe_3O_4/C_2H_6O_2$) and analyzed its entropy generation and the flow over a porous stretchable sheet with Joule heating and the slip conditions. Thermal radiation and a magnetic field influencing the flow were also under consideration to assess this flow. Khashi'ie *et al.* [66] looked into the nanofluid flow water based hybrid nanofluid, constituting of the element copper nanoparticles and the nanoparticles of alumina compound, along a shrinking surface. The single phase (homogeneous) model of nanofluid was adopted and Joule heating impacted on it. Taking Joule heating as the most influential factor, Shoaib *et al.* [67], applied the implicit Lobatto scheme to study the computational mechanisms of an aqueous fluid and its three-dimensional flow via a revolving surface, being under the effects of thermal radiation, with the nanometer sized particles of copper and the compound of aluminium oxide. Ramzan *et al.* [68] took into account an aqueous hybrid nanofluid with the nanoparticles of magnesia and observed its flow over a surface. Joule heating and its influence showed effects on the flow. Radiative heat was another major component of the model, along with the slip conditions. Alqahtani *et al.* [69] investigated the hybrid nanofluid composed of ethylene glycol with the nanoparticles of aluminium oxide, as well as copper oxide, creating ($Cuo - Al_2O_3/C_2H_6O_2$) so that the transfer of thermal energy, and frictional resistance could be explored while the flow was affected by Ohmic heating and prescribed heat flux. Khashi'ie *et al.* [70] presented the results via the boundary value problem solver (bvp4c) for the model of suspended alumina particles along with the copper nanoparticles in pure H_2O. The fluid is flowing over a shrinking surface with Ohmic heating and convective boundary conditions. Rasool *et al.* [71] used the revised form of the Buongiorno framework and took the aspects of thermal diffusion, nonlinear radiation, Ohmic heating and magnetism into account and studied their involvement in the transfer of a fluid formed by submerging $Ag - MoS_2$ particles into 1:1 of water-ethylene glycol basefluid, and the resulting blend of ($Ag - MoS_2/50\%C_2H_6O_2 - 50\%\ H_2O$) . The procedure of Newton-Raphson elaborated the features of Falkner-Skan. Hayat *et al.* [72] elaborated the influence of Lorentz force and Joule heating on a hybrid nanofluid ($Cu - CoFe_2O_4/H_2O$). The flow was observed over a surface with pores where Darcy-Forchheimer, heat generation, and thermal radiation had their direct effect on the flow. Jayanthi and Niranjan [73] tackled the flow of time-independent, incompressible, 2-D, electromagnetic nanofluid when Joule heating, chemical processes and thermal radiation act on it. Bvp4c was employed and numerous dimensionless variables were assessed. Zainodin *et al.* [74] determined the efficiency of the nanoparticles of $CoFe_2O_4$ -Fe_3O_4 immersed in water when the flow is affected by Joule heating, mixed convection and viscous dissipation. Jameel *et al.* [75] interpreted the impact of Joule heating on Maxwell nanofluid whose Darcy-Forchheimer flow was the subject of research with Cattaneo-Christov framework. Viscous dissipation and thermal radiation, along with other physical variables were a part of the analysis. Muhammad *et al.* [76] focused on the Darcy-Forchheimer flow of an MHD, aqueous hybrid nanofluid with MoS_2 and Ag nanoparticles scattered within. A magnetic field was applied on the surface and Joule heating was the major factor of impact. Rafique *et al.* [77] identified the results of a ternary hybrid nanofluid ($TiO_2 - Al_2O_3 - Cu$) with pure water, with the factors of Ohmic heating, temperature stratification, variable viscosity and suction. The effect of viscous dissipation was also explored for the flow near a stagnation point. Tanveer et *al.* [78] studied the entropy generation and heat transfer phenomenon of an alumimnium oxide and copper-based aqueous nanofluid within a material with pores in the midst of gyro-oriented microbes with Ohmic heating. The gravity-stricken microbes give rise to bioconvection. Razzaq *et al.* [79] examined the flow of an aqueous hybrid nanofluid made of copper element nanoparticles and those of aluminium oxide and an inclined magnetic force is applied while Ohmic heating was regarded as the primary component.

In light of the prior stated research analysis, it can be concluded that the stagnation point flow of a hybrid nanofluid over a shrinking surface immersed in a porous medium in the presence of Joule heating has not been addressed yet. The influence of inclined magnetohydrodynamics is also explored. The numerical interpretation of the results via bvp4c has been done from the reduced mathematical equations evolved as ODEs by means of similarity factors. The graphical representation for the temperature and velocity distributions have also been attained in a similar manner. The present work aims to benefit the scientific and technical communities by fostering a thorough analysis and paving the way for potential initiatives and endeavors.

1.6 Thesis Organization

The thesis is comprised of five chapters. A brief description of each chapter is mentioned below.

Chapter 1 embodies the foundational introduction of the crucial factors constituted in the study, accompanied by a rigorous review of the existing work in literature relevant to the associated effects.

Chapter 2 proposes all the significant terminologies and laws to develop the mandatory understanding of the present investigation.

Chapter 3 describes the mechanism of three fluids, two nanofluids and one hybrid nanofluid, moving over a shrinking sheet, with the stagnation point flow being conditional upon thermal radiation, viscous dissipation and convective boundary conditions. The mathematical model is simplified and investigated numerically through the medium of MATLAB software.

Chapter 4 assesses the fluid flow over a shrinking surface in a porous medium for the hybrid nanofluid in addition to the nanofluids with the important variables of Joule heating and inclined magnethydrodynamics. The Darcy Forchheimer flow is also a part of the analysis. The numerical conclusions obtained via bvp4c have been represented graphically for the velocity and temperature distributions as well as surface friction coefficient and Nusselt number.

Chapter 5 elaborates the concluded insights of the study and provides a few pathways to some fascinating potential research projects.

Chapter 2

Fundamental Concepts and Laws

This chapter addresses some of the key definitions, fundamental terminologies and basic laws which are necessary for the effective comprehension of the evaluation presented in the next chapters.

2.1 Fluid

A liquid, gas or any substance in motion is referred to as a fluid when it is unable to withstand an applied external force and deform continuously as a consequence of the applied shear force. This indicates that a fluid does not possess the ability to endure shear stress. Basic examples include kerosene oil, air, blood, water etc. [80]

2.2 Fluid Mechanics

One of the most fundamental branches of physics, fluid mechanics explores the flow of fluids, behavior of fluids under the influence of forces exerted on them and the consequent effects on the physical characteristics of the fluid. It includes two prime fields [80].

2.2.1 Fluid Dynamics

This sub-branch of fluid mechanics primarily focuses on the particular interactions, forces and their impact on the fluid flow properties when a fluid is in motion. [80]

2.2.2 Fluid Statics

Another major domain of fluid mechanics, fluid statics, also described as hydrostatics, examines the physical attributes of a fluid that is stationary i.e. at rest. [80]

2.3 Fluid Flow and its Types

Fluid flow describes the transport of a fluid through a particular point as a consequence of uneven forces exerted on the fluid. The movement of fluid goes on continuously, so long as the imbalanced forces remain present. The flow of a fluid is categorized by the following types [80].

2.3.1 Steady Flow

The flow is identified as a steady flow [80] when certain necessary aspects of the fluid, including fluid temperature, fluid velocity, fluid density and pressure are time-independent and remain unchanged at a specific point in time. Representing fluid features by $\emptyset$, mathematically:

$$\frac{\partial\phi}{\partial t} = 0. \quad (2.1)$$

2.3.2 Unsteady Flow

When the fluid motion and its parameters of pressure, velocity, density, etc. become time-dependent and alter with the passing of time at a particular point, then such a flow is referred to as unsteady [80]. Mathematically,

$$\frac{\partial\phi}{\partial t} \neq 0. \quad (2.2)$$

2.3.3 Laminar Flow

When the flow of fluid is observed along smooth parallel layers or designated pathways, without significant overlapping or blending between layers, then the flow can be specified as laminar. [80]

2.3.4 Turbulent Flow

Turbulent flow is defined as an incredibly disordered fluid movement. Such a flow displays erratic and unpredictable patterns and emerges with a rise in velocity and decline in viscosity. [80]

2.3.5 Compressible Flow

If a fluid's density varies on a continuous form with the fluid's motion, the flow is regarded as compressible. Variations in other physical aspects (velocity, pressure etc.) are the outcomes of this compressibility. [80]

2.3.6 Incompressible Flow

This type of flow is accompanied by little to no changes in the fluid's density as the fluid flows with the passage of time. In other words, density of the fluid is time-independent and thus remains constant. [80]

2.4 Thermal and Physical Properties of Fluid

2.4.1 Viscosity

Viscosity [81] is termed as the rate of fluid's resistance to the flow when an external force acts on it. It is the influence of internal friction as the layers of fluid move simultaneously.

2.4.2 Kinematic Viscosity

A fluid's kinematic viscosity [81] is characterized as the dynamic viscosity-to-density ratio. Mathematical representation of kinematic viscosity is,

$$\upsilon = \frac{\mu}{\rho}. \tag{2.3}$$

Its units in the SI are m^2/s and dimensionally elaborated as $[L^2T^{-1}]$.

2.4.3 Dynamic Viscosity

Dynamic (absolute) viscosity [81] associates shear stress to the rate of variation in velocity i.e. velocity gradient of the fluid. It is mathematically expressed as,

$$\text{Viscosity } (\mu) = \frac{\text{Strees(shear)}}{\text{Gradient of velocity}}. \tag{2.4}$$

Dimensionally, viscosity is depicted as $[ML^{-1}T^{-1}]$ and its unit of measurement is $\frac{kg}{ms}$.

2.4.4 Pressure

Pressure [81] is the ratio of the perpendicularly applied force on a material, to the cross-sectional area of the material's surface. It represents the physical forces implemented on an object. It is indicated in mathematical terms as,

$$\text{Pressure} = \frac{F}{A}. \tag{2.5}$$

It is estimated in N/m^2 units.

2.4.5 Stress

Stress [81] is the quantity that measures the magnitude of the shear forces which trigger deformation in a material. Mathematically,

$$\sigma = \frac{F}{A}, \tag{2.6}$$

where F is the force exerted, A denotes the area of cross-section and σ indicates the stress induced. This mathematical concept has the SI units of $\frac{N}{m^2}$.

2.4.6 Normal Stress

This kind of stress is prompted when the force implemented on a surface acts in a direction perpendicular (normal) to the area of cross-section of the material. [81]

2.4.7 Shear Stress

When the administered force works in a parallel direction to the surface of a material, the resulting stress is termed as shear stress [81].

2.4.8 Density

Density [81] is an essential physical attribute of matter, define as the mass-to-volume ratio of a substance or material. Mathematically,

$$\rho = \frac{m}{V}. \tag{2.7}$$

The SI unit of density is kg/m^3.

2.5 Newton's Law of Viscosity

This law [82] demonstrates that the shear stress between two consecutive fluid layers and the gradient of velocity have a direct relationship between them, with a mathematical formulation as,

$$\tau \propto \frac{\partial v}{\partial y}, \tag{2.10}$$

$$\tau = \mu \frac{\partial v}{\partial y}, \tag{2.11}$$

where the rate at which the component of fluid is subjected to shear strain is governed by $\frac{\partial v}{\partial y}$, dynamic viscosity is identified as μ and τ symbolizes shear stress.

2.6 Types of Fluid

2.6.1 Newtonian Fluid

Newtonian fluids [81] linearly relate the gradient of velocity with shear stress, elaborating the compliance of Newton’s law of viscosity. Some basic forms of Newtonian fluids include air, mineral oils, water, ethyl alcohol etc.

2.6.2 Non-Newtonian Fluid

Non-Newtonian fluids [81] relate the rate of shear stress and strain in a nonlinear manner and as a result, do not comply with Newton’s law of viscosity. A few notable non-Newtonian fluids include ketchup, toothpaste, paint, slurries and starch.

2.7 Mechanisms of Heat Transmission

There are three primary mechanisms [82] by which the transmission of heat occurs between two systems of different temperatures.

2.7.1 Conduction

Conduction [82] of heat signifies the flow of energy from a material's particles with high energy to the neighbouring particles of low energy as an immediate effect of particle-to-particle interactions.

2.7.2 Convection

Convection [82] incorporates the effects of fluid motion with conduction when the energy is transmitted from a surface to the surrounding fluid in motion.

2.7.2.1 Forced Convection

Forced convection [82] induces the motion of fluid over a surface by utilizing external sources such as mechanical instruments, pumps etc.

2.7.2.2 Free/Natural Convection

This procedure is characterized by fluid motion stimulated when temperature alterations cause the density to vary and give rise to buoyancy forces. [82]

2.7.2.3 Mixed Convection

Mixed convection [82] is powered by both the external and buoyant forces, generating a combined effect of forced as well as free (natural) convection.

2.7.3 Radiation

When matter releases energy as electromagnetic waves due to the variations in the arrangement of molecules or atoms, the consequent phenomenon is known as radiation [82]. Heat radiation does not need a transition medium for heat transfer.

2.8 Thermal Diffusivity

The thermal diffusivity [82] of any material can be regarded as the ratio of the heat that the material transmits to the amount of energy stored per unit of volume. It is mathematically designated as,

$$\alpha = \frac{k}{\rho C_p}, \tag{2.8}$$

where the thermal conductivity k, reflects how heat is transmitted effectively, ρ proposes the density and C_p, the heat capacity.

2.9 Thermal Conductivity

Thermal conductivity [82] is categorized as the rate of heat transfer per unit area of an object with a per unit difference of temperature. In mathematical form,

$$k = \frac{qL}{A(\Delta T)}, \tag{2.9}$$

where the amount of thermal energy q is being conducted over an area A, creating a difference in the temperature.

W/mK is the unit used to characterize thermal heat conductivity.

2.10 Dimensionless Numbers

2.10.1 Prandtl Number

Prandtl number [83] is a number having no dimensions and illustrates how the kinematic viscosity and thermal diffusivity are associated with each other. Mathematically,

$$\mathrm{Pr} = \frac{u}{\alpha_f}, \tag{2.12}$$

where α_f quantifies the thermal diffusivity and υ elaborates the kinematic viscosity of the fluid.

2.10.2 Nusselt Number

This non-dimensional parameter [83] is specified as the conducted heat-to-convective heat energy ratio of a fluid. It has an expression as,

$$Nu_x = \frac{Q_{convetion}}{Q_{conduction}} = \frac{hL}{k}, \tag{2.13}$$

where k signifies the heat conductivity, the characteristic length is indicated by L and coefficient of heat convection is given by h.

2.10.3 Eckert Number

Eckert number [83] is a dimensionless variable, used to link the heat transfer by convection with the kinetic energy of the fluid, with the help of the following ratio,

$$Ec = \frac{v^2}{c_p \Delta T}, \tag{2.14}$$

where v^2 is the velocity of flow, specific heat is denoted by c_p and the temperature variation is given by ΔT.

2.10.4 Skin Friction Coefficient

The skin friction [83] is a particular form of drag that is induced by the variation in velocities of a fluid's layers when the fluid encounters a solid boundary. Its mathematical expression is,

$$C_f = \frac{\tau_w}{\frac{1}{2}\rho u_\infty^2}, \tag{2.15}$$

where the wall's stress (shear) is τ_w, the free stream velocity is described by u_∞ and the fluid's density is designated by ρ.

2.10.5 Reynolds Number

This non-dimensional quantity [83] helps to clarify the connection between the forces due to inertia and viscous forces. The flow pattern of the fluid is specified as turbulent or laminar with the aid of Reynold's number. It is calculated as,

$$Re = \frac{uL}{u}, \tag{2.16}$$

where u states the velocity, L is for denoting characteristic length and υ symbolizes the dynamic viscosity.

2.10.6 Biot Number

The Biot number Bi quantifies the ratio of internal thermal resistance to external thermal resistance during convective heat transfer [83]. Mathematically,

$$Bi = \frac{hL}{k}, \tag{2.17}$$

Here, h signifies the convective heat transfer coefficient, L is the characteristic length and k is the thermal conductivity of the material.

Chapter 3

Stagnation Point Flow of Hybrid Nanofluid with Magnetohydrodynamics and Viscous Dissipation

3.1 Introduction

Hybrid nanofluids are an innovative and highly evolved type of heat transfer fluids that exhibit exceptional thermal attributes. This chapter examines the two dimensional, time-independent flow of three distinctive fluids in close proximity to the stagnation point. The surface under consideration is assumed to be shrinking. The elements of convective boundary conditions accompanied by viscous dissipation are also involved. The problem of fluid flow is a mathematical illustration of differential equations in cartesian coordinates. The subsequent ODEs are acquired by utilizing appropriate similarity variables on the principal PDEs. The strategy of bvp4c in the software of MATLAB is implemented to explore the profiles of velocity and temperature graphically.

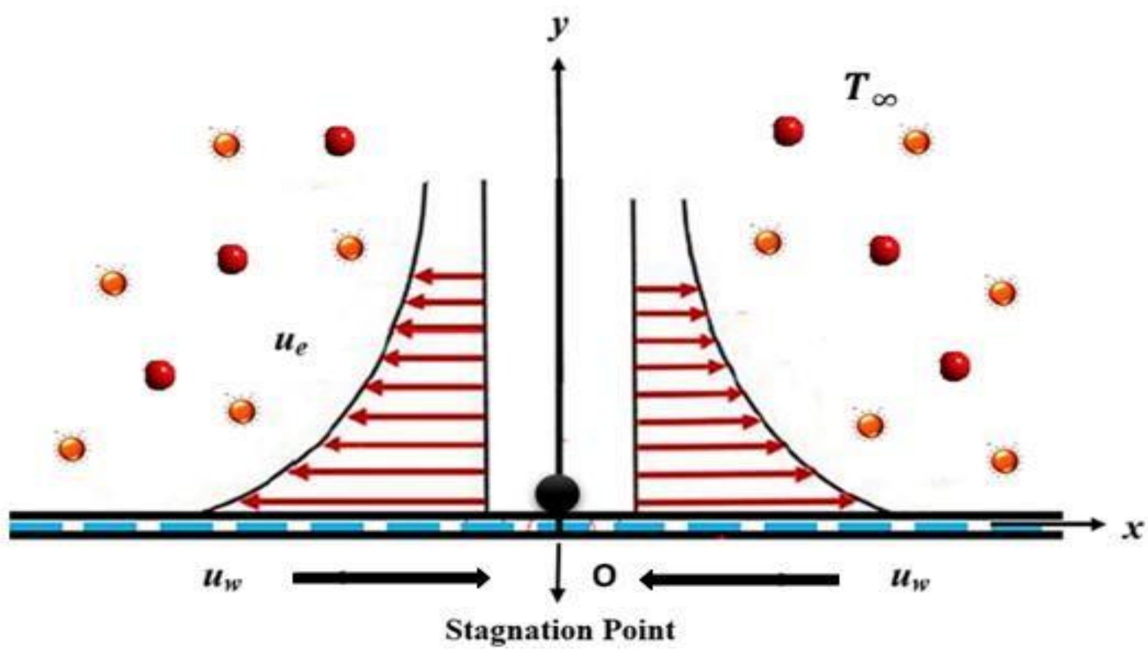

Fig. 3.1: Flow Configuration Model.

3.2 Mathematical Formulation

The current framework relies on the incompressible, time-independent (steady), two-dimensional flow of three nanofluids, adjacent to the stagnation point. The first fluid is comprised of alumina Al_2O_3 and ZnO nanoparticles saturated in kerosene oil, while the other two are ZnO-kerosene oil and Al_2O_3-kerosene oil based nanofluids. This flow, giving rise to a boundary layer, is investigated over a shrinking surface in the horizontal direction. The velocity for the shrinking/stretching surface is designated as $u_w = ax$, along the horizontal x-axis. Perpendicular to the surface under observation, a magnetic field B_o is taken into account. Due to the stagnation point, $u_e = bx$ is the free stream velocity. The phenomenon of viscous dissipation coupled with convective boundary conditions are also examined.

The velocity field prescribed for this model is,

$$\mathbf{V} = [u(x, y), v(x, y), 0]. \tag{3.1}$$

The following equations govern the fluid flow problem,

$$\boldsymbol{\nabla}.\mathbf{V} = 0, \tag{3.2}$$

$$\rho_{hnf}[(\mathbf{V}.\boldsymbol{\nabla})\mathbf{V}] = \boldsymbol{\nabla}.\boldsymbol{\tau} + \rho_{hnf}\mathbf{b}, \tag{3.3}$$

$$(\rho C_p)_{hnf}[(\mathbf{V}.\boldsymbol{\nabla})T] = -\boldsymbol{\nabla}.\mathbf{q} + \mathrm{Tr}(\boldsymbol{\tau}.\mathbf{L}) + q_r, \tag{3.4}$$

with

$$\mathbf{q} = -k\,\mathrm{grad}\,T. \tag{3.5}$$

Here, $\mathbf{V}$ indicates the field of velocity, ρ denotes the fluid's density, $\boldsymbol{\tau}$ is categorized as the Cauchy stress tensor, the temperature of the fluid is T, $\mathbf{q}$ gives the heat flux and the radiative heat flux is symbolized by q_r.

The equations listed below are attained by implementing relevant boundary layer assumptions.

$$\frac{\partial u}{\partial x} + \frac{\partial v}{\partial y} = 0, \tag{3.6}$$

$$u\frac{\partial u}{\partial x} + v\frac{\partial u}{\partial y} = u_e\frac{\partial u_e}{\partial x} + \frac{\mu_{hnf}}{\rho_{hnf}}\frac{\partial^2 u}{\partial y^2} + \frac{\sigma_{hnf}}{\rho_{hnf}}B_o^2(u_e - u), \tag{3.7}$$

$$u\frac{\partial T}{\partial x} + v\frac{\partial T}{\partial y} = \frac{k_{hnf}}{(\rho c_p)_{hnf}}\frac{\partial^2 T}{\partial y^2} - \frac{1}{(\rho C_p)_{hnf}}\frac{\partial q_r}{\partial y} + \frac{\mu_{hnf}}{(\rho C_p)_{hnf}}\left(\frac{\partial u}{\partial y}\right)^2. \tag{3.8}$$

The fluid flow is assessed under the following boundary conditions:

$$u = u_w = ax, v = 0, -k_{hnf}\left(\frac{\partial T}{\partial y}\right) = h(T_f - T), \text{when } y = 0, \tag{3.9}$$

$$u \to u_e = bx, T \to T_\infty, v \to 0, \text{ when } y \to \infty. \tag{3.10}$$

In the formerly stated conditions, u signifies the velocity in the horizontal direction, v represents the velocity vertical to the horizontal direction, a and b show arbitrary constants, u_w and T_f designate the velocity and temperature at the wall and u_e and T_∞ characterize the free stream velocity and temperature.

The non-dimensional similarity variables are taken to be

$$\eta = \left(\frac{\rho_f b}{\mu_f}\right)^{\frac{1}{2}} y, \;\; \theta(\eta) = \frac{T - T_\infty}{T_f - T_\infty}, \tag{3.11}$$

$$u = f'(\eta)bx, \;\; v = -\left(\frac{\mu_f b}{\rho_f}\right)^{\frac{1}{2}} f(\eta). \tag{3.12}$$

Table 3.1: Thermophysical Attributes of Kerosene Oil, Zinc Oxide and Alumina. [84]

Characteristics	**Kerosene Oil**	$\boldsymbol{ZnO}$	$\boldsymbol{Al_2O_3}$
$\rho(kg/m^3)$	783	5700	3970
$k(W/mK)$	0.15	25	40
$\sigma((\Omega\text{m}))^{-1}$	0.0000000006	9.999	0.0000000001
$C_p(J/kg\text{K})$	2090	523	765

Table 3.2: Thermophysical attributes under consideration for both Nanofluids. [84]

Characteristics	Nanofluid
Electrical Conductivity (σ)	$\frac{\sigma_{nf}}{\sigma_f} = \frac{\sigma_{s1} - 2\phi_{s1}(\sigma_f - \sigma_{s1}) + 2\sigma_f}{\sigma_{s1} + (\sigma_f - \sigma_{s1}) + 2\sigma_f}$
Dynamic Viscosity (μ)	$\frac{\mu_{nf}}{\mu_f} = \frac{1}{(1-\phi_{s1})^{2.5}}$
Specific Heat Capacity (C_p)	$(\rho C_p)_{nf} = (1-\phi_{s1})(\rho C_p)_f + \phi_{s1}(\rho C_p)_{s1}$
Density (ρ)	$\rho_{nf} = (1-\phi_{s1})\rho_f + \phi_{s1}\rho_{s1}$
Thermal Conductivity (k)	$\frac{k_{nf}}{k_f} = \frac{k_{s1} - 2\phi_{s1}(k_f - k_{s1}) + 2k_f}{k_{s1} + \phi_{s1}(k_f - k_{s1}) + 2k_f}$

Table 3.3: Thermophysical attributes of Hybrid Nanofluid ($ZnO - Al_2O_3$/Kerosene Oil) [84].

Characteristics	Hybrid Nanofluid
Electrical Conductivity (σ)	$\frac{\sigma_{hnf}}{\sigma_f} = [\frac{\sigma_{s2} - 2\phi_{s2}(\sigma_{nf} - \sigma_{s2}) + 2\sigma_{nf}}{\sigma_{s2} + \phi_{s2}(\sigma_{nf} - \sigma_{s2}) + 2\sigma_{nf}}] \times [\frac{\sigma_{s1} - 2\phi_{s1}(\sigma_f - \sigma_{s1}) + 2\sigma_f}{\sigma_{s1} + \phi_{s1}(\sigma_f - \sigma_{s1}) + 2\sigma_f}]$
Dynamic Viscosity (μ)	$\frac{\mu_{hnf}}{\mu_f} = \frac{1}{(1-\phi_1)^{2.5}(1-\phi_2)^{2.5}}$
Specific Heat Capacity (C_p)	$\frac{(\rho C_P)_{hnf}}{(\rho C_P)_f} = \frac{(\rho C_P)_{s2}\,\phi_{s2}}{(\rho C_P)_f} + [\frac{(\rho C_P)_{s1}\,\phi_{s1}}{(\rho C_P)_f} + (1-\phi_{s1})](1-\phi_{s2})$
Density (ρ)	$\frac{\rho_{hnf}}{\rho_f} = \frac{\rho_{s2}\phi_{s2}}{\rho_f} + [\frac{\rho_{s1}\phi_{s1}}{\rho_f} + (1-\phi_{s1})](1-\phi_{s2})$
Thermal conductivity (k)	$\frac{k_{hnf}}{k_f} = [\frac{k_{s2} - 2\phi_{s2}(k_{nf} - k_{s2}) + 2k_{nf}}{k_{s2} + \phi_{s2}(k_{nf} - k_{s2}) + 2k_{nf}}] \times [\frac{k_{s1} - 2\phi_{s1}(k_f - k_{s1}) + 2k_f}{k_{s1} + \phi_{s1}(k_f - k_{s1}) + 2k_f}]$

For the Eq. (3.8), in the expression $\frac{\partial q_r}{\partial y}$, q_r is established as

$$q_r = -\frac{4}{3}\frac{\sigma^*}{k^*}\frac{\partial T^4}{\partial y}, \tag{3.13}$$

The terms σ^* and k^*define the coefficient of mean absorption. The expression described below is obtained when for T^4, the Taylor's expansion is utilized as

$$T^4 \approx 4T_\infty{}^3 T - 3T_\infty{}^4, \tag{3.14}$$

leading to

$$\frac{\partial T^4}{\partial y} = 4\frac{\partial T}{\partial y}T_\infty{}^3. \tag{3.15}$$

Hence, the Eq. (3.13) becomes

$$q_r = -\frac{16}{3}\frac{\sigma^* T_\infty^3}{k^*}\frac{\partial T}{\partial y}. \tag{3.16}$$

Consequently, Eq. (3.8) is obtained as

$$u\frac{\partial T}{\partial x}+v\frac{\partial T}{\partial y}=\frac{k_{hnf}}{(C_P\rho)_{hnf}}\frac{\partial^2 T}{\partial y^2}+\frac{1}{(C_P\rho)_{hnf}}\left(\frac{16\sigma^* T_\infty^3}{3k^*}\frac{\partial^2 T}{\partial y^2}\right)+\frac{\mu_{hnf}}{(C_p\rho)_{hnf}}\left(\frac{\partial u}{\partial y}\right)^2. \tag{3.17}$$

The equation (3.6) is readily satisfied via the application of Eqs. (3.11) - (3.12). Therefore, the aforementioned PDEs from Eqs. (3.7) and (3.8) take the following form

$$f'^2(\eta)-f(\eta)f''(\eta)-1-\frac{\frac{\mu_{hnf}}{\mu_f}}{\frac{\rho_{hnf}}{\rho_f}}f'''(\eta)-M\frac{\frac{\sigma_{hnf}}{\sigma_f}}{\frac{\rho_{hnf}}{\rho_f}}(1-f'(\eta))=0, \tag{3.18}$$

$$\left(\frac{k_{hnf}}{k_f}+R\right)\theta''(\eta)+\frac{\mu_{hnf}}{\mu_f}EcPrf''^2(\eta)+\frac{(\rho C_P)_{hnf}}{(\rho C_P)_f}Prf(\eta)\theta'(\eta)=0, \tag{3.19}$$

$$f(0)=0,\quad \theta'(0)=-Bi(1-\theta(0)),\quad f'(0)=\lambda_1, \text{when } \eta=0, \tag{3.20}$$

$$\theta(\infty)\to 0,\quad f'(\infty)\to 1, \text{when } \eta\to\infty. \tag{3.21}$$

The above stated equations include certain dimensionless entities, where $M=\frac{B_o^2\sigma_f}{\rho_f b}$ illustrates the magnetic parameter, the parameter for thermal radiation is depicted by $R=\frac{16T_\infty^3\sigma_1}{3k_1k_f}$, the Eckert number is symbolized as $Ec=\frac{(bx)^2}{(T_f-T_\infty)(C_p)_f}$, Prandtl number is denoted by $Pr=\frac{\mu_f(C_p)_f}{k_f}$ and the parameter of velocity ratio is demonstrated as $\lambda_1=\frac{a}{b}$.

The mathematical expression for the factors of skin friction and Nusselt number are described as,

$$C_f=\frac{1}{\rho_f u_e^2}\tau_w,\quad Nu_x=-\left[-(q_r)_{y=0}+k_{hnf}\left(\frac{\partial T}{\partial y}\right)_{y=0}\right]\frac{xq_w}{k_f(T_f-T_\infty)}, \tag{3.22}$$

where $q_w=-\left(\frac{\partial T}{\partial y}\right)_{y=0}k_{hnf}$ is indicating the heat flux and $\tau_w=\left(\frac{\partial u}{\partial y}\right)_{y=0}\mu_{hnf}$ characterizes the shear stress at the surface.

Then, Eq. (3.16) is reduced as

$$C_f(Re)^{\frac{1}{2}}=\frac{\mu_{hnf}}{\mu_f}f''(0),\quad Nu_x(Re)^{-\frac{1}{2}}=-\left(\frac{4}{3}R+\frac{k_{hnf}}{k_f}\right)\theta'(0), \tag{3.23}$$

Furthermore, to prevent complexity in calculations, the ratios depicted below are utilized.

$$A=\frac{\mu_{hnf}}{\mu_f},\quad B=\frac{\rho_{hnf}}{\rho_f},\quad C=\frac{(\rho C_P)_{hnf}}{(\rho C_P)_f}, \tag{3.24}$$

$$S = \frac{\sigma_{hnf}}{\sigma_f}, \qquad K = \frac{k_{hnf}}{k_f}. \tag{3.25}$$

Consequently, Eqs. (3.18), (3.19) and (3.23) are reduced to the following arrangement

$$f'^2(\eta) - f(\eta)f''(\eta) - 1 - \frac{A}{B}f'''(\eta) - M\frac{S}{B}(1 - f'(\eta)) = 0\,, \tag{3.26}$$

$$(K + R)\theta''(\eta) + AEcPrf''^2(\eta) + CPrf(\eta)\,\theta'(\eta) = 0, \tag{3.27}$$

$$(Re)^{\frac{1}{2}}C_f = Af''(0), \;\; (Re)^{-\frac{1}{2}}Nu_x = -\left(\frac{4}{3}R + K\right)\theta'(0). \tag{3.28}$$

Here, Re signifies the local Reynold's number.

3.3 Numerical Stratagem

The bvp4c module of MATLAB is implemented to work out the previously obtained ODEs for the flow model. The differential equations involved in the problem are of higher order. Hence, they are initially converted to the form of first order DEs and then, as a result, the aid of bvp4c process is taken into consideration.

$$y(1) = f, \tag{3.29}$$

$$y(2) = f', \tag{3.30}$$

$$y(3) = f'', \tag{3.31}$$

$$y(4) = \theta, \tag{3.32}$$

$$y(5) = \theta', \tag{3.33}$$

$$y'(3) = [\{y(2)\}^2 - y(1)y(3) - 1 - M\frac{S}{B}\{(1 - y(2))\}]\left(\frac{B}{A}\right), \tag{3.34}$$

$$y'(5) = [-CPr\{y(1)y(5)\} - AEcPr\{y(3)\}^2]\left(\frac{1}{K+R}\right). \tag{3.35}$$

And the relevant boundary conditions are

$$y_0(1) = 0, \quad y_0(5) = -Bi(1 - y_0(4)), \quad y_0(2) = \lambda_1 \tag{3.36}$$

$$y_\infty(4) \to 0, \quad y_\infty(2) \to 1. \tag{3.37}$$

3.4 Graphical Analysis and Discussion

The analysis of several effects that arise as a consequence of numerous dimensional entities on the profiles of velocity and temperature is fundamental to the study. This section emphasizes the essential flow attributes by extensively investigating the fluid problem. The notable impacts of dimensionless parameters on the quantities under scrutiny are demonstrated. Figures 3.2, 3.3 and 3.4 depict the velocity profile for the magnetic parameter (M) and the corresponding volume fractions of Al_2O_3 and ZnO nanoparticles $\phi_1$and ϕ_2 respectively. Figure 3.2 portrays that an upsurge in the values of M also upsurges the velocity of the hybrid nanofluid as well as the two nanofluids. Figure 3.3 and 3.4 illustrate the velocity profile under the influence of increasing values of the nanoparticle volume fractions. It is found that the velocity of the nanofluids and hybrid nanofluid diminishes for larger values of ϕ_1 and ϕ_2, because the momentum boundary layer thickness is minimized with the accumulation of volume fractions of nanoparticles. Figures 3.5-3.9 clarify the considerable influence of different dimensionless factors on the temperature profile of the hybrid and nanofluids, which include Prandtl number (Pr), Eckert number, (Ec), Radiation parameter (R), Biot number (Bi), and ϕ_1, ϕ_2 i.e. the volume fractions of the nanoparticles of ZnO and Al_2O_3. Figure 3.5 exemplifies a deterioration in the temperature of the three distinct fluids with heightened Pr values. Figure 3.6 depicts the temperature profile for the variation in Eckert number (Ec). With a spike in Ec, the thermal field is intensified due to a surge in the boundary layer thickness and the kinetic energy of the fluid. This directly amplifies all three fluid's temperature. Figure 3.7 shows that temperature of the nanofluids as well as the hybrid nanofluid amplifies as the radiation factor is augmented. When the convective heat transfer is boosted, it offsets the outcomes of thermal radiation, leading to a heightened temperature profile. Figure 3.8 displays the growing trend of the temperature profile of the fluids with an enhancement in the Biot number (Bi), owing to the fact that the increment in the Biot number (Bi) causes the temperature gradient near the surface to increase as well due the enhancement in the thermal boundary layer thickness. Figure 3.9 and 3.10 represent a rise in the temperature for all the three fluids under considerations. As the nanoparticles volumetric fractions are elevated, it results in a greater temperature profile. This behavior is justified by the better accumulation of heat energy as a result of rise in thermal conductivity. Figures 3.11-3.14 analyze the pivotal effects of the distinguished parameters of M, λ_1, Ec and R with variations of ϕ_2 on skin friction and Nusselt number. For ϕ_1, the skin friction coefficient shows an upsurging trend with the magnetic parameter (M) in Figure 3.9. This behaviour remains the same for the hybrid and both the nanofluids respectively. This is because of the fact that the magnetic field hinders the fluid movement and the strength of magnetic field defies the flow, driving up the drag force and ultimately increasing the skin friction coefficient. Fig 3.10 is sketched to illustrates the conduct of friction drag with the velocity ratio parameter λ_1 when ϕ_1 is raised. It is revealed that the friction drag is elevated when ϕ_2 is accumulated for the fluids for growing λ_1. Concerning the three fluids, Figure 3.11 exhibits a drop in the heat transmission rate for increased Eckert number (Ec) when ϕ_1 is altered in an increasing manner. Figure 3.12 demonstrates a decay in the Nusselt number with a boost in ϕ_1 when the radiation parameter (R) is under consideration.

Table 3.1-3.3 represent the thermophysical features of the hybrid nanofluids and both the nanofluids. This information is essential for the execution of the study. Table 3.4 is presented to show the excellent agreement of the present analysis with the available published data. The comparison validates the ongoing analysis. Table 3.5 shows the ranges of the values used in the computation of the study.

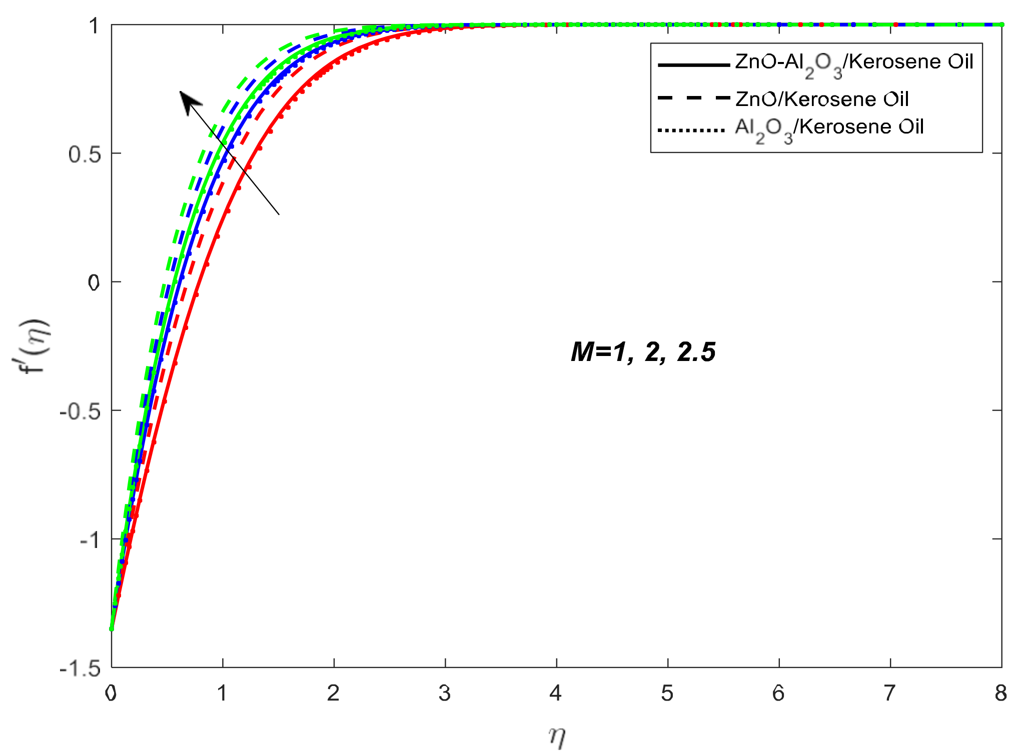

Fig. 3.2: Variation of velocity distribution $f'(\eta)$ for magnetic parameter M.

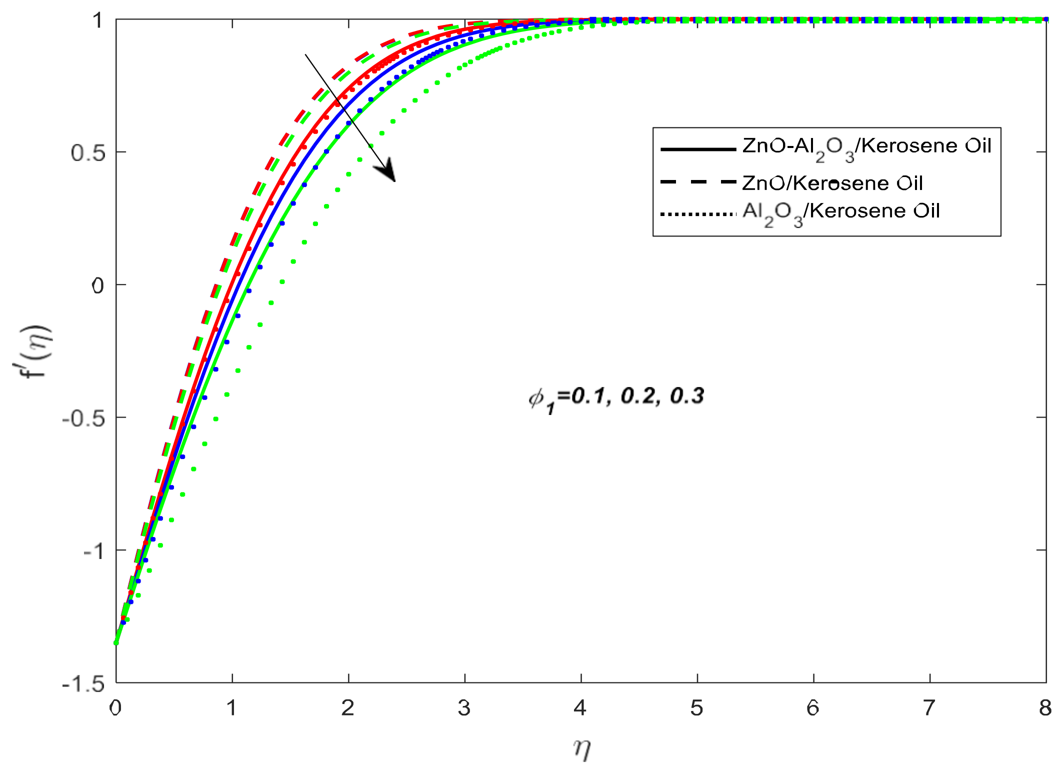

Fig. 3.3: Variation of velocity distribution $f'(\eta)$ for volumetric fraction ϕ_1.

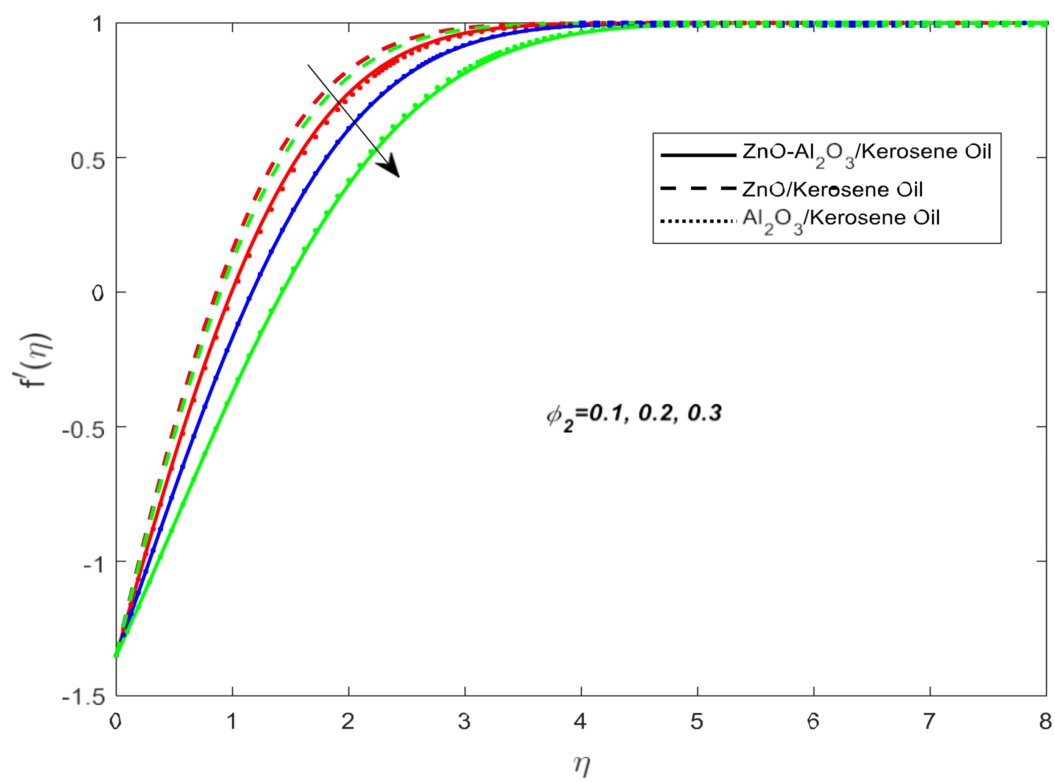

Fig. 3.4: Variation of velocity distribution $f'(\eta)$ for volumetric fraction ϕ_2.

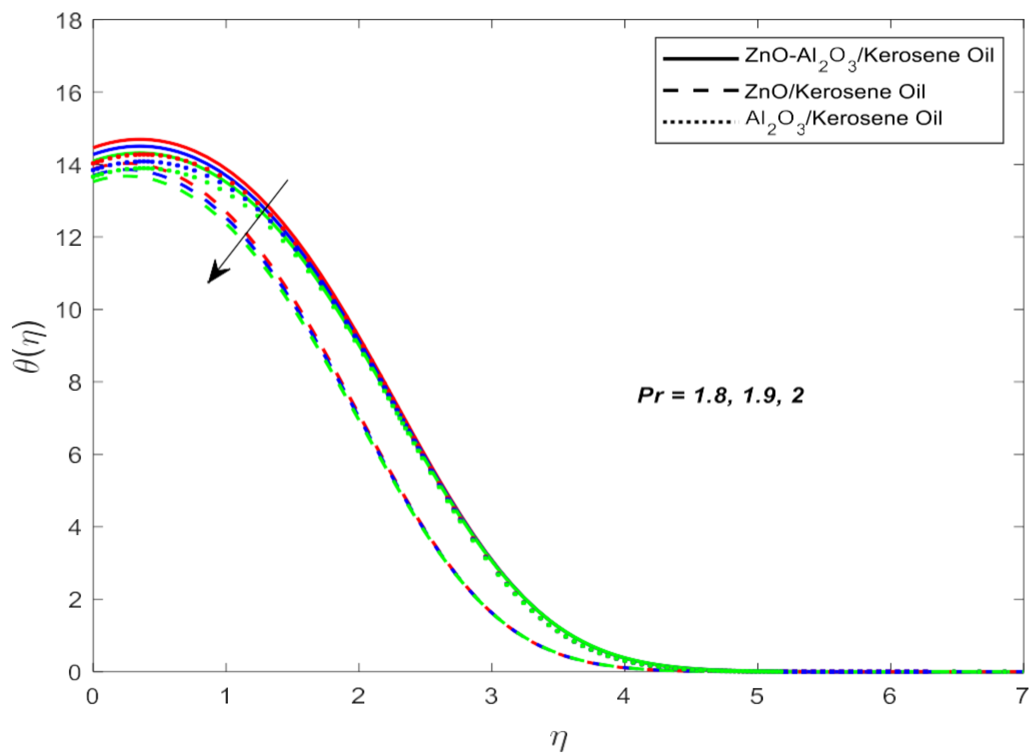

Fig. 3.5: Variation of temperature distribution $\theta(\eta)$ for Prandtl number Pr.

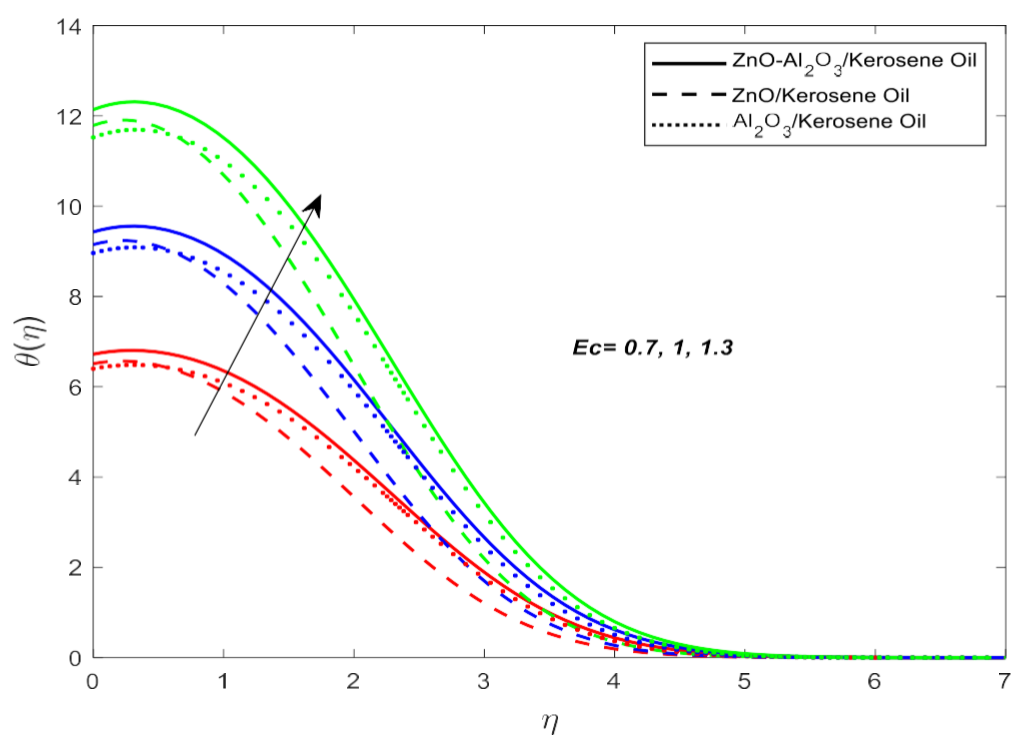

Fig. 3.6: Variation of temperature distribution $\theta(\eta)$ for Eckert number Ec.

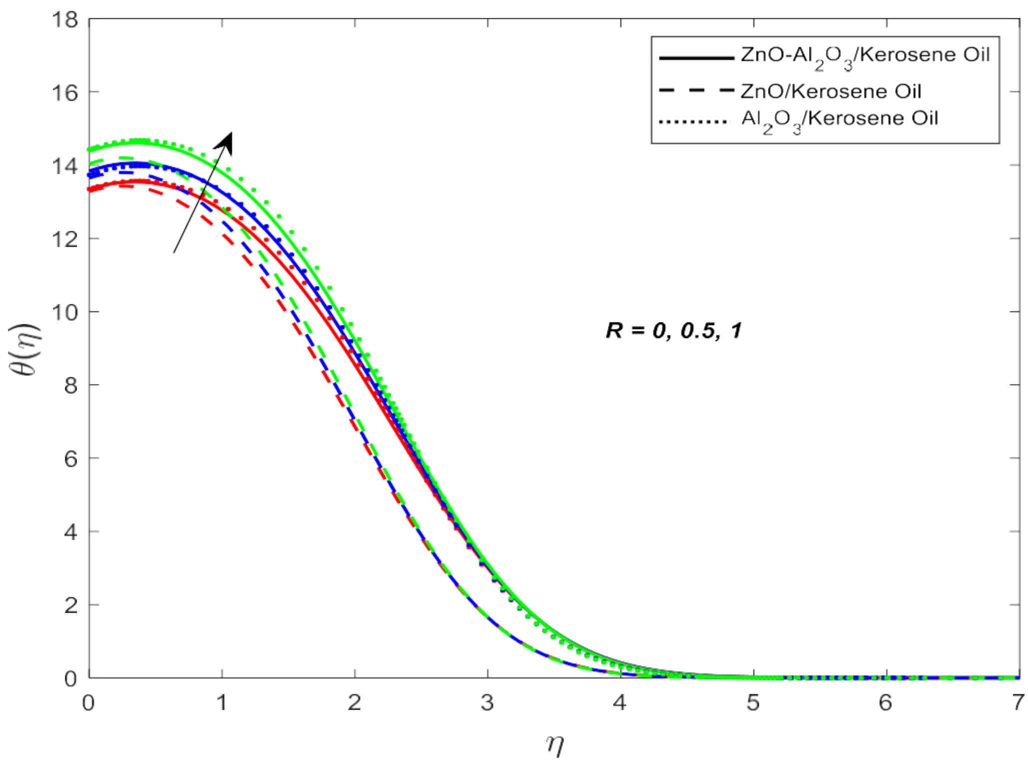

Fig. 3.7: Variation of temperature distribution $\theta(\eta)$ for radiation parameter R.

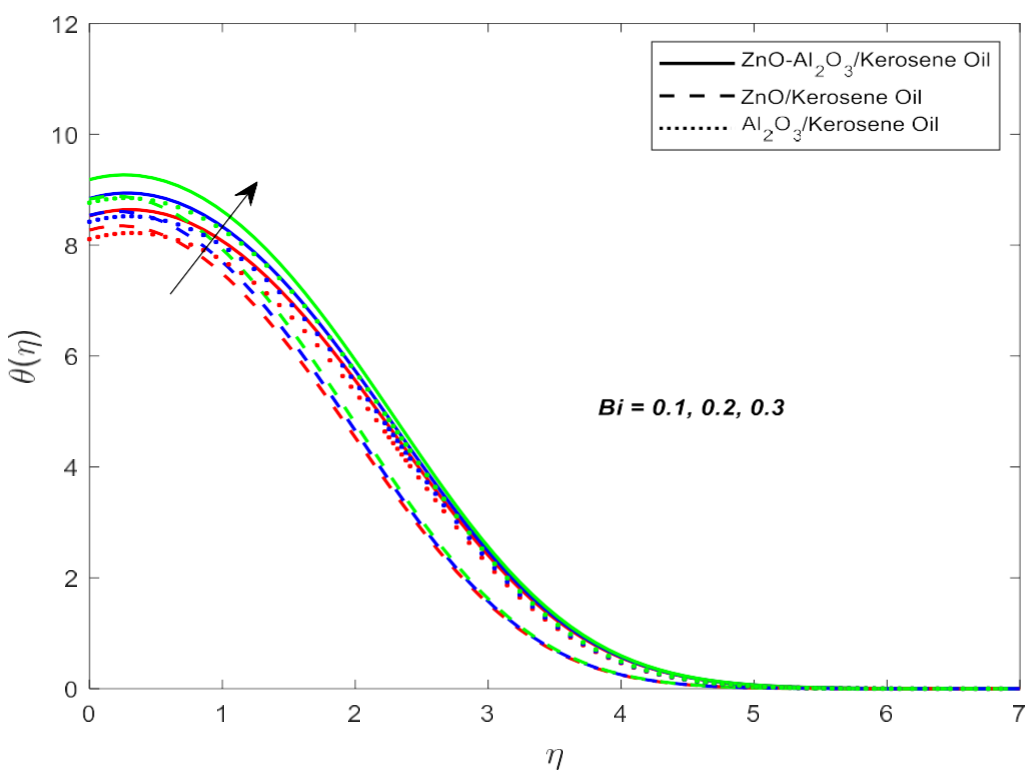

Fig. 3.8: Variation of temperature distribution $\theta(\eta)$ for Biot number Bi.

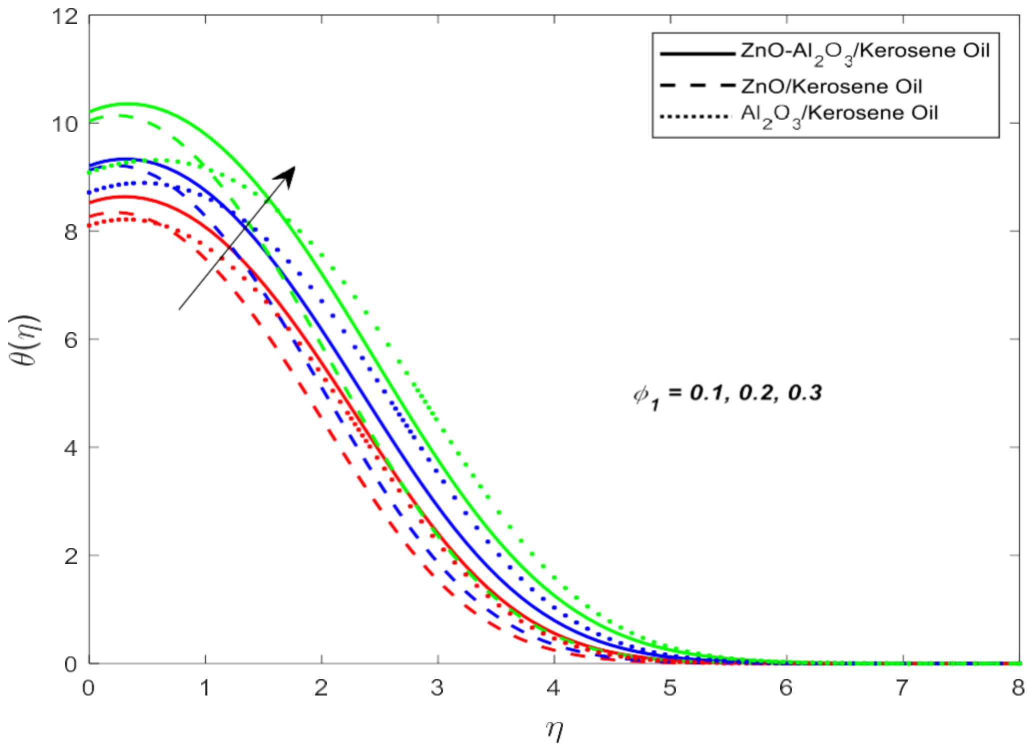

Fig. 3.9: Variation of temperature distribution $\theta(\eta)$ for volumetric fraction ϕ_1.

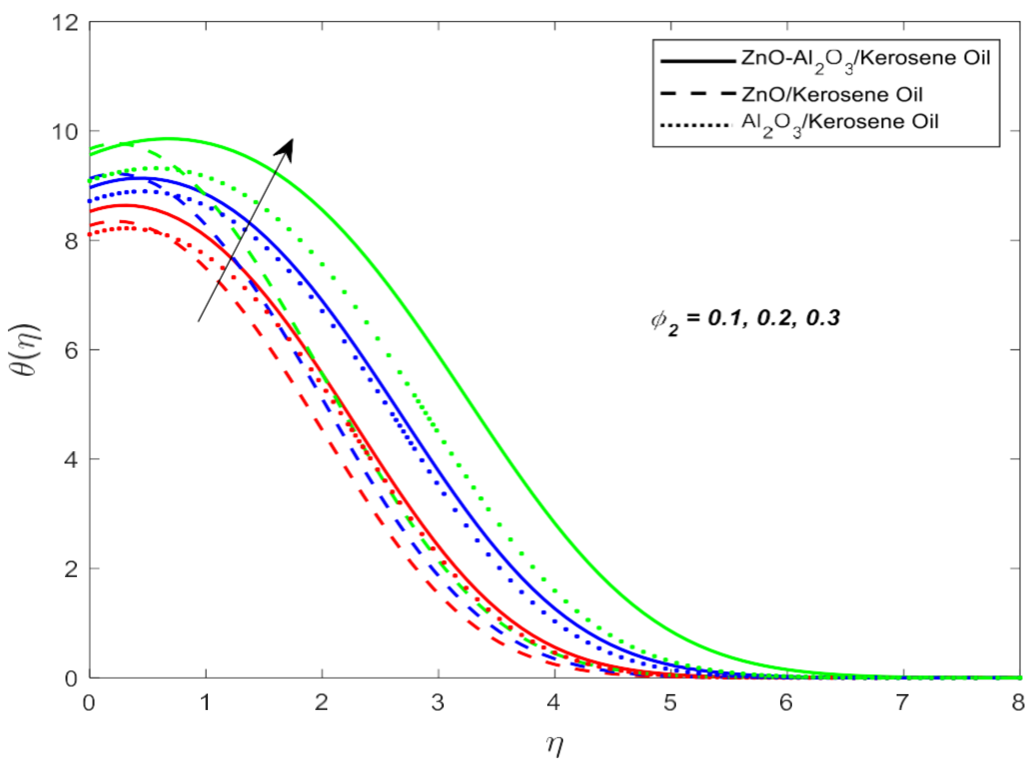

Fig. 3.10: Variation of temperature distribution $\theta(\eta)$ for volumetric fraction ϕ_2.

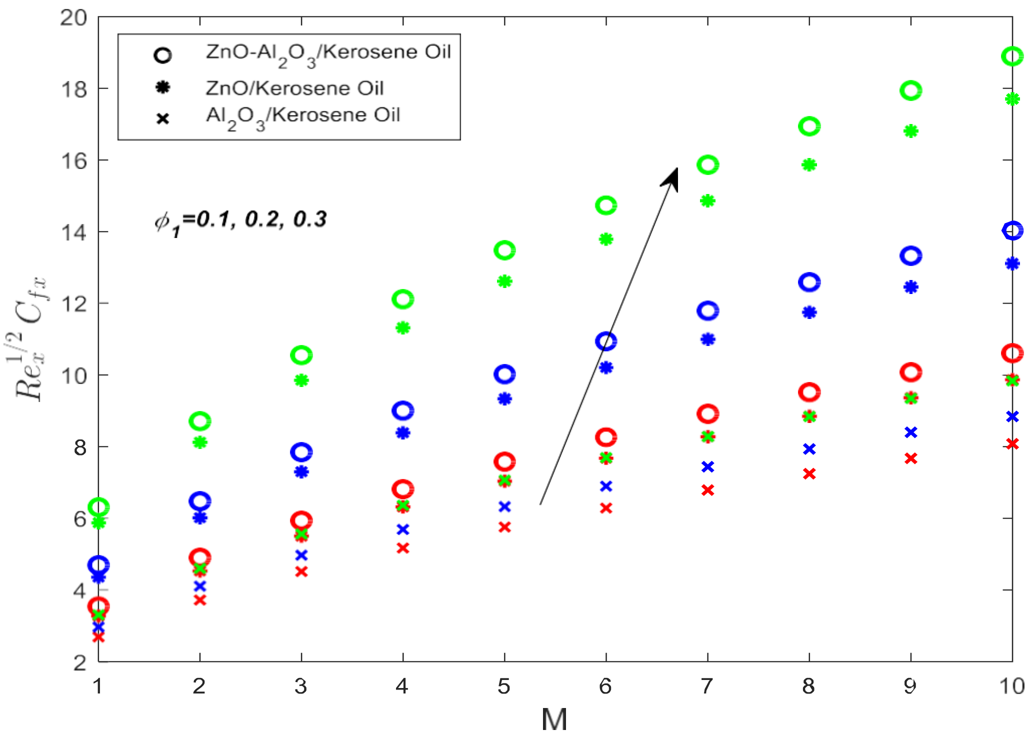

Fig. 3.11: Variation of Skin friction for M with ϕ_1.

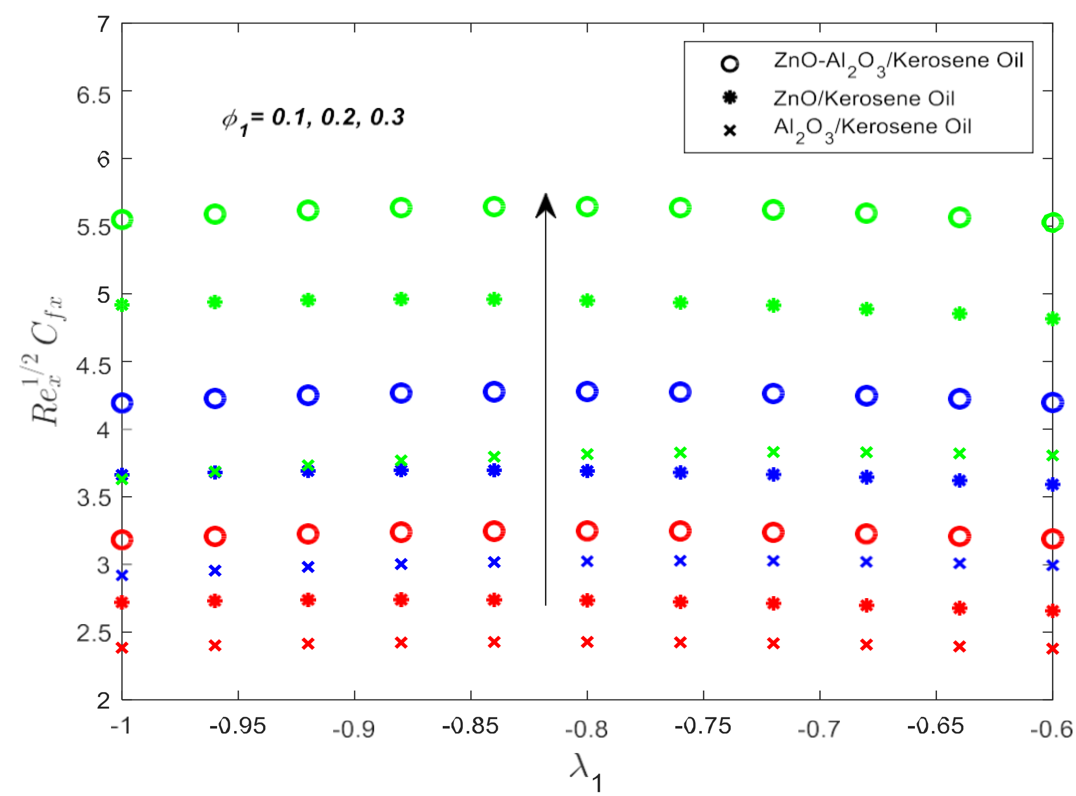

Fig. 3.12: Variation of Skin friction for λ_1 with ϕ_1.

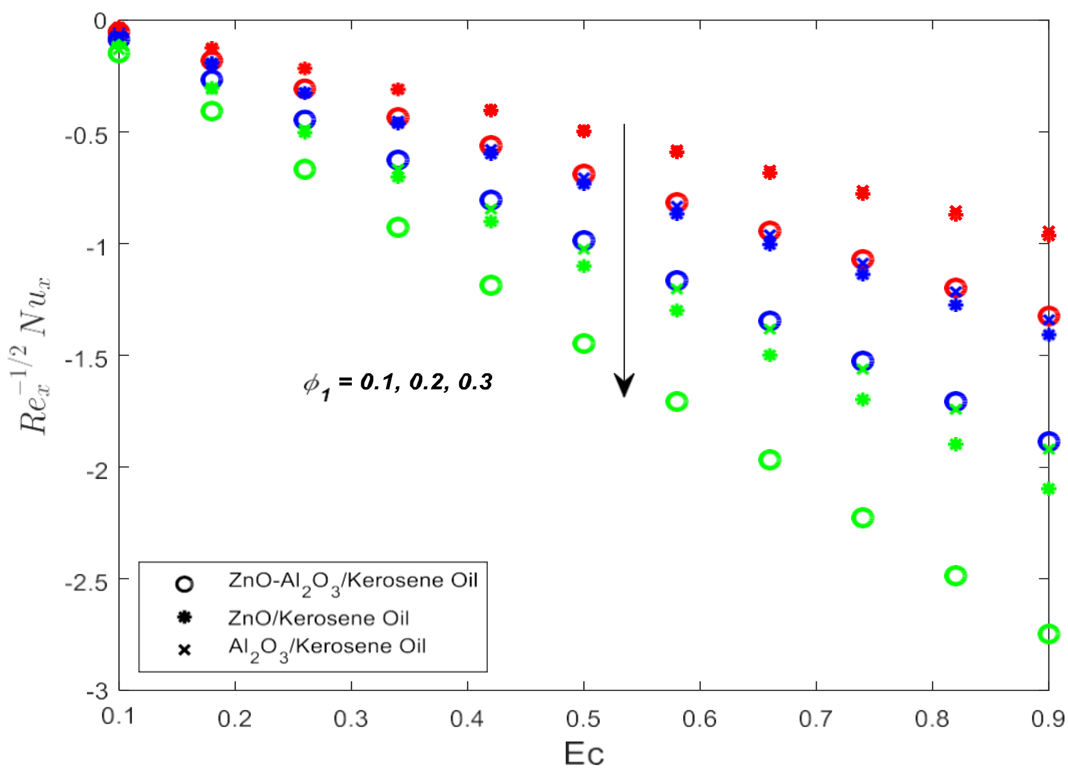

Fig. 3.13: Variation of Nusselt number for Ec with ϕ_1.

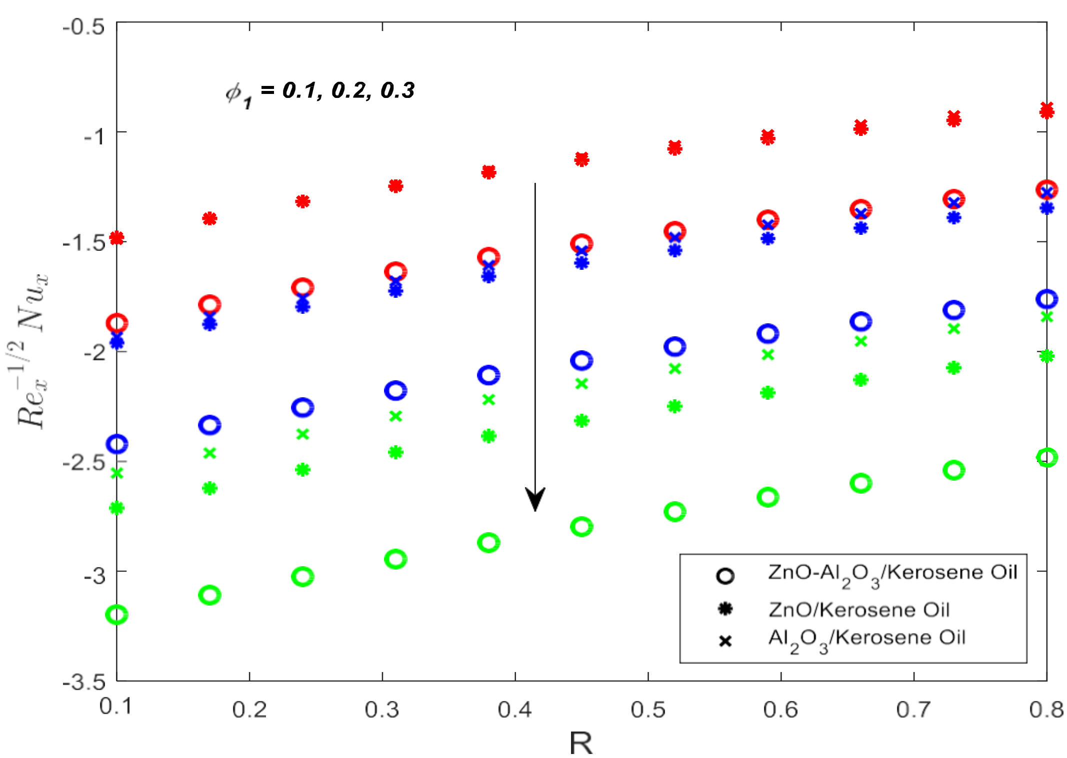

Fig. 3.14: Variation of Nusselt number for R with ϕ_1.

Table 3.4: Comparison of values of λ_1 on $f''(0)$ when $M = 0,\ Pr = 0,\ R = 0,\ Ec = 0,$ $Bi = \ 0,\ \phi_1 = 0,\ \phi_2 = 0.$

λ_1	Wang [89]	Rehman *et al.* [84]	Current results
	$f''(0)$	$f''(0)$	$f''(0)$
-1.15	1.08223	1.08220	1.08223
-1	1.32882	1.32880	1.32882
-0.75	1.48930	1.48930	1.48930
-0.5	1.49567	1.49567	1.49567
-0.25	1.40224	1.40224	1.40224
0	1.23258	1.23258	1.23258
0.5	0.71330	0.71330	0.71330
1	0	0	0

Table 3.5: Parametric values incorporated in the current analysis.

Parameters	**Values**	**References**
M	1, 2, 2.5	Saleem *et al.* [85]
Pr	1.8, 1.9, 2	Saleem *et al.* [85]
R	0, 0.5, 1	Saleem *et al.* [85]
Ec	0.7, 1, 1.3	Saleem *et al.* [85]
λ_1	-1.35	Saleem *et al.* [85]
Bi	0.1, 0.2, 0.3	Saleem *et al.* [85]
ϕ_1	0.1, 0.2, 0.3	Saleem *et al.* [85]
ϕ_2	0.1, 0.2, 0.3	Saleem *et al.* [85]

Chapter 4

Thermally Radiative and Magnetohydrodynamic Flow of Hybrid Nanofluid in the presence of Joule Heating

4.1 Introduction

The prime objective of this chapter is to investigate the behavior and nature of three different fluids ($ZnO -$ Kerosene Oil, $Al_2O_3 -$ Kerosene Oil and $ZnO - Al_2O_3 -$ Kerosene Oil) flowing past a shrinking surface in a porous medium. The flow is examined when the effect of Darcy Forchheimer is involved while the fluid flow is being directly impacted as the consequence of Joule heating, inclined magnetohydrodynamics and convective boundary conditions. Viscous dissipation, along with thermal radiation also significantly affect the flow. By means of certain adequate transformations, the governing mathematical equations are reconstructed into a nonlinear system of ODEs and are eventually solved via bvp4c, a tool of the MATLAB program, in order to obtain numerical outcomes. The temperature and velocity profiles, in addition to the Nusselt number and skin friction are analyzed graphically. In order to validate the present findings, a comparative investigation with the available literature has also been performed.

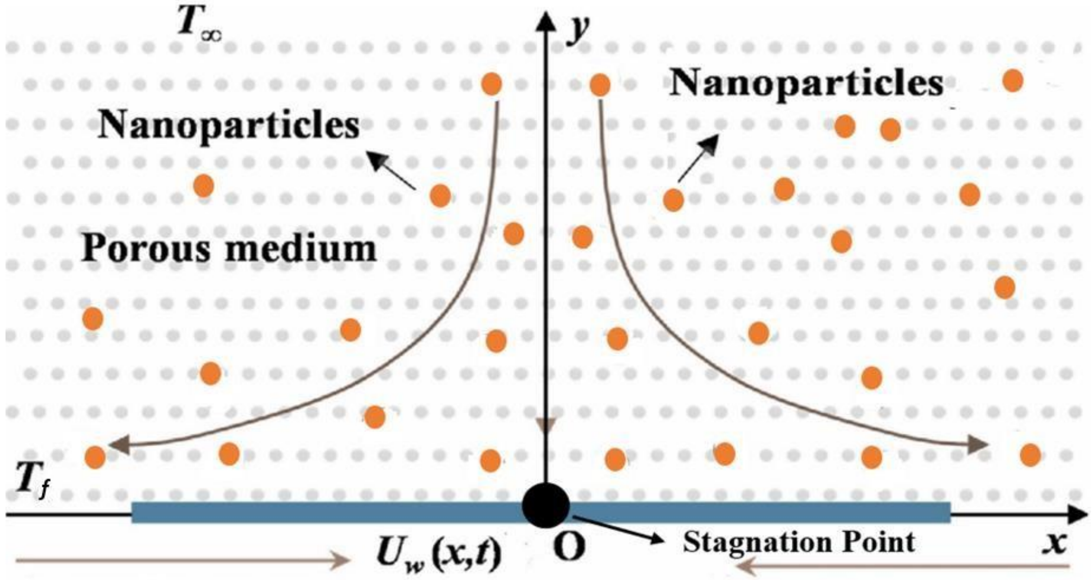

Fig. 4.1: Flow Configuration Model.

4.2 Mathematical Formulation of the Problem

The model under consideration is based on the steady, 2-D flow of two distinct nanofluids and a hybrid nanofluid, with kerosene oil taken to be the basefluid and the nanoparticles considered to be ZnO and Al_2O_3. The fluid flows over a shrinking sheet dispersed in a porous medium. The vertical axis is subject to an induced inclined magnetic field $\mathbf{B} = (0, B_o, 0)$**.** The additional factors of Joule heating, thermal radiation, viscous dissipation along with the implications of Darcy Forchheimer are also employed. The linear shrinking is described by $u_w = ax$. The wall temperature T_f is less than T_∞, the temperature of free stream. The free stream velocity is given by $u_e = bx$, where b indicates the stagnation point intensity. The equations governing the fluid flow are acquired with the enforcement of specific boundary layer theory approximations and are stated as

$$\frac{\partial u}{\partial x} + \frac{\partial v}{\partial y} = 0, \tag{4.1}$$

$$u\frac{\partial u}{\partial x}+v\frac{\partial u}{\partial y}=u_e\frac{\partial u_e}{\partial x}+\frac{\mu_{hnf}}{\rho_{hnf}}\frac{\partial^2 u}{\partial y^2}-\frac{\sigma_{hnf}}{\rho_{hnf}}B_o^2(sin\alpha)^2(u-u_e)+\mathcal{F}(u_e^2-u^2)-\frac{\mu_{hnf}}{\rho_{hnf}K_o^*}(u-u_e), \tag{4.2}$$

$$u\frac{\partial T}{\partial x}+v\frac{\partial T}{\partial y}=\frac{k_{hnf}}{(\rho c_p)_{hnf}}\frac{\partial^2 T}{\partial y^2}-\frac{1}{(\rho C_p)_{hnf}}\frac{\partial q_r}{\partial y}+\frac{\sigma_{hnf}}{(\rho C_p)_{hnf}}B_o^2(u-u_e)^2+\frac{\mu_{hnf}}{(\rho C_p)_{hnf}}\left(\frac{\partial u}{\partial y}\right)^2. \tag{4.3}$$

The system is being monitored with the help of the following boundary conditions:

$$u=u_w=ax, v=0, -k_{hnf}\left(\frac{\partial T}{\partial y}\right)=h(T_f-T), \text{when } y=0, \tag{4.4}$$

$$u\to u_e=bx,\ v\to 0,\ T\to T_\infty,\ \text{when } y\to\infty, \tag{4.5}$$

where u and v denote the horizontal and vertical components of velocity, a and b are considered to be arbitrary constants, u_w and u_e are the velocity elements at the wall and free stream, while T_f and T_∞ provide the wall and ambient temperature respectively. Furthermore, in Eq. (4.3), the thermal radiation throughout the surface is demonstrated as $\frac{\partial q_r}{\partial y}$ and has an approximated value to be [86]

$$q_r=-\frac{4}{3}\frac{\sigma^*}{k^*}\frac{\partial T^4}{\partial y}, \tag{4.6}$$

Here, the Stefan Boltzmann constant is σ^* and k^* nominates the mean absorption coefficient. When the Taylor's expansion of T^4 is implemented around T_∞, the following form is acquired

$$T^4\approx 4T_\infty{}^3T-3T_\infty{}^4, \tag{4.7}$$

which generates

$$\frac{\partial T^4}{\partial y}=4\frac{\partial T}{\partial y}T_\infty{}^3. \tag{4.8}$$

and therefore, Eq. (4.6) becomes

$$q_r=-\frac{16}{3}\frac{\sigma^*T_\infty^3}{k^*}\frac{\partial T}{\partial y}. \tag{4.9}$$

After substituting Eq. (4.6) in (4.3), it leads to the following equation

$$u\frac{\partial T}{\partial x}+v\frac{\partial T}{\partial y}=\frac{k_{hnf}}{(C_p\rho)_{hnf}}\frac{\partial^2 T}{\partial y^2}+\frac{1}{(C_p\rho)_{hnf}}\left(\frac{16\sigma^*T_\infty^3}{3k^*}\frac{\partial^2 T}{\partial y^2}\right)+\frac{\sigma_{hnf}}{(C_p\rho)_{hnf}}B_o^2(u-u_e)^2+\frac{\mu_{hnf}}{(C_p\rho)_{hnf}}\left(\frac{\partial u}{\partial y}\right)^2. \tag{4.10}$$

The following transformations have been selected for the current model [85]

$$\eta = \left(\frac{\rho_f b}{\mu_f}\right)^{\frac{1}{2}} y, \quad \theta(\eta) = \frac{T - T_\infty}{T_f - T_\infty}, \tag{4.11}$$

$$u = f'(\eta) bx, \quad v = -\left(\frac{\mu_f b}{\rho_f}\right)^{\frac{1}{2}} f(\eta). \tag{4.12}$$

Table 4.1: Thermo-physical attributes of Kerosene Oil, Zinc Oxide and Alumina. [84], [85], [87]

Characteristics	**Kerosene Oil**	ZnO	Al_2O_3
$\rho(kg/m^3)$	783	5700	3970
$k(W/mK)$	0.15	25	40
$\sigma((\Omega m))^{-1}$	0.0000000006	9.999	0.0000000001
$C_p(J/kgK)$	2090	523	765

Table 4.2: Thermo-physical attributes under consideration for nanofluids [84], [85], [87].

Characteristics	Nanofluid
Electrical Conductivity (σ)	$\frac{\sigma_{nf}}{\sigma_f} = \frac{\sigma_{s1} - 2\phi_{s1}(\sigma_f - \sigma_{s1}) + 2\sigma_f}{\sigma_{s1} + \phi_{s1}(\sigma_f - \sigma_{s1}) + 2\sigma_f}$
Dynamic Viscosity (μ)	$\frac{\mu_{nf}}{\mu_f} = \frac{1}{(1-\phi_{s1})^{2.5}}$
Specific Heat Capacity (C_p)	$(\rho C_p)_{nf} = (1-\phi_{s1})(\rho C_p)_f + \phi_{s1}(\rho C_p)_{s1}$
Density (ρ)	$\rho_{nf} = (1-\phi_{s1})\rho_f + \phi_{s1}\rho_{s1}$
Thermal Conductivity (k)	$\frac{k_{nf}}{k_f} = \frac{k_{s1} - 2\phi_{s1}(k_f - k_{s1}) + 2k_f}{k_{s1} - \phi_{s1}(k_f - k_{s1}) + 2k_f}$

Table 4.3: Thermo-physical attributes of hybrid nanofluid ($ZnO - Al_2O_3$/Kerosene Oil) [83], [84], [87].

Characteristics	Hybrid Nanofluid
Electrical Conductivity (σ)	$\frac{\sigma_{hnf}}{\sigma_f} = [\frac{\sigma_{s2} - 2\phi_{s2}(\sigma_{nf} - \sigma_{s2}) + 2\sigma_{nf}}{\sigma_{s2} + \phi_{s2}(\sigma_{nf} - \sigma_{s2}) + 2\sigma_{nf}}] \times [\frac{\sigma_{s1} - 2\phi_{s1}(\sigma_f - \sigma_{s1}) + 2\sigma_f}{\sigma_{s1} + \phi_{s1}(\sigma_f - \sigma_{s1}) + 2\sigma_f}]$
Dynamic Viscosity (μ)	$\frac{\mu_{hnf}}{\mu_f} = \frac{1}{(1-\phi_1)^{2.5}(1-\phi_2)^{2.5}}$
Specific Heat Capacity (C_p)	$\frac{(\rho C_P)_{hnf}}{(\rho C_P)_f} = \frac{(\rho C_P)_{s2}\,\phi_{s2}}{(\rho C_P)_f} + [\frac{(\rho C_P)_{s1}\,\phi_{s1}}{(\rho C_P)_f} + (1-\phi_{s1})](1-\phi_{s2})$
Density (ρ)	$\frac{\rho_{hnf}}{\rho_f} = \frac{\rho_{s2}\phi_{s2}}{\rho_f} + [\frac{\rho_{s1}\phi_{s1}}{\rho_f} + (1-\phi_{s1})](1-\phi_{s2})$
Thermal conductivity (k)	$\frac{k_{hnf}}{k_f} = [\frac{k_{s2}-2\phi_{s2}(k_{nf}-k_{s2})+2k_{nf}}{k_{s2}+\phi_{s2}(k_{nf}-k_{s2})+2k_{nf}}] \times [\frac{k_{s1}-2\phi_{s1}(k_f-k_{s1})+2k_f}{k_{s1}+\phi_{s1}(k_f-k_{s1})+2k_f}]$

The crucial parameters of Nusselt number and coefficient of surface friction are clarified as

$$C_f = \frac{\tau_w}{\rho_f\, u_e^2},\quad Nu_x = -\frac{x q_w}{k_f\,(T_f - T_\infty)}, \tag{4.13}$$

where the shear stress at the surface and the heat transfer rate is demonstrated as

$$\tau_w = \left(\frac{\partial u}{\partial y}\right)_{y=0} \mu_{hnf}, \tag{4.14}$$

$$q_w = -\left(\frac{\partial T}{\partial y}\right)_{y=0} k_{hnf}. \tag{4.15}$$

when the chosen transformation variables (4.11) – (4.12) are utilized, Eq. (4.1) is promptly satisfied and as a result, Eqs. (4.2) – (4.5) are transformed to the form

$$f(\eta)f''(\eta) - f'^2(\eta) + 1 + \frac{\frac{\mu_{hnf}}{\mu_f}}{\frac{\rho_{hnf}}{\rho_f}} f'''(\eta) + M\frac{\frac{\sigma_{hnf}}{\sigma_f}}{\frac{\rho_{hnf}}{\rho_f}}(sin\alpha)^2(1 - f'(\eta))$$
$$+Fr[1 - f'^2(\eta)] - \frac{\frac{\mu_{hnf}}{\mu_f}}{\frac{\rho_{hnf}}{\rho_f}}\omega_o[f'(\eta) - 1] = 0\,, \tag{4.16}$$

$$\frac{1}{\frac{(\rho C_p)_{hnf}}{(\rho C_p)_f}}\frac{1}{Pr}\left(\frac{k_{hnf}}{k_f}+\frac{4}{3}R\right)\theta''(\eta)+\frac{\frac{\mu_{hnf}}{\mu_f}}{\frac{(\rho C_p)_{hnf}}{(\rho C_p)_f}}Ecf''^2(\eta)+f(\eta)\theta'(\eta)+$$

$$\frac{\frac{\sigma_{hnf}}{\sigma_f}}{\frac{(\rho C_p)_{hnf}}{(\rho C_p)_f}}MEc[f'(\eta)-1]^2=0, \tag{4.17}$$

and the boundary conditions are

$$f(0)=0,\quad \theta'(0)=-Bi(1-\theta(0)),\quad f'(0)=\lambda_1, \text{when } \eta=0, \tag{4.18}$$

$$\theta(\infty)\to 0,\quad f'(\infty)\to 1,\quad \text{when } \eta\to\infty. \tag{4.19}$$

Eqs. (4.16) – (4.19) include substantial dimensionless quantities such as magnetic parameter, porosity parameter, thermal radiation parameter, velocity ratio parameter, Eckert number, Prandtl number and Forchheimer parameter, which possess the following mathematical forms:

$$M=\frac{B_o^2\sigma_f}{\rho_f b},\ \omega_o=\frac{v_f}{K_o^* b},\ R=\frac{4T_\infty^3\sigma_1}{3k_1k_f},\ \lambda_1=\frac{a}{b}, \tag{4.20}$$

$$Ec=\frac{(bx)^2}{(T_f-T_\infty)(C_p)_f},\ Pr=\frac{(C_p)_f\mu_f}{k_f},\ Fr=\frac{C_b}{\sqrt{K}}. \tag{4.21}$$

Also, Eq. (4.13) can be simplified in the form

$$C_f(Re)^{\frac{1}{2}}=\frac{\mu_{hnf}}{\mu_f}f''(0),\ Nu_x(Re)^{-\frac{1}{2}}=-\frac{k_{hnf}}{k_f}\theta'(0). \tag{4.22}$$

The expressions can be easier to understand with the aid of the following ratios.

$$A=\frac{\mu_{hnf}}{\mu_f},\quad B=\frac{\rho_{hnf}}{\rho_f},\quad C=\frac{(\rho C_p)_{hnf}}{(\rho C_p)_f}, \tag{4.23}$$

$$S=\frac{\sigma_{hnf}}{\sigma_f},\quad K=\frac{k_{hnf}}{k_f}. \tag{4.24}$$

Finally, Eqs. (4.16), (4.17) and (4.22) can now be expressed as,

$$f(\eta)f''(\eta)-f'^2(\eta)+1+\frac{A}{B}f'''(\eta)+M\frac{S}{B}(sin\alpha)^2(1-f'(\eta))+$$
$$Fr[1-f'^2(\eta)]-\frac{A}{B}\omega_o[f'(\eta)-1]=0, \tag{4.25}$$

$$\frac{1}{Pr}\cdot\frac{1}{C}(K+\frac{4}{3}R)\,\theta''(\eta)+\frac{A}{C}Ecf''^2(\eta)+f(\eta)\theta'(\eta)+\frac{S}{C}MEc$$
$$[f'(\eta)-1]^2=0, \tag{4.26}$$

$$(Re)^{\frac{1}{2}}C_f = Af''(0), \quad (Re)^{-\frac{1}{2}}Nu_x = -K\theta'(0). \tag{4.27}$$

4.3 Numerical Stratagem

The flow model, typically, consists of nonlinear differential equations, which are coupled as well and are somewhat complicated to reduce. The numerical findings can be yielded by first acquiring a system of ODEs retaining first order and then the bvp4c technique further solves the system.

$$y(1) = f, \tag{4.28}$$

$$y(2) = f', \tag{4.29}$$

$$y(3) = f'', \tag{4.30}$$

$$y(4) = \theta, \tag{4.31}$$

$$y(5) = \theta', \tag{4.32}$$

$$\begin{aligned} y'(3) = {} & [\{y(2)\}^2 - y(1)y(3) - 1 - M\frac{S}{B}(sin\alpha)^2\{(1 - y(2))\} \\ & -Fr(1 - \{y(2)\}^2) + \frac{A}{B}\omega_o\{y(2)\}]\left(\frac{B}{A}\right), \end{aligned} \tag{4.33}$$

$$y'(5) = [-y(1)y(5) - \frac{A}{C}Ec\{y(3)\}^2 + \frac{S}{C}MEc\{y(2) - 1\}^2]PrC\left(\frac{1}{K + \frac{4}{3}R}\right). \tag{4.34}$$

$$y_0(1) = 0, \quad y_0(2) = \lambda_1, \quad y_0(5) = -Bi(1 - y_0(4)) \tag{4.35}$$

$$y_\infty(2) \to 1, \quad y_\infty(4) \to 0. \tag{4.36}$$

4.4 Graphical Analysis and Discussion

This section involves the graphical conduct of a number of factors included in the study, on the profiles of temperature and velocity. Additionally, the performance of key variables is also highlighted for the Nusselt number and skin friction coefficient. The parameters affecting the velocity profile consist of the concentration of ZnO nanoparticles (ϕ_1), concentration of Al_2O_3 nanoparticles (ϕ_2), magnetic parameter (M), parameter of porosity (ω_o), inclination angle (α) and the Forchheimer parameter (Fr) respectively. Figures 4.2-4.7 illustrate the results of these variables. Figure 4.2 along with Figure 4.3 display the decreasing trend of velocity profile for the two nanofluids and the hybrid nanofluid when the volumetric concentrations ϕ_1 and ϕ_2 are increased. The kerosene-based fluids experience a greater level of viscosity and density for increased nanoparticles volumetric concentration and hence the velocity level falls. Figure 4.4 shows that as the parameter of magnetism surges, the three different fluids exhibit an elevated velocity profile. This occurs as the magnetic damping is dominated by the momentum transfer from the surface and resulting, dominating the Lorentz force. Figure 4.5 displays that an amplification in porosity parameter triggers a decline in the velocity for the fluids, owing to the fact that velocity and porosity have an inverse relation. Figure 4.6 reflects that a loss in the velocity profile is observed for an in increase in the inclination angle (α). The flow is usually facilitated by wall movement. For an inclined surface, the component of shrinking force declines with gravity, lessening the fluid inertia and lowering the velocity. The amplification of the Forchheimer number (Fr) on the velocity profile is emphasized in Figure 4.7. In a porous medium, the nonlinear resistance to flow becomes dominant with bigger values of Fr. This number minimizes the three fluids' velocity, optimizing the permeability and suppressing the porous drag force. Figures 4.8 to 4.14 portray the temperature distribution when the parameters of Pr, Ec, R, Bi, ϕ_1, ϕ_2 and M are at work. The behaviour of temperature distribution for varied Prandtl number (Pr) is depicted in Figure 4.8. With the increase in the magnitude of Pr, the temperature profile lessens for the two nanofluids as well as for the hybrid nanofluid, caused by the dominant thermal boundary layer. In accordance to higher quantities of Eckert number (Ec), the overall temperature also experiences an increment as depicted in Figure 4.9. This is due to the heat production in the medium caused by enhanced friction in the three fluids, yielding consistent particle collisions, all as a consequence of the boosted Ec. Figure 4.10 illustrates that the temperature for the three fluids ascends for the rise in the radiation parameter (R). As R increases, the transfer of energy is extremely affected by the thermal radiation contribution, which causes the fluid to absorb more heat and so the thermal boundary layer also grows. Figure 4.11 demonstrates that when the Biot number (Bi) is raised, the nanofluids witness an upraised profile of temperature. The same demeanor is noted for the kerosene-based hybrid nanofluid. Enhancement in Bi suggests higher convective heat transmission at the surface, ultimately rising the temperature. Figure 4.12 as well as Figure 4.13 describe the boosted temperature distribution against the volume fractions ϕ_1 and ϕ_2 for the fluids. The rise in ϕ_1 and ϕ_2 will also strengthen the thermal boundary layer and its thickness, resulting in a high temperature. Figure 4.14 exemplifies the energy transport for the fluids when the parameter of magnetism (M) is under consideration. The temperature gradient is uplifted by amplified magnetic strength. Figures 4.15-4.18 highlight the influence of crucial variables for Fr, M, ω_o and α on skin friction with the deviations in ϕ_1. Figure 4.15 reflects the effect of the Forchheimer constant (Fr) on the skin friction coefficient for the varied values of ϕ_1. It is found that when Fr ascends, the surface friction drag for the fluids involved also rapidly grows, on account of intensified force of inertial drag. Figure 4.16 shows an uplifted pattern of the skin friction coefficient for the three fluids when the magnetic parameter (M) is extended in addition to ϕ_1. Figure 4.17 indicates the performance of the porosity parameter (ω_o) for diverse values of ϕ_1, implying that the skin friction coefficient undergoes an increment for enhancement in ω_o and ϕ_1. Figure 4.18 clarifies an enhanced pattern of the skin friction term for the inclination angle α in terms of uplifted ϕ_1. Figures 4.19, 4.20, 4.21 and 4.22 clarify the interaction of R, M, Pr and Ec with the Nusselt number in compliance with ϕ_1. Figure 4.19 demonstrates that with increasing values of ϕ_1, the heat transfer coefficient gets diminished when being dealt against the parameter of radiation (R). The Nusselt number declines for the fluids when variations of ϕ_1 with magnetic parameter (M) are being scrutinized in Figure 4.20. The same conduct is perceived for the association of the Prandtl number (Pr) in Figure 4.21 when the Nusselt number is of consideration. Figure 4.22 elaborates the decline of the Nusselt number when Eckert number (Ec) is being estimated with boosted values of ϕ_1.

Table 4.1- 4.3 give the details of the necessary data required to perform the current analysis. This data includes the properties of the two different nanofluids and the hybrid nanofluid. Table 4.4 is the comparative study of the research work with existing literature available in the related studies. The comparison points out good out the validity of the results. The suitable ranges of the dimensionless parameters taken in the study in illustrated in Table 3.5.

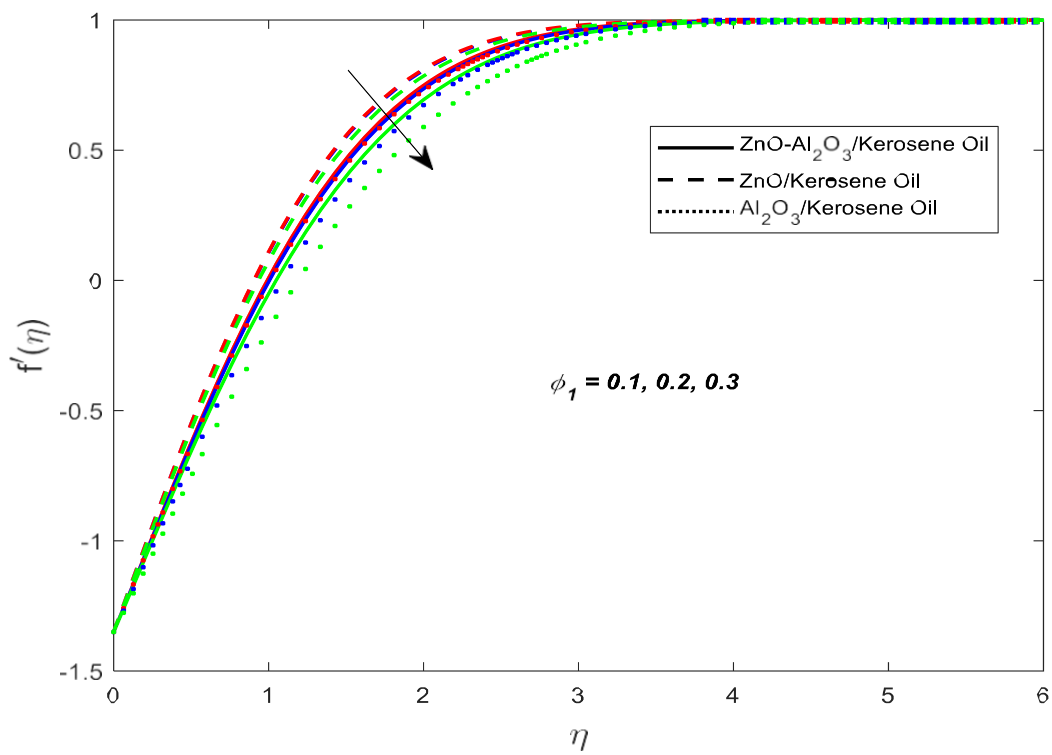

Fig. 4.2: Variation of velocity distribution $f'(\eta)$ for volumetric fraction ϕ_1.

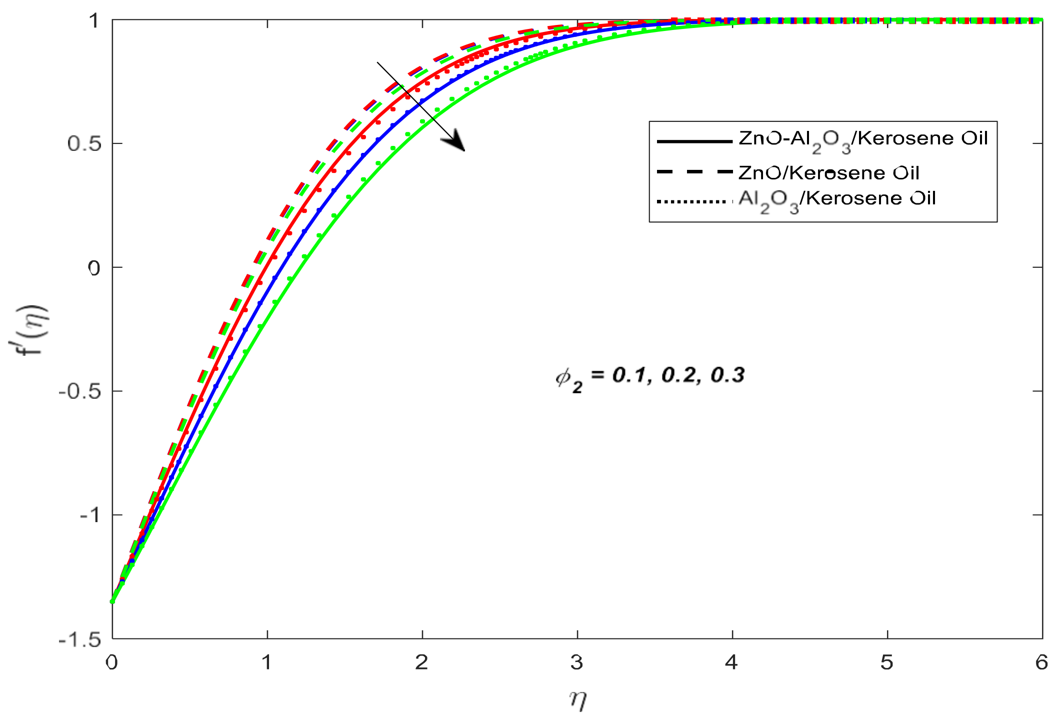

Fig. 4.3: Variation of velocity distribution $f'(\eta)$ for volumetric fraction ϕ_2.

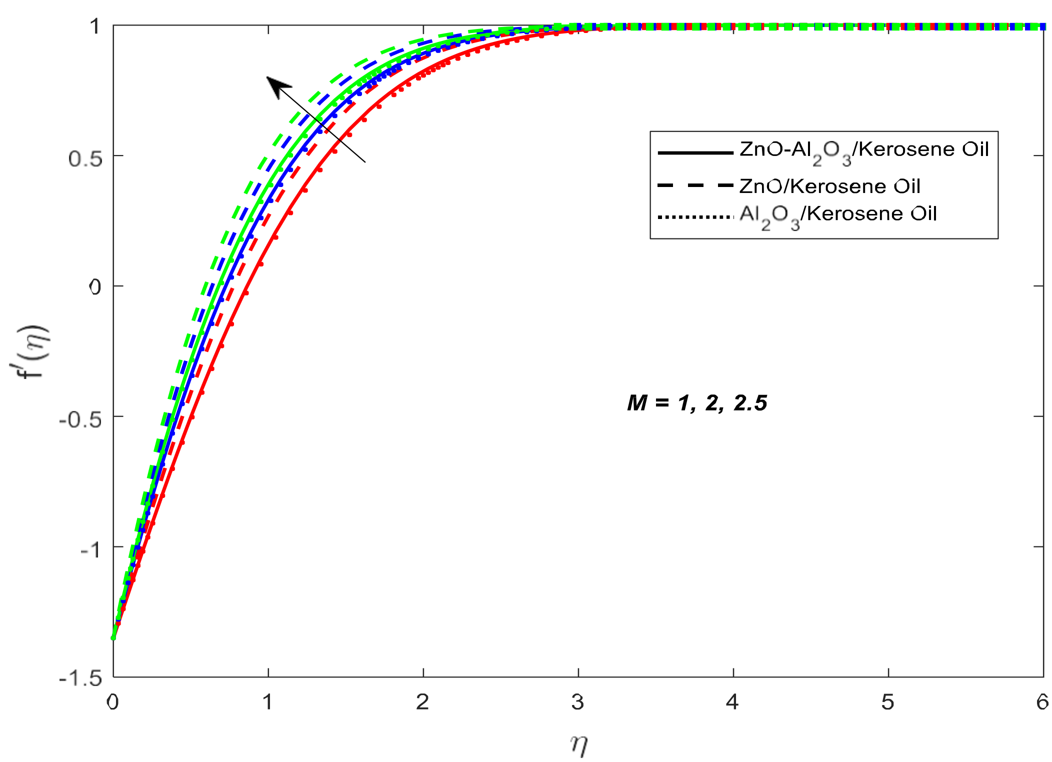

Fig. 4.4: Variation of velocity distribution $f'(\eta)$ for magnetic parameter M.

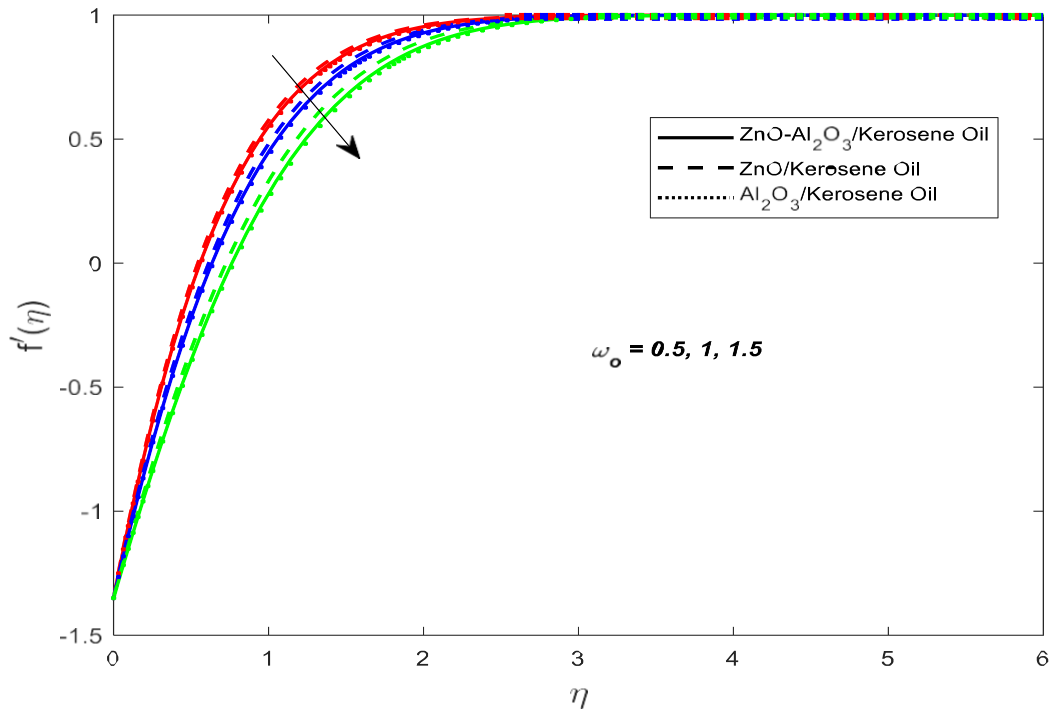

Fig. 4.5: Variation of velocity distribution $f'(\eta)$ for porosity parameter ω_o.

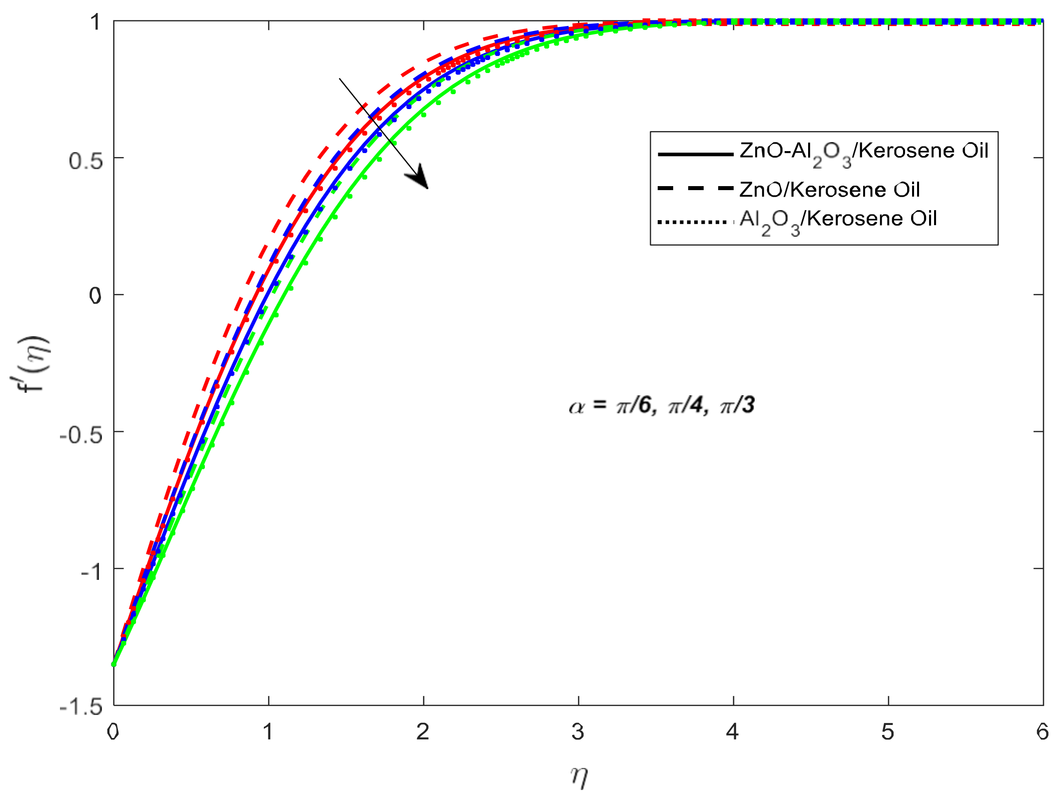

Fig. 4.6: Variation of velocity distribution $f'(\eta)$ for angle of inclination α.

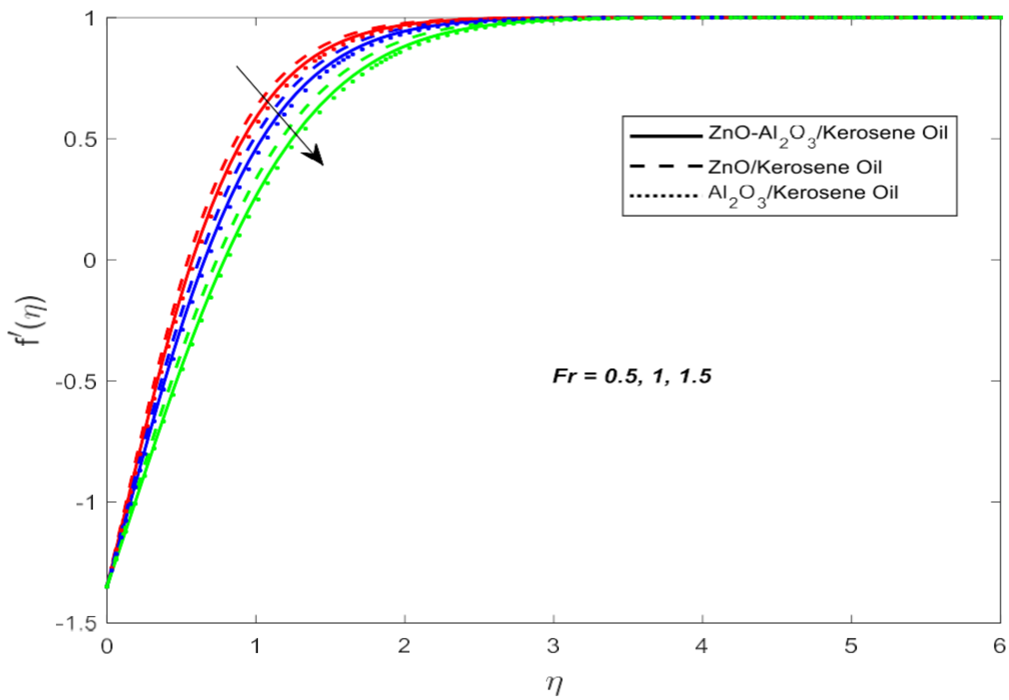

Fig. 4.7: Variation of velocity distribution $f'(\eta)$ for Forchheimer number Fr.

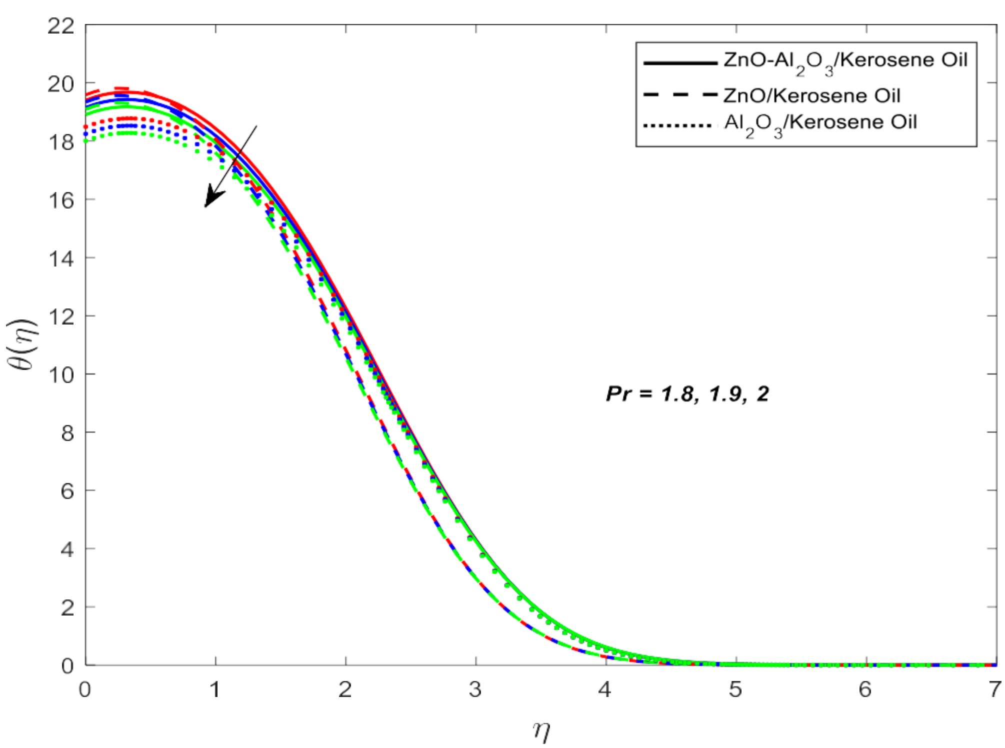

Fig. 4.8: Variation of temperature distribution $\theta(\eta)$ for Prandtl number Pr.

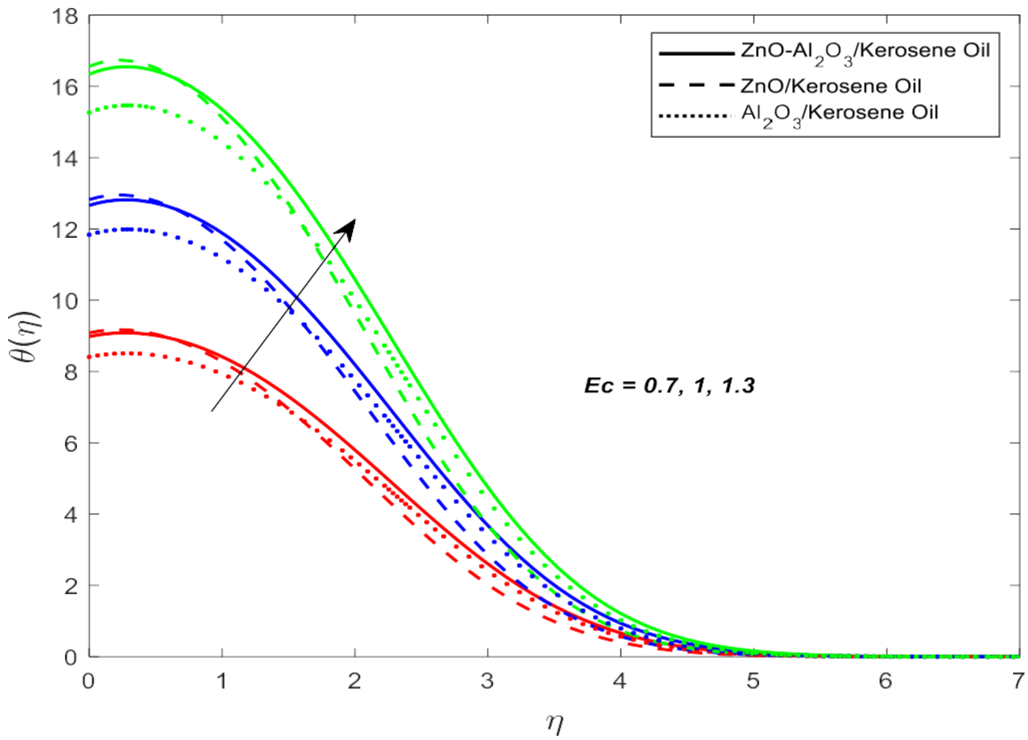

Fig. 4.9: Variation of temperature distribution $\theta(\eta)$ for Eckert number Ec.

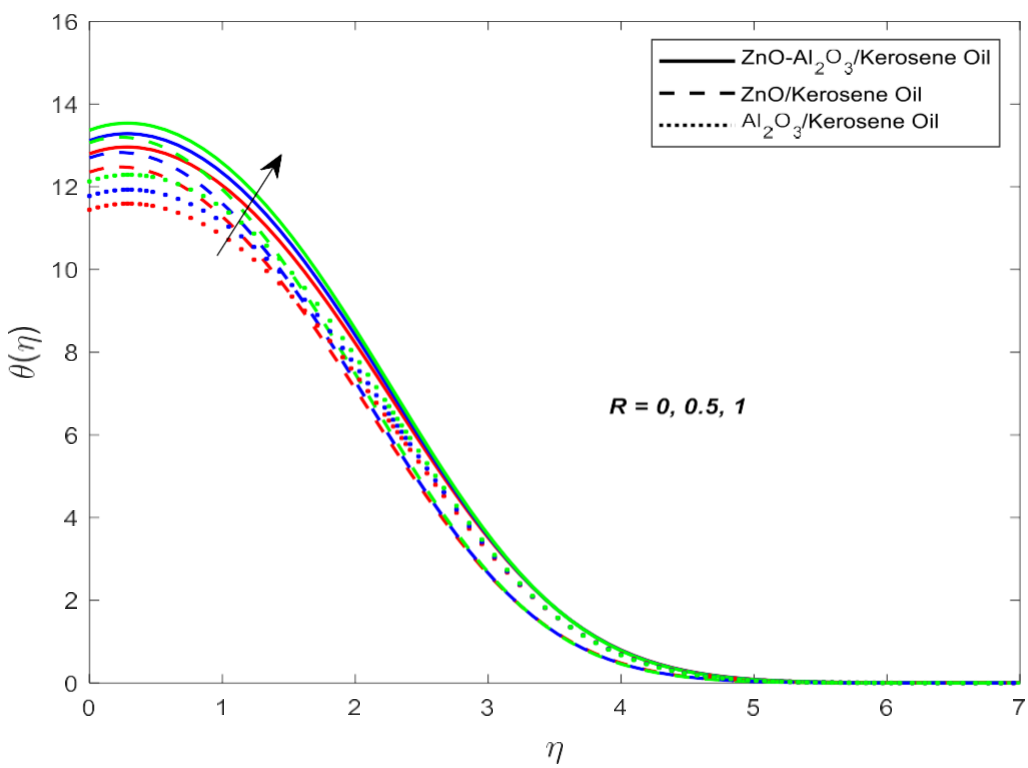

Fig. 4.10: Variation of temperature distribution $\theta(\eta)$ for radiation parameter R.

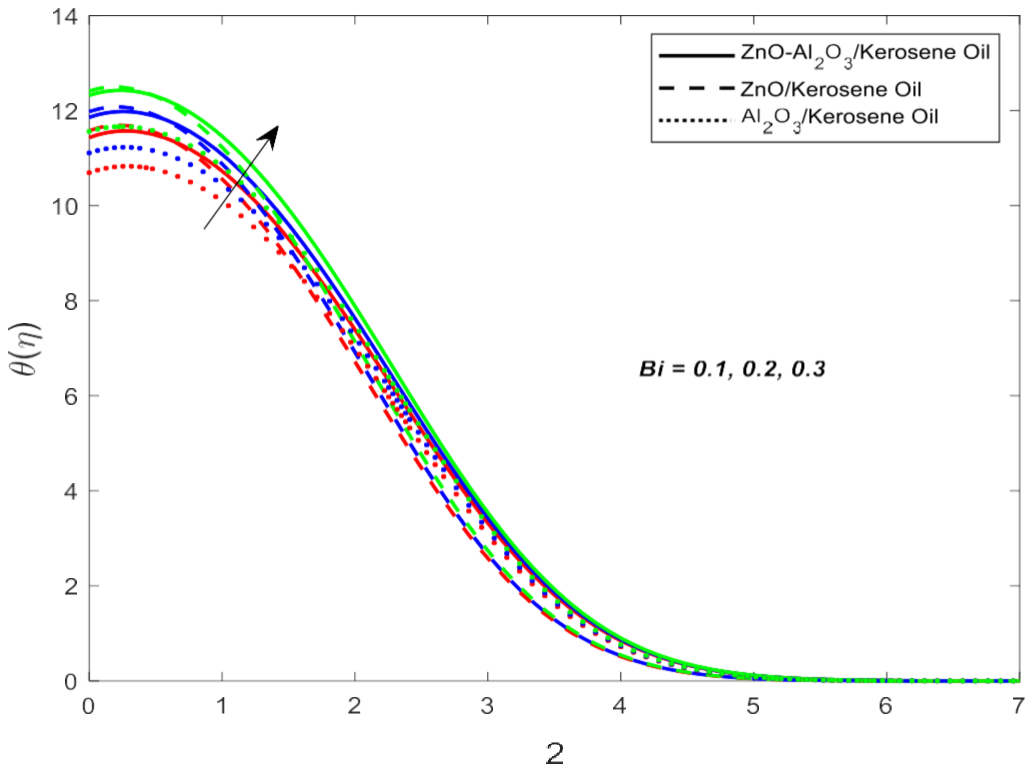

Fig. 4.11: Variation of temperature distribution $\theta(\eta)$ for Biot number Bi.

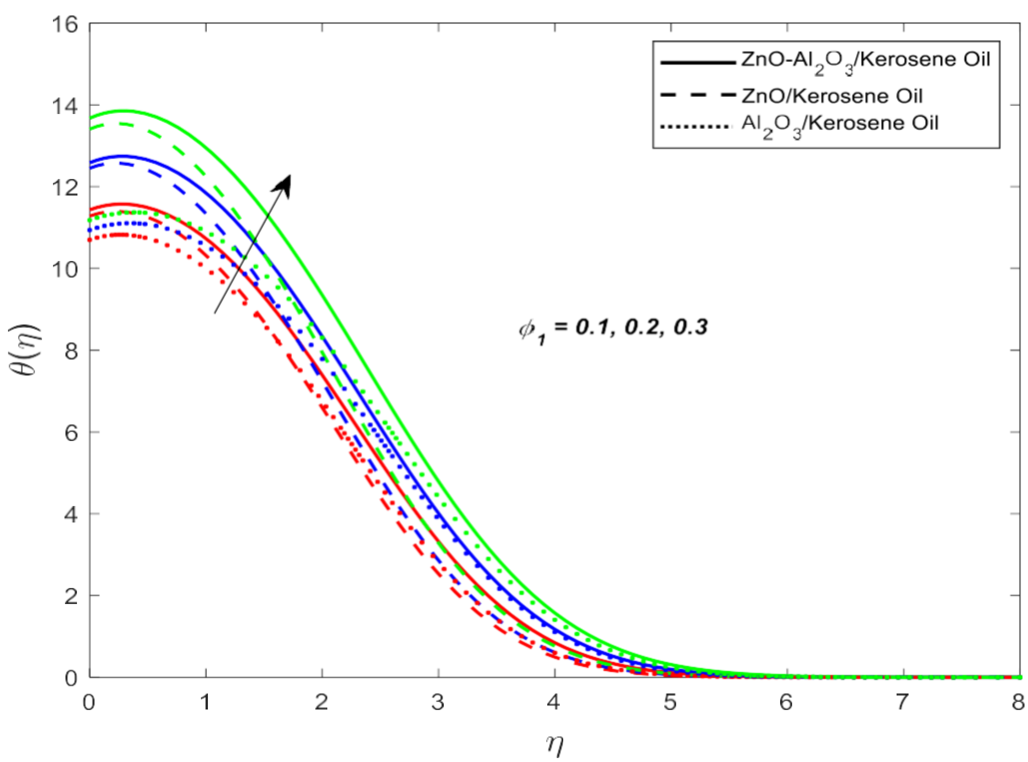

Fig. 4.12: Variation of temperature distribution $\theta(\eta)$ for volumetric fraction ϕ_1.

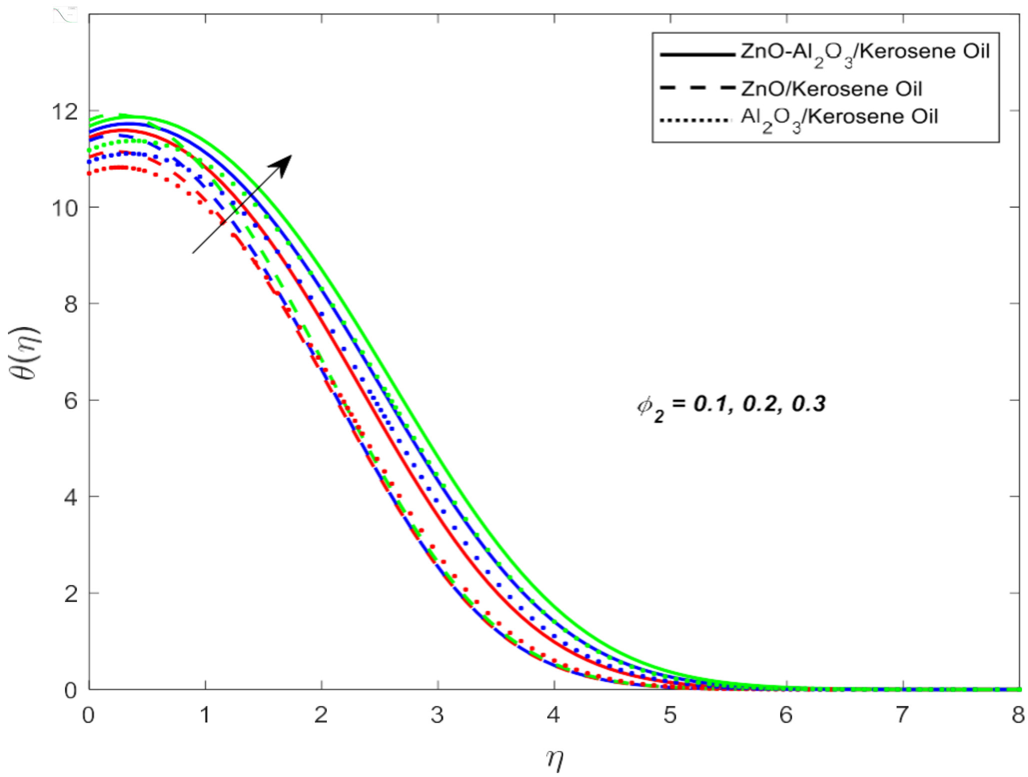

Fig. 4.13: Variation of temperature distribution $\theta(\eta)$ for volumetric fraction ϕ_2.

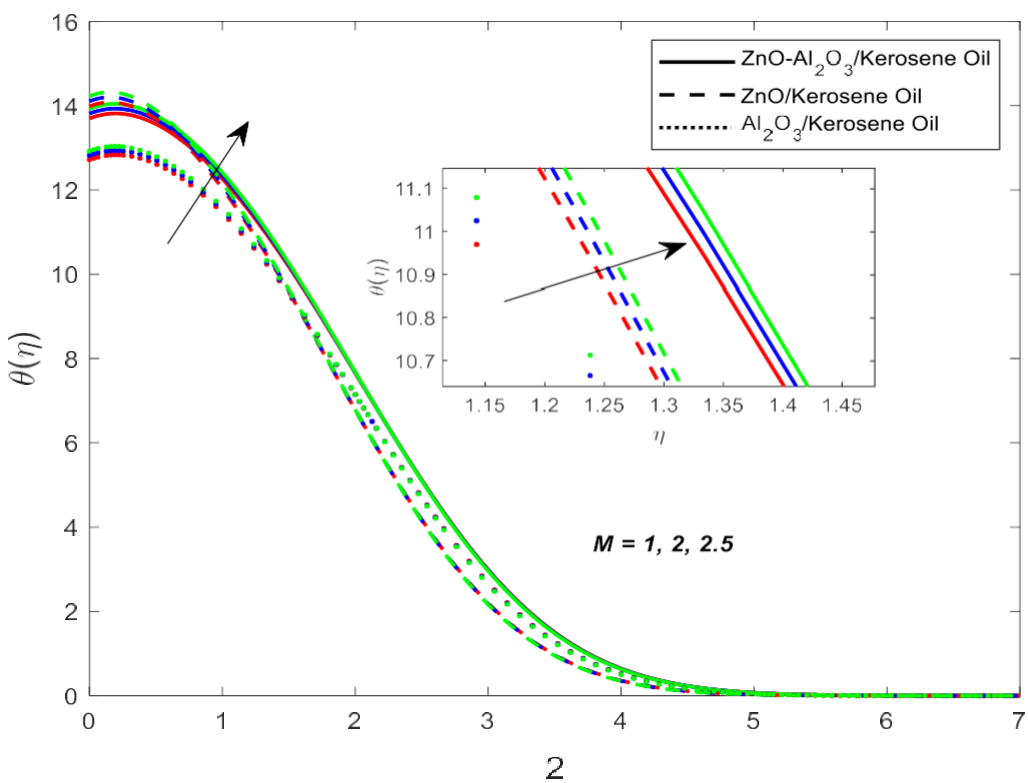

Fig. 4.14: Variation of temperature distribution $\theta(\eta)$ for magnetic parameter *M*.

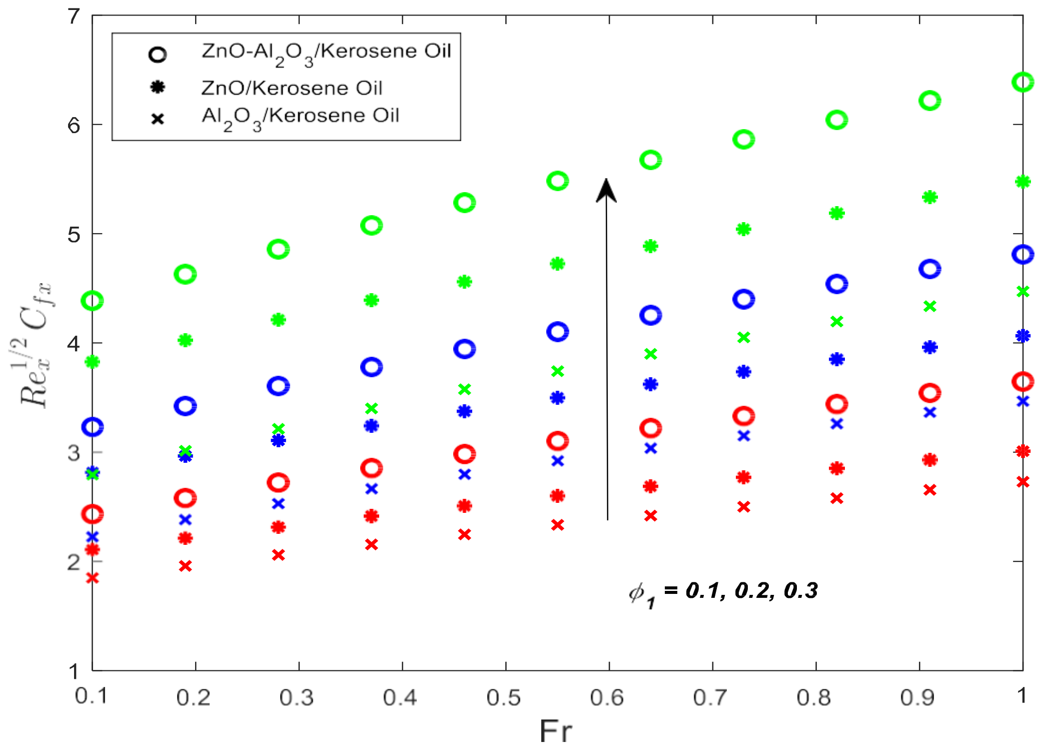

Fig. 4.15: Variation of Skin friction for *Fr* with ϕ_1.

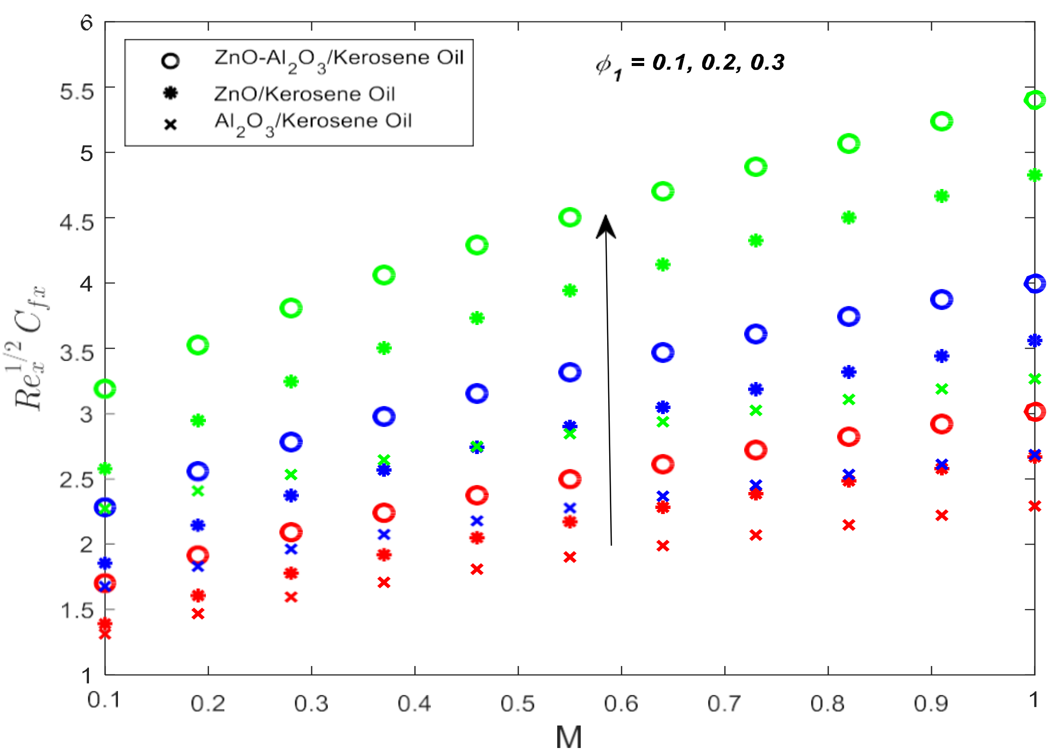

Fig. 4.16: Variation of Skin friction for *M* with ϕ_1.

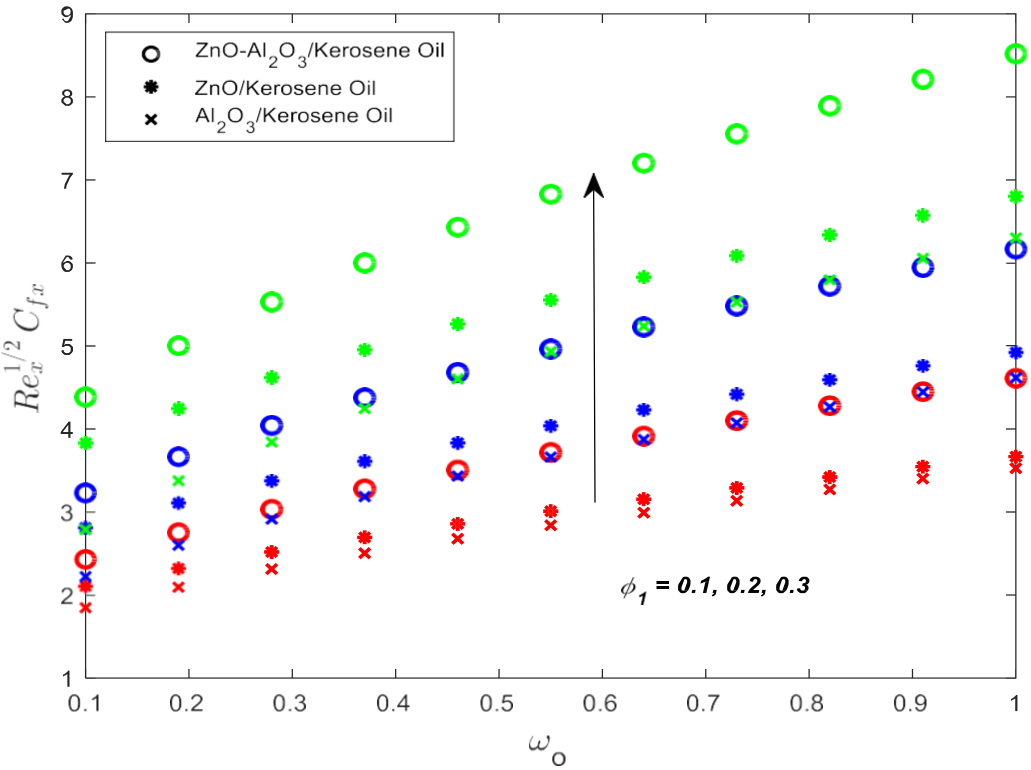

Fig. 4.17: Variation of Skin friction for ω_o with ϕ_1.

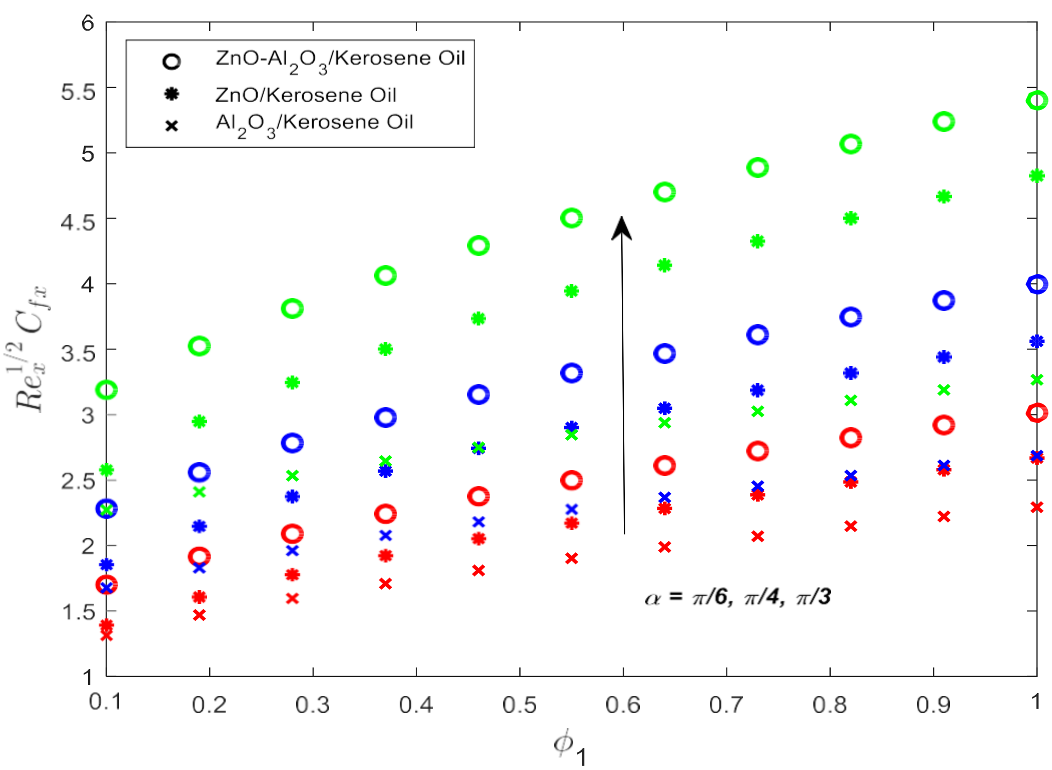

Fig. 4.18: Variation of Skin friction for α with ϕ_1.

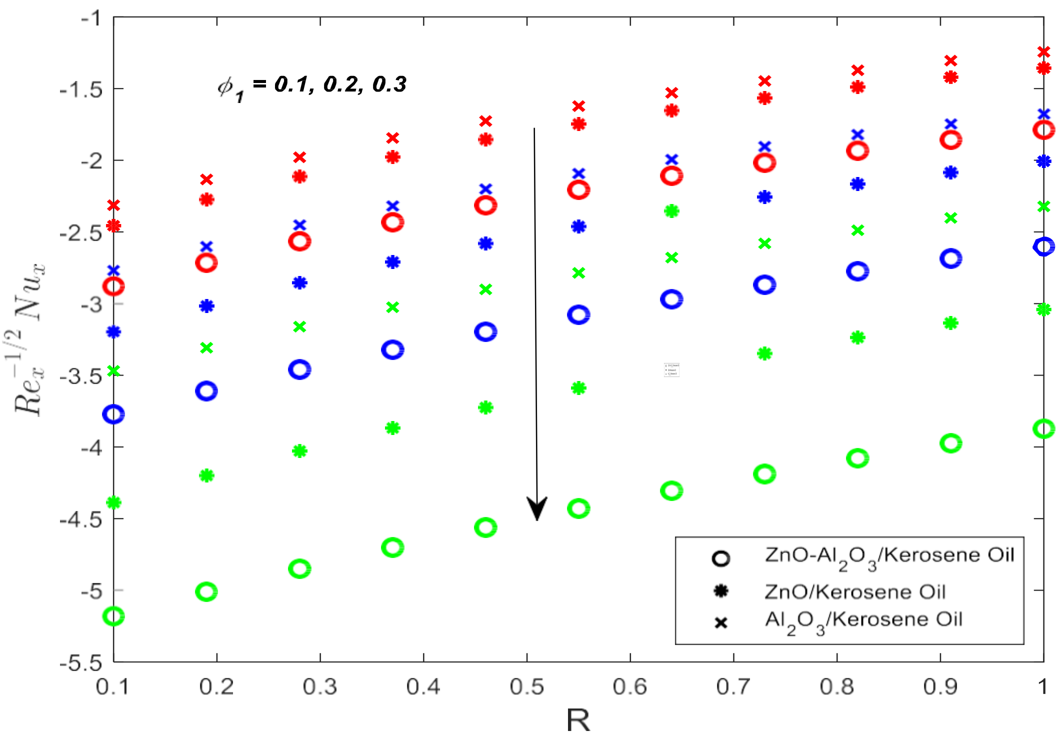

Fig. 4.19: Variation of Nusselt number for R with ϕ_1./

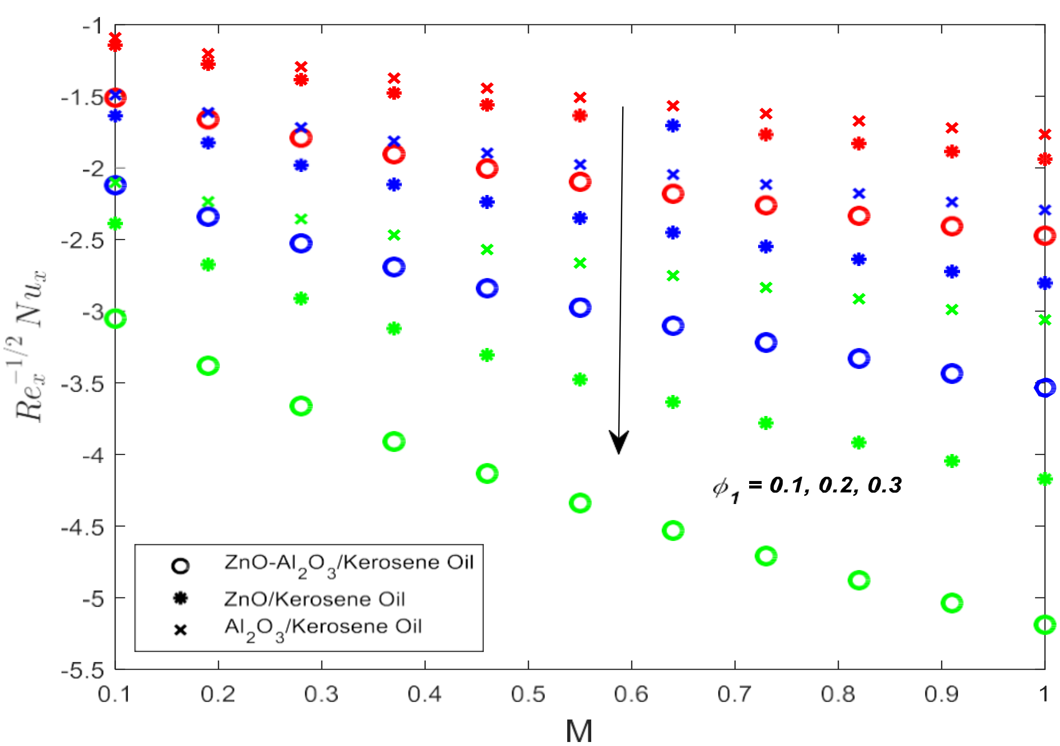

Fig. 4.20: Variation of Nusselt number for M with ϕ_1.

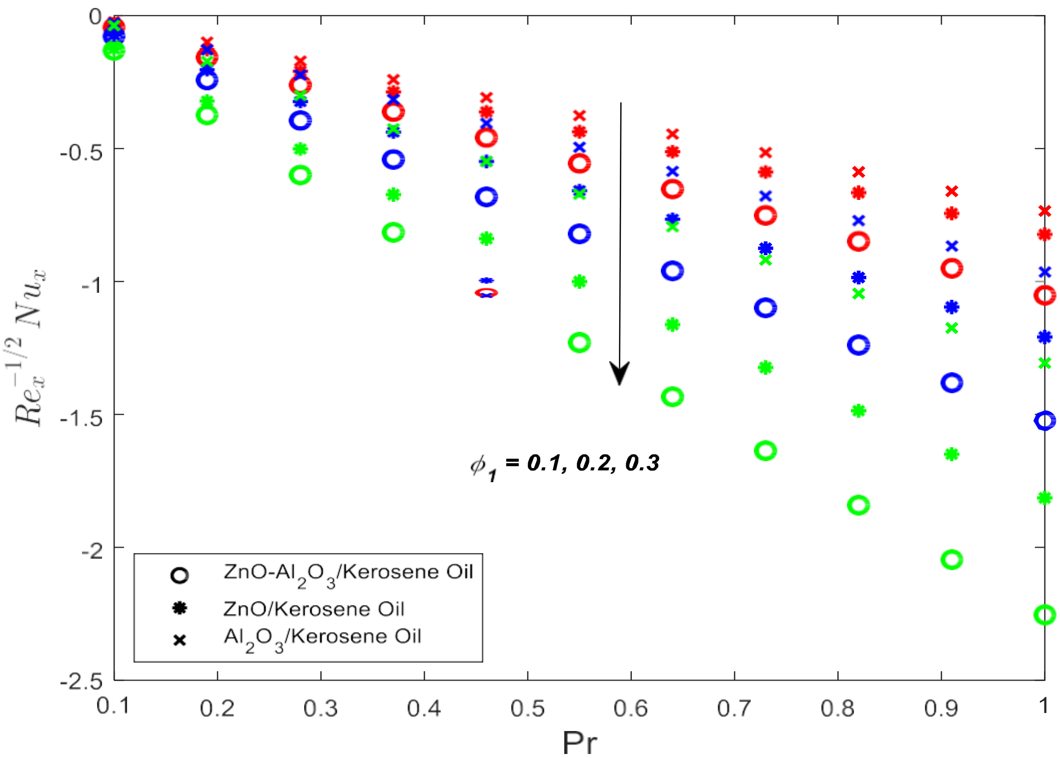

Fig. 4.21: Variation of Nusselt number for Pr with ϕ_1.

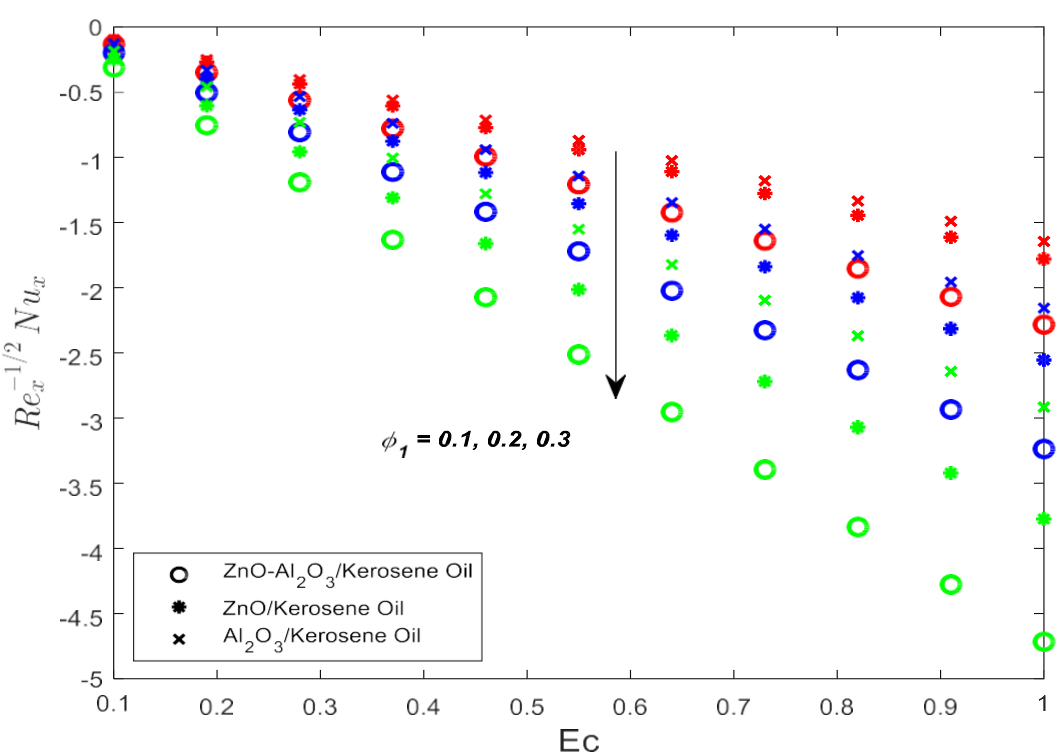

Fig. 4.22: Variation of Nusselt number for Ec with ϕ_1.

Table 4.4: Parametric values incorporated in the current analysis.

Parameters	Values	References
M	1, 2, 2.5	Saleem *et al.* [85]
Pr	1.8, 1.9, 2	Saleem *et al.* [85]
R	0, 0.5, 1	Saleem *et al.* [85]
Ec	0.7, 1, 1.3	Saleem *et al.* [85]
λ_1	-1.35	Saleem *et al.* [85]
Bi	0.1, 0.2, 0.3	Saleem *et al.* [85]
Fr	0.5, 1, 1.5	Ullah *et al.* [88]
ω_o	0.5, 1, 1.5	Ullah *et al.* [88]
ϕ_1	0.1, 0.2, 0.3	Saleem *et al.* [85]
ϕ_2	0.1, 0.2, 0.3	Saleem *et al.* [85]
α	$\frac{\pi}{6}, \frac{\pi}{4}, \frac{\pi}{3}$	Sneha *et al.* [90]

Table 4.5: Comparison of values of λ_1 on $f''(0)$ when $M = 0,\ Pr = 0,\ R = 0,\ Ec = 0,$ $Bi = 0,\ \phi_1 = 0,\ \phi_2 = 0.$

λ_1	Wang [89]	Rehman *et al.* [84]	Saleem *et al.* [85]	Current results
	$f''(0)$	$f''(0)$	$f''(0)$	$f''(0)$
-1.15	1.08223	1.08220	1.08223	1.08223
-1	1.32882	1.32880	1.32882	1.32882
-0.75	1.48930	1.48930	1.48930	1.48930
-0.5	1.49567	1.49567	1.49567	1.49567
-0.25	1.40224	1.40224	1.40224	1.40224
0	1.23258	1.23258	1.23258	1.23258
0.5	0.71330	0.71330	0.71330	0.71330
1	0	0	0	0

Chapter 5

Conclusion & Future Work

5.1 Conclusion Remarks

Hybrid nanofluids possess remarkable attributes and are regarded to have diverse and distinct applications encompassing a wide range of systems and industries. Unlike conventional nanofluids that use a single type of nanoparticle, HNFs combine two or more nanoparticles to achieve synergistic effects, resulting in significantly higher thermal conductivity than either component alone. This synergy allows engineers to tailor the fluid's behavior—balancing thermal performance with viscosity and stability—for specific industrial needs. In some cases, different nanoparticles are chosen not only for thermal enhancement but also to introduce multifunctional traits like corrosion resistance, catalytic effects, or even non-Newtonian flow characteristics, further expanding their application in microfluidic, biomedical, and energy systems. Exhibiting refined and exceptional thermal features in contrast to classic fluids and nanofluids, they facilitate more efficient heat conductivity, heat transfer and viscosity. This study highlights the stagnation point and Darcy Forchheimer flow of a kerosene oil-based hybrid fluid, with zinc oxide and alumina nanoparticles blended within. The hybrid nanofluid is investigated along with the two nanofluids separately. The flow is being inspected over a shrinking sheet in a porous medium, driven by the aspects of inclined magentohydrodynamics and Joule heating. The modeled equations of the flow problem are presented as partial differential equations and are adapted to be ordinary differential equations by implementing adequate similarity variables. Important numerical outcomes for multiple involved parameters have been deduced with respect to the temperature and velocity profiles. The factor of inclined magentohydrodynamics (α) and the magnetic parameter (M) cause a prominent elevation in the velocity distribution when their values are increased. On the other hand, the velocity profile encounters a reduced magnitude as the volumetric fractions ϕ_1 and ϕ_2, porosity parameter (ω_o) and Darcy Forchheimer variable (Fr) are elevated. For the temperature profile, Biot number (Bi) and thermal radiation parameter (R) induce a decay in the fluid's temperature. The temperature distribution endures an increment as nanoparticles volume concentrations ϕ_1 and ϕ_2, Eckert number (Ec), magnetic parameter (M) and Prandtl number (Pr) are augmented. The Nusselt number is lowered for the thermal radiation parameter (R) with higher quantities of ϕ_1. The same behavior is obtained when the Nusselt number is evaluated for magnetic parameter (M) and Eckert number (Ec) for ϕ_1. The skin friction coefficient ascends with the increase in ϕ_1 against the magnetic parameter (M), angle of inclination (α) and the Forchheimer constant (Fr) respectively. All the three fluids execute the same behaviour for all the parameters discussed above. The comparison between the two nanofluids and the hybrid nanofluid yield significant results. The prominence of hybrid nanofluid over the nanofluid is apparent from the obtained results.

5.2 Future Work

The aforementioned study has been conducted for the stagnation point fluid flow of a hybrid nanofluid with two nanofluids through a shrinking surface under the impact of Joule heating and some more appropriate assumptions. This work, however, has the potential to lead to various insightful future projects, a few of which are stated below.

- Unsteady and Darcy Forchheimer flow of hybrid nanofluid across a stretching/shrinking sheet in the presence of mixed convection.
- Numerical analysis of a ternary hybrid nanofluid with Ohmic heating and activation energy.

- Stagnation point flow of an unsteady hybrid nanofluid over a nonlinear stretching sheet in a porous medium.
- Heat and Mass Transfer of a ternary hybrid nanofluid employing the Cattaneo Christov framework with Ohmic heating and inclined magnetohydrodynamics.

References

[1] R. Turcu, A. L. Darabont, A. Nan, N. Aldea, D. Macovei, D. Bica, and L. P. Biro, "New polypyrrole-multiwall carbon nanotubes hybrid materials," *J. Optoelectron. Adv. Mater.*, vol. 8, no. 2, pp. 643–647, Apr. 2006.

[2] H. Alfvén, "Existence of electromagnetic-hydrodynamic waves," *Nature*, vol. 150, no. 3805, pp. 405–406, 1942, doi: 10.1038/150405d0.

[3] M. A. Mahmoud, "Thermal radiation effects on MHD flow of a micropolar fluid over a stretching surface with variable thermal conductivity," *Physica A*, vol. 375, no. 2, pp. 401–410, Mar. 2007, doi: 10.1016/j.physa.2006.09.010.

[4] S. Nadeem, R. Mehmood, and N. S. Akbar, "Non-orthogonal stagnation point flow of a nano non-Newtonian fluid towards a stretching surface with heat transfer," *Int. J. Heat Mass Transf.*, vol. 57, no. 2, pp. 679–689, Feb. 2013, doi: 10.1016/j.ijheatmasstransfer.2012.10.019.

[5] M. H. Abolbashari, N. Freidoonimehr, F. Nazari, and M. M. Rashidi, "Entropy analysis for an unsteady MHD flow past a stretching permeable surface in nano-fluid," *Powder Technol.*, vol. 267, pp. 256–267, Nov. 2014, doi: 10.1016/j.powtec.2014.07.028.

[6] S. S. Ghadikolaei, M. Yassari, H. Sadeghi, K. Hosseinzadeh, and D. D. Ganji, "Investigation on thermophysical properties of TiO_2–Cu/H_2O hybrid nanofluid transport dependent on shape factor in MHD stagnation point flow," *Powder Technol.*, vol. 322, pp. 428–438, Dec. 2017, doi: 10.1016/j.powtec.2017.09.006.

[7] A. Jamaludin, K. Naganthran, R. Nazar, and I. Pop, "MHD mixed convection stagnation-point flow of Cu-Al_2O_3/water hybrid nanofluid over a permeable

stretching/shrinking surface with heat source/sink," *Eur. J. Mech. B Fluids*, vol. 84, pp. 71–80, Nov. 2020, doi: 10.1016/j.euromechflu.2020.05.017.

[8] E. H. Aly and I. Pop, "MHD flow and heat transfer near stagnation point over a stretching/shrinking surface with partial slip and viscous dissipation: Hybrid nanofluid versus nanofluid," *Powder Technol.*, vol. 367, pp. 192–205, 2020, doi: 10.1016/j.powtec.2020.03.030.

[9] A. S. Khan, H. Y. Xu, and W. Khan, "Magnetohydrodynamic hybrid nanofluid flow past an exponentially stretching sheet with slip conditions," *Mathematics*, vol. 9, no. 24, p. 3291, Dec. 2021, doi: 10.3390/math9243291.

[10] U. Yashkun, K. Zaimi, N. A. Abu Bakar, A. Ishak, and I. Pop, "MHD hybrid nanofluid flow over a permeable stretching/shrinking sheet with thermal radiation effect," *Int. J. Numer. Methods Heat Fluid Flow*, vol. 31, no. 3, pp. 1014–1031, Jul. 2021, doi: 10.1108/HFF-02-2020-0083.

[11] B. Kumbhakar and S. Nandi, "Unsteady MHD radiative-dissipative flow of Cu-Al_2O_3/H_2O hybrid nanofluid past a stretching sheet with slip and convective conditions: A regression analysis," *Math. Comput. Simul.*, vol. 194, pp. 563–587, Apr. 2022, doi: 10.1016/j.matcom.2021.12.018.

[12] N. A. M. Noor and S. Shafie, "Magnetohydrodynamics squeeze flow of sodium alginate-based Jeffrey hybrid nanofluid with heat sink or source," *Case Stud. Therm. Eng.*, vol. 49, p. 103303, Sep. 2023, doi: 10.1016/j.csite.2023.103303.

[13] M. Nadeem, I. Siddique, Z. Riaz, B. M. Makhdoum, R. M. Zulqarnain, and M. Sallah, "Numerical study of unsteady tangent hyperbolic fuzzy hybrid nanofluid over an exponentially stretching surface," *Sci. Rep.*, vol. 13, no. 1, p. 15551, Apr. 2023, doi: 10.1016/j.matcom.2021.12.018.

[14] M. Mumtaz, S. Islam, H. Ullah, and Z. Shah, "Chemically reactive MHD convective flow and heat transfer performance of ternary hybrid nanofluid past a curved stretching sheet," *J. Mol. Liq.*, vol. 390, p. 123179, Nov. 2023, doi: 10.1016/j.molliq.2023.123179.

[15] R. I. Yahaya, N. Md Arifin, I. Pop, F. Md Ali, and S. S. P. Mohamed Isa, "Dual solutions for MHD hybrid nanofluid stagnation point flow due to a radially shrinking

disk with convective boundary condition," *Int. J. Numer. Methods Heat Fluid Flow*, vol. 33, no. 2, pp. 456–476, Aug. 2023, doi: 10.1108/HFF-05-2022-0301.

[16] N. M. Lisha, A. G. Vijaya Kumar, and N. A. Shah, "Numerical investigation of homogeneous–heterogeneous reactions in 3D MHD non-Newtonian hybrid nanofluid with heat source and shape factor in permeable media over a stretching sheet," *J. Therm. Anal. Calorim.*, vol. 149, no. 13, pp. 6933–6954, Dec. 2024, doi: 10.1007/s10973-023-12708-x.

[17] S. A. Anand Kumar, S. Sreedhar, M. Gayathri, and M. V. Krishna, "Darcy–Forchheimer modelling on unsteady MHD convection flow of a hybrid nanofluids (CNTs–Al_2O_3/H_2O) over a stretching sheet," *ZAMM – J. Appl. Math. Mech.*, vol. 104, no. 9, p. e202300800, Jul. 2024, doi: 10.1002/zamm.202300800.

[18] Z. Hussain, F. Aljuaydi, M. Ayaz, and S. Islam, "Enhancing thermal efficiency in MHD kerosene oil-based ternary hybrid nanofluid flow over a stretching sheet with convective boundary conditions," *Results Eng.*, vol. 22, p. 102151, Jun. 2024, doi: 10.1016/j.rineng.2024.102151.

[19] A. Rehman, D. Khan, I. Mahariq, M. A. Elkotb, and T. Elnaqeeb, "Viscous dissipation effects on time-dependent MHD Casson nanofluid over stretching surface: A hybrid nanofluid study," *J. Mol. Liq.*, vol. 408, p. 125370, Aug. 2024, doi: 10.1016/j.molliq.2024.125370.

[20] Z. H. Khan, W. A. Khan, S. M. Ibrahim, K. Swain, and Z. Huang, "Impact of multiple slips and thermal radiation on heat and mass transfer in MHD Maxwell hybrid nanofluid flow over porous stretching sheet," *Case Stud. Therm. Eng.*, vol. 61, p. 104906, Sep. 2024, doi: 10.1016/j.csite.2024.104906.

[21] M. A. A. Hamad, M. J. Uddin, and A. M. Ismail, "Radiation effects on heat and mass transfer in MHD stagnation-point flow over a permeable flat plate with thermal convective surface boundary condition, temperature dependent viscosity and thermal conductivity," *Nucl. Eng. Des.*, vol. 242, pp. 194–200, Jan. 2012, doi: 10.1016/j.nucengdes.2011.09.005.

[22] Y. Lin, L. Zheng, and X. Zhang, "Radiation effects on Marangoni convection flow and heat transfer in pseudo-plastic non-Newtonian nanofluids with variable thermal

conductivity," *Int. J. Heat Mass Transf.*, vol. 77, pp. 708–716, Oct, 2014, doi: 10.1016/j.ijheatmasstransfer.2014.06.028.

[23] M. Imtiaz, T. Hayat, and A. Alsaedi, "Flow of magneto nanofluid by a radiative exponentially stretching surface with dissipation effect," *Adv. Powder Technol.*, vol. 27, no. 5, pp. 2214–2222, Sep. 2016, doi: 10.1016/j.apt.2016.08.006.

[24] G. K. Ramesh, B. C. Prasannakumara, B. J. Gireesha, S. A. Shehzad, and F. M. Abbasi, "Three-dimensional flow of Maxwell fluid with suspended nanoparticles past a bidirectional porous stretching surface with thermal radiation," *Therm. Sci. Eng. Prog.*, vol. 1, pp. 6–14, Mar. 2017, doi: 10.1016/j.tsep.2017.02.006.

[25] M. Usman, M. Hamid, T. Zubair, R. U. Haq, and W. Wang, "Cu-Al_2O_3/Water hybrid nanofluid through a permeable surface in the presence of nonlinear radiation and variable thermal conductivity via LSM," *Int. J. Heat Mass Transf.*, vol. 126, pp. 1347–1356, Nov. 2018, doi: 10.1016/j.ijheatmasstransfer.2018.06.005.

[26] T. A. Yusuf, F. Mabood, W. A. Khan, and J. A. Gbadeyan, "Irreversibility analysis of Cu-TiO_2-H_2O hybrid-nanofluid impinging on a 3-D stretching sheet in a porous medium with nonlinear radiation: Darcy-Forchheimer's model," *Alex. Eng. J.*, vol. 59, no. 6, pp. 5247–5261, Dec. 2020, doi: 10.1016/j.aej.2020.09.053.

[27] S. Masood and M. Farooq, "Influence of thermal stratification and thermal radiation on graphene oxide-Ag/H_2O hybrid nanofluid," *J. Therm. Anal. Calorim.*, vol. 143, pp. 1361–1370, Sep. 2021, doi: 10.1007/s10973-020-10227-7.

[28] A. Ali, T. Kanwal, M. Awais, Z. Shah, P. Kumam, and P. Thounthong, "Impact of thermal radiation and non-uniform heat flux on MHD hybrid nanofluid along a stretching cylinder," *Sci. Rep.*, vol. 11, no. 1, p. 20262, Sep. 2021, doi: 10.1038/s41598-021-99800-0.

[29] T. S. Neethu, A. S. Sabu, A. Mathew, A. Wakif, and S. Areekara, "Multiple linear regression on bioconvective MHD hybrid nanofluid flow past an exponential stretching sheet with radiation and dissipation effects," *Int. Commun. Heat Mass Transf.*, vol. 135, p. 106115, Jun. 2022, doi: 10.1016/j.icheatmasstransfer.2022.106115.

[30] M. Arshad, A. Hassan, Q. Haider, F. M. Alharbi, N. Alsubaie, A. Alhushaybari, and A. M. Galal, "Rotating hybrid nanofluid flow with chemical reaction and thermal

radiation between parallel plates," *Nanomaterials*, vol. 12, no. 23, p. 4177, Nov. 2022, doi: 10.3390/nano12234177.

[31] A. S. Oke, B. C. Prasannakumara, W. N. Mutuku, R. P. Gowda, B. A. Juma, R. N. Kumar, and O. I. Bada, "Exploration of the effects of Coriolis force and thermal radiation on water-based hybrid nanofluid flow over an exponentially stretching plate," *Sci. Rep.*, vol. 12, no. 1, p. 21733, Oct. 2022, doi: 10.1038/s41598-022-21799-9.

[32] M. Arshad, F. M. Alharbi, A. Hassan, Q. Haider, A. Alhushaybari, S. M. Eldin, and A. M. Galal, "Effect of inclined magnetic field on radiative heat and mass transfer in chemically reactive hybrid nanofluid flow due to dual stretching," *Sci. Rep.*, vol. 13, no. 1, p. 7828, May. 2023, doi: 10.1038/s41598-023-34871-9.

[33] K. V. Nagaraja, U. Khan, J. K. Madhukesh, A. M. Hassan, B. C. Prasannakumara, N. Ben Kahla, and J. Singh Chohan, "Heat and mass transfer analysis of assisting and opposing radiative flow conveying ternary hybrid nanofluid over an exponentially stretching surface," *Sci. Rep.*, vol. 13, no. 1, p. 14795, Sep. 2023, doi: 10.1038/s41598-023-41916-6.

[34] W. Ibrahim and T. Gizewu, "Stability analysis of dual solutions for mixed convection and thermal radiation with hybrid nanofluid flow past shrinking/stretching curved surface," *Sci. Rep.*, vol. 13, no. 1, p. 21676, Nov. 2023, doi: 10.1038/s41598-023-48728-8.

[35] M. Arshad, F. M. Alharbi, A. Alhushaybari, S. M. Eldin, Z. Ahmad, and A. M. Galal, "Exploration of heat and mass transfer subjected to first order chemical reaction and thermal radiation: Comparative dynamics of nano, hybrid and tri-hybrid particles over dual stretching surface," *Int. Commun. Heat Mass Transf.*, vol. 146, p. 106916, Jul. 2023, doi: 10.1016/j.icheatmasstransfer.2023.106916.

[36] S. Hashim, A. S. Alqahatni, S. Rehman, S. Alshehery, and S. Bibi, "Computational investigation of magnetized hybrid nanofluids heat transport and flow through elongational surface with thermal radiation and wall slip," *Heliyon*, vol. 9, no. 10, p. e11104, Oct. 2023, doi: 10.1016/j.heliyon.2023.e20056.

[37] K. Varatharaj, R. Tamizharasi, R. Sivaraj, and K. Vajravelu, "Simulation of MHD-Casson hybrid nanofluid dynamics over a permeable stretching sheet: Effects of heat

transfer and thermal radiation," *J. Therm. Anal. Calorim.*, vol. 149, no. 15, pp. 8693–8711, May 2024, doi: 10.1007/s10973-024-13347-6.

[38] M. Rahman, B. Kada, F. Haq, J. Younis, A. Hussain, M. H. Ahmed, and A. A. Pasha, "Thermal radiation and permeability effects in thermal transportation of Maxwell hybrid nanofluid flow with irreversibility optimization," *Case Stud. Therm. Eng.*, vol. 61, p. 105052, Sep. 2024, doi: 10.1016/j.csite.2024.105052.

[39] J. Madhu, J. K. Madhukesh, I. Sarris, B. C. Prasannakumara, G. K. Ramesh, N. A. Shah, and H. Ashraf, "Influence of quadratic thermal radiation and activation energy impacts over oblique stagnation point hybrid nanofluid flow across a cylinder," *Case Stud. Therm. Eng.*, vol. 104624, Aug. 2024, doi: 10.1016/j.csite.2024.104624.

[40] F. Waseem, M. Sohail, N. Ilyas, E. M. Awwad, M. Sharaf, M. J. Khan, and A. Tulu, "Entropy analysis of MHD hybrid nanoparticles with OHAM considering viscous dissipation and thermal radiation," *Sci. Rep.*, vol. 14, no. 1, p. 1096, Dec. 2024, doi: 10.1038/s41598-023-50865-z.

[41] U. Farooq, C. Maatki, K. Kriaa, B. Hadrich, M. Imran, S. Noreen, and A. Akgül, "Characteristics of sodium alginate-based hybrid nanofluid and Darcy–Forchheimer flow induced by stretching surface with thermal radiation and Cattaneo–Christov heat flux model," *J. Comput. Sci.*, vol. 76, p. 102209, Mar. 2024, doi: 10.1016/j.jocs.2024.102209.

[42] R. Nazar, N. Amin, D. Filip, and I. Pop, "Stagnation point flow of a micropolar fluid towards a stretching sheet," *Int. J. Non-Linear Mech.*, vol. 39, no. 7, pp. 1227–1235, Sep. 2004, doi: 10.1016/j.ijnonlinmec.2003.08.007.

[43] Z. Abbas, Y. Wang, T. Hayat, and M. Oberlack, "Mixed convection in the stagnation-point flow of a Maxwell fluid towards a vertical stretching surface," *Nonlinear Anal. Real World Appl.*, vol. 11, no. 4, pp. 3218–3228, Aug. 2010, doi: 10.1016/j.nonrwa.2009.11.016.

[44] N. F. M. Noor, R. U. Haq, S. Nadeem, and I. Hashim, "Mixed convection stagnation flow of a micropolar nanofluid along a vertically stretching surface with slip effects," *Meccanica*, vol. 50, pp. 2007–2022, Mar. 2015, doi: 10.1007/s11012-015-0145-9.

[45] M. N. Rostami, S. Dinarvand, and I. Pop, "Dual solutions for mixed convective stagnation-point flow of an aqueous silica–alumina hybrid nanofluid," *Chin. J. Phys.*, vol. 56, no. 5, pp. 2465–2478, Oct. 2018, doi: 10.1016/j.cjph.2018.06.013.

[46] A. Jamaludin, R. Nazar, and I. Pop, "Mixed convection stagnation-point flow of a nanofluid past a permeable stretching/shrinking sheet in the presence of thermal radiation and heat source/sink," *Energies*, vol. 12, no. 5, p. 788, Feb. 2019, doi: 10.3390/en12050788.

[47] N. A. Zainal, R. Nazar, K. Naganthran, and I. Pop, "Unsteady MHD mixed convection flow in hybrid nanofluid at three-dimensional stagnation point," *Mathematics*, vol. 9, no. 5, p. 549, Mar. 2021, doi: 10.3390/math9050549.

[48] H. Waqas, S. A. Khan, T. Muhammad, and S. M. R. S. Naqvi, "Heat transfer enhancement in stagnation point flow of ferro-copper oxide/water hybrid nanofluid: A special case study," *Case Stud. Therm. Eng.*, vol. 28, p. 101615, Dec. 2021, doi: 10.1016/j.csite.2021.101615.

[49] T. A. Shatnawi, N. Abbas, and W. Shatanawi, "Mathematical analysis of unsteady stagnation point flow of radiative Casson hybrid nanofluid flow over a vertical Riga sheet," *Mathematics*, vol. 10, no. 19, p. 3573, Sep. 2022, doi: 10.3390/math10193573.

[50] J. Kayalvizhi and A. G. Vijaya Kumar, "Entropy analysis of EMHD hybrid nanofluid stagnation point flow over a porous stretching sheet with melting heat transfer in the presence of thermal radiation," *Energies*, vol. 15, no. 21, p. 8317, Nov. 2022, doi: 10.3390/en15218317.

[51] Z. Mahmood and U. Khan, “Unsteady three-dimensional nodal stagnation-point flow of polymer-based ternary-hybrid nanofluid past a stretching surface with suction and heat source,” *Science Progress*, vol. 106, no. 1, p. 00368504231152741, Jan. 2023, doi: 10.1177/00368504231152741.

[52] S. A. Lone, F. Ali, A. Saeed, and G. Bognár, “Irreversibility analysis with hybrid cross nanofluid of stagnation point and radiative flow (TiO_2+CuO) based on engine oil past a stretchable sheet,” *Heliyon*, vol. 9, no. 4, Mar. 2023, doi: 10.1016/j.heliyon.2023.e15056.

[53] N. A. Zainal *et al.*, “Stagnation point hybrid nanofluid flow past a stretching/shrinking sheet driven by Arrhenius kinetics and radiation effect,” *Alexandria Engineering Journal*, vol. 68, pp. 29–38, Apr. 2023, doi: 10.1016/j.aej.2023.01.005.

[54] N. A. Zainal *et al.*, “Dual solutions for general three-dimensional MHD boundary layer stagnation-point flow of hybrid nanofluid and heat transfer,” *International Journal of Numerical Methods for Heat & Fluid Flow*, vol. 33, no. 12, pp. 4015–4036, Sep. 2023, doi: 10.1108/HFF-02-2023-0078.

[55] K. A. M. Alharbi *et al.*, “Stagnation point flow of hybrid nanofluid flow passing over a rotating sphere subjected to thermophoretic diffusion and thermal radiation,” *Scientific Reports*, vol. 13, no. 1, p. 19093, Oct. 2023, doo: 10.1038/s41598-023-46353-z.

[56] G. Karthik and P. V. Kumar, “EMHD stagnation point flow of dusty hybrid nanofluid over a permeable stretching sheet: Radiative solar applications,” *Case Studies in Thermal Engineering*, vol. 54, p. 104044, Feb. 2024, doi: 10.1016/j.csite.2024.104044.

[57] M. A. Fadhel *et al.*, “Dual numerical solutions of Casson SA–hybrid nanofluid toward a stagnation point flow over stretching/shrinking cylinder,” *Nanotechnology Reviews*, vol. 13, no. 1, p. 20230191, Feb. 2024, doi: 10.1515/ntrev-2023-0191.

[58] Z. Mahmood, K. Rafique, U. Khan, M. Abd El-Rahman, and R. Alharbi, “Analysis of mixed convective stagnation point flow of hybrid nanofluid over sheet with variable thermal conductivity and slip Conditions: A Model-Based study,” *International Journal of Heat and Fluid Flow*, vol. 106, p. 109296, Apr. 2024, doi: 10.1016/j.ijheatfluidflow.2024.109296.

[59] Y. Ouyang, M. F. M. Basir, K. Naganthran, and I. Pop, “Triple solutions for unsteady stagnation flow of tri-hybrid nanofluid with heat generation/absorption in a porous medium,” *Case Studies in Thermal Engineering*, vol. 61, p. 105027, Sep. 2024, doi: 10.1016/j.csite.2024.105027.

[60] T. Singla, S. Sharma, and B. Kumar, “Convective slip flow of a hybrid nanofluid near a non-orthogonal stagnation point over a stretching surface,” *ZAMM-Journal of*

Applied Mathematics and Mechanics, vol. 104, no. 10, p. e202300392, Aug. 2024, doi: 10.1002/zamm.202300392.

[61] M. Nawaz, A. Zeeshan, R. Ellahi, S. Abbasbandy, and S. Rashidi, "Joules and Newtonian heating effects on stagnation point flow over a stretching surface by means of genetic algorithm and Nelder-Mead method," *International Journal of Numerical Methods for Heat & Fluid Flow*, vol. 25, no. 3, pp. 665–684, Apr. 2015, doi: 10.1108/HFF-04-2014-0103.

[62] T. Hayat, M. Imtiaz, and A. Alsaedi, "Melting heat transfer in the MHD flow of Cu–water nanofluid with viscous dissipation and Joule heating," *Advanced Powder Technology*, vol. 27, no. 4, pp. 1301–1308, Jul. 2016, doi: 10.1016/j.apt.2016.04.024.

[63] A. Kamran, S. Hussain, M. Sagheer, and N. Akmal, "A numerical study of magnetohydrodynamics flow in Casson nanofluid combined with Joule heating and slip boundary conditions," *Results in Physics*, vol. 7, pp. 3037–3048, 2017, doi: 10.1016/j.rinp.2017.08.004.

[64] S. S. Ghadikolaei, K. Hosseinzadeh, and D. D. Ganji, "Numerical study on magnetohydrodynamic CNTs-water nanofluids as a micropolar dusty fluid influenced by non-linear thermal radiation and joule heating effect," *Powder Technology*, vol. 340, pp. 389–399, Dec. 2018, doi: 10.1016/j.powtec.2018.09.023.

[65] A. Aziz, W. Jamshed, Y. Ali, and M. Shams, "Heat transfer and entropy analysis of Maxwell hybrid nanofluid including effects of inclined magnetic field, Joule heating and thermal radiation," *Discrete and Continuous Dynamical Systems - Series S*, vol. 13, pp. 2667, Jul. 2020, doi: 10.3934/dcdss.2020142.

[66] N. S. Khashi'ie, N. M. Arifin, I. Pop, and N. S. Wahid, "Flow and heat transfer of hybrid nanofluid over a permeable shrinking cylinder with Joule heating: A comparative analysis," *Alexandria Engineering Journal*, vol. 59, no. 3, pp. 1787–1798, Jun. 2020, doi: 10.1016/j.aej.2020.04.048.

[67] M. Shoaib *et al.*, "Numerical analysis of 3-D MHD hybrid nanofluid over a rotational disk in presence of thermal radiation with Joule heating and viscous dissipation effects using Lobatto IIIA technique," *Alexandria Engineering Journal*, vol. 60, no. 4, pp. 3605–3619, Aug. 2021, doi: 10.1016/j.aej.2021.02.015.

[68] M. Ramzan *et al.*, “Heat transfer analysis of the mixed convective flow of magnetohydrodynamic hybrid nanofluid past a stretching sheet with velocity and thermal slip conditions,” *PLoS ONE*, vol. 16, no. 12, p. e0260854, Dec. 2021, doi: 10.1371/journal.pone.0260854.

[69] A. M. Alqahtani *et al.*, “Transport properties of two-dimensional dissipative flow of hybrid nanofluid with Joule heating and thermal radiation,” *Scientific Reports*, vol. 12, no. 1, p. 19374, Oct. 2022, doi: 10.1038/s41598-022-23337-z.

[70] N. S. Khashi’ie, N. S. Wahid, N. Md Arifin, and I. Pop, “MHD stagnation-point flow of hybrid nanofluid with convective heated shrinking disk, viscous dissipation and Joule heating effects,” *Neural Computing and Applications*, vol. 34, no. 20, pp. 17601–17613, Apr. 2022, doi: 10.1007/s00521-022-07371-6.

[71] G. Rasool, A. Wakif, X. Wang, A. Alshehri, and A. M. Saeed, "Falkner-Skan aspects of a radiating (50% ethylene glycol+ 50% water)-based hybrid nanofluid when Joule heating as well as Darcy-Forchheimer and Lorentz forces affect significantly," *Propulsion and Power Research*, vol. 12, no. 3, pp. 428–442, Sep. 2023, doi: 10.1016/j.jppr.2023.07.001.

[72] A. U. Hayat, I. Ullah, H. Khan, M. M. Alam, A. M. Hassan, and H. Khan, "Numerical analysis of radiative hybrid nanomaterials flow across a permeable curved surface with inertial and Joule heating characteristics," *Heliyon*, vol. 9, no. 11, Oct. 2023, doi: 10.1016/j.heliyon.2023.e21452.

[73] S. Jayanthi and H. Niranjan, "Effects of Joule heating, viscous dissipation, and activation energy on nanofluid flow induced by MHD on a vertical surface," *Symmetry*, vol. 15, no. 2, p. 314, Jan. 2023, doi: 10.3390/sym15020314.

[74] S. Zainodin, A. Jamaludin, R. Nazar, and I. Pop, "MHD Mixed Convection Flow of Hybrid Ferrofluid through Stagnation-Point over the Nonlinearly Moving Surface with Convective Boundary Condition, Viscous Dissipation, and Joule Heating Effects," *Symmetry*, vol. 15, no. 4, p. 878, Apr. 2023, 10.3390/sym15040878.

[75] M. Jameel, Z. Shah, M. Rooman, M. H. Alshehri, and N. Vrinceanu, "Entropy generation analysis on Darcy-Forchheimer Maxwell nanofluid flow past a porous stretching sheet with threshold Non-Fourier heat flux model and Joule heating," *Case Stud. Therm. Eng.*, vol. 52, p. 103738, Dec. 2023, doi: 10.1016/j.csite.2023.103738.

[76] K. Muhammad, B. Ahmed, M. Sharaf, M. Afikuzzaman, and E. A. Az-Zo'bi, "Multiscale tribology analysis of MHD hybrid nanofluid flow over a curved stretching surface," *Nanoscale Adv.*, vol. 6, no. 3, pp. 855–866, Dec. 2023, doi: 10.1039/D3NA00688C.

[77] K. Rafique, Z. Mahmood, Muhammad Adnan, H. Alqahtani, and A. A. Shaaban, "Dynamics of shape factor with Joule heating and thermal stratification on magnetohydrodynamic Al_2O_3-Cu-TiO_2/H_2O nanofluid of stretching disk: an irreversibility analysis," *J. Therm. Anal. Calorim.*, pp. 1–24, Jul. 2024, doi: 10.1007/s10973-024-13269-3.

[78] A. Tanveer, M. Aneja, M. B. Ashraf, and R. Nawaz, "Bioconvection heat and mass transfer across a nonlinear stretching sheet with hybrid nanofluids, joule dissipation, and entropy generation," *ZAMM-J. Appl. Math. Mech.*, vol. 104, no. 5, p. e202300550, Mar. 2024, doi: 10.1002/zamm.202300550.

[79] I. Razzaq et al., "Effects of viscous and Joule dissipation on hydromagnetic hybrid nanofluid flow over nonlinear stretching surface with Hamilton-Crosser model," *Case Stud. Therm. Eng.*, p. 105125, Sep. 2024, doi: 10.1016/j.csite.2024.105125.

[80] R. W. Fox, A. McDonald, and P. Pitchard, *Introduction to Fluid Mechanics*, 2004 ed. New York, NY, USA: John Wiley & Sons, Inc., 2006.

[81] F. Durst and I. Arnold, *Fluid Mechanics: An Introduction to the Theory of Fluid Flows*, vol. 675. Berlin, Germany: Springer, 2008.

[82] S. Whitaker, *Fundamental Principles of Heat Transfer*, 1st ed. United Kingdom: Elsevier Science and Technology Books, 1977.

[83] S. Whitaker, *Fundamental Principles of Heat Transfer*, 1st ed. United Kingdom: Elsevier Science and Technology Books, 1977.

[84] A. Rehman and Z. Abbas, "Stability analysis of heat transfer in nanomaterial flow of boundary layer towards a shrinking surface: Hybrid nanofluid versus nanofluid," *Alexandria Eng. J.*, vol. 61, no. 12, pp. 10757–10768, Dec. 2022, doi: 10.1016/j.aej.2022.04.020.

[85] S. Saleem, B. Ahmad, A. Naseem, M. B. Riaz, and T. Abbas, "Mono and hybrid nanofluid analysis over shrinking surface with thermal radiation: a numerical

approach," *Case Stud. Therm. Eng.*, vol. 54, p. 104023, Feb. 2024, doi: 10.1016/j.csite.2024.104023.

[86] E. M. Sparrow and R. Cess, *Radiation Heat Transfer*. Washington, DC, USA: Hemisphere Publishing Corp., 1978.

[87] L. Zhang, T. Nazar, M. M. Bhatti, and E. E. Michaelides, "Stability analysis on the kerosene nanofluid flow with hybrid zinc/aluminum-oxide (ZnO-Al2O3) nanoparticles under Lorentz force," *Int. J. Numer. Methods Heat Fluid Flow*, vol. 32, no. 2, pp. 740–760, Jan. 2022, doi: 10.1108/HFF-02-2021-0103.

[88] B. Ullah, B. M. Fadhl, B. M. Makhdoum, K. S. Nisar, H. A. Wahab, and U. Khan, "Heat transfer analysis in Darcy Forchheimer flow of hybrid nanofluid for multiple shape effects over a curved stretching surface," *Case Stud. Therm. Eng.*, vol. 40, p. 102538, Dec. 2022, doi: 10.1016/j.csite.2022.102538.

[89] C. Y. Wang, "Stagnation flow towards a shrinking sheet," *Int. J. Non-Linear Mech.*, vol. 43, no. 5, pp. 377–382, Jun. 2008, doi: 10.1016/j.ijnonlinmec.2007.12.021.

[90] K. N. Sneha, U. S. Mahabaleshwar, and S. Bhattacharyya, "An effect of thermal radiation on inclined MHD flow in hybrid nanofluids over a stretching/shrinking sheet," *J. Therm. Anal. Calorim.*, vol. 148, no. 7, pp. 2961–2975, Sep. 2023, doi: 10.1007/s10973-022-11552-9.